




**ADVERTIMENT.** L'accés als continguts d'aquesta tesi queda condicionat a l'acceptació de les condicions d'ús establertes per la següent llicència Creative Commons:  [http://cat.creativecommons.org/?page\\_id=184](http://cat.creativecommons.org/?page_id=184)

**ADVERTENCIA.** El acceso a los contenidos de esta tesis queda condicionado a la aceptación de las condiciones de uso establecidas por la siguiente licencia Creative Commons:  <http://es.creativecommons.org/blog/licencias/>

**WARNING.** The access to the contents of this doctoral thesis it is limited to the acceptance of the use conditions set by the following Creative Commons license:  <https://creativecommons.org/licenses/?lang=en>



# **Electronic tongues based on electropolymerized molecularly imprinted polymers for pharmaceutical analysis**

**Mingyue Wang**

**Doctoral Thesis**

Doctoral Studies in Chemistry

Directors: Prof. Manel del Valle Zafra

Dr. Xavier Cetó Alsedà

Department of Chemistry

July 2022



Per aspera ad astra.

功不唐捐 玉汝于成





# Declaration

---

Thesis submitted to aspire for the doctoral degree of Mingyue Wang.

Mingyue Wang

Director's approval:

Pro. Manel del Valle Zafra

Dr. Xavier Cetó Alsedà

Bellaterra, 2 July 2022



## Funding support

---

The present thesis work has been carried out in the laboratory of the Group of Sensors and Biosensors of Chemistry Department in Universitat Autònoma de Barcelona. Research was financially supported by the Ministry of Economy and Innovation (MINECO) through projects CTQ2016-80170-P and PID2019-107102RB-C21.

Group of Sensors and Biosensors



Universitat Autònoma de Barcelona



Ministry of Economy and Innovation (Spain)





# Summary

---

In the past decades, as the increasing use of drugs for treating various diseases contributed to the progressively improved life quality of human being, pharmaceutical analysis has been regarded as an important issue that is demanded in several fields, such as pharmaceutical industry, clinical monitoring, and environmental protection. However, to date, the detection methods to pharmaceuticals suffer from some drawbacks of being expensive, laborious, and inefficient. To this end, in this work, two electronic tongues (ETs) were built by combining molecularly imprinted polymers (MIPs) based electrochemical sensors and chemometric tools, and applied to detect the two sets of pharmaceutical analytes. The one is related to the commonly used active pharmaceutical ingredients including paracetamol, ascorbic acid, and uric acid, while the other belongs to fluoroquinolone antibiotics including ciprofloxacin, levofloxacin, and moxifloxacin.

On the one hand, efforts have been made to enhance the sensing performance of electropolymerized MIPs in terms of conductivity, sensitivity, and structural porosity, mainly through two ways. First,  $pTS^-$  was incorporated into the MIPs backbone as doping anion to form the MIPs films. Second, multiwall carbon nanotubes (MWCNTs) and gold nanoparticles (AuNPs) were integrated into MIPs to produce the hybrid materials. Both kinds of fabricated MIPs-based sensors were characterized morphologically and electrochemically. After then, their voltammetric responses toward different analytes were investigated individually, from which series of linear relationships and analytical parameters were obtained.

On the other hand, certain difficulties facing most conventional sensors can be solved by ET approach through combining MIPs-based sensor arrays with chemometric tools. Based on the qualitative and quantitative models, the two developed ETs present excellent capability of simultaneously analyzing the families of pharmaceutical analytes that share similar structure and nature.



## ***TABLE OF CONTENTS***





# Table of Contents

---

1	Introduction .....	1
1.1	Chemical sensors and sensor arrays .....	3
1.1.1	Chemical sensors .....	3
1.1.2	Electrochemical sensors .....	6
1.1.3	Chemical sensor arrays .....	10
1.2	Electronic tongues .....	12
1.2.1	Taste system: from biological to artificial .....	12
1.2.2	Data processing and chemometric tools .....	14
1.3	Molecularly imprinted polymers .....	18
1.3.1	Synthesis and polymerization .....	20
1.3.2	Electropolymerization of MIPs .....	26
1.4	Electrochemical sensing based on MIPs .....	32
1.4.1	MIPs-based electrochemical sensors .....	32
1.4.2	Strategies to improve MIPs-based electrochemical sensors .....	35
1.4.3	MIPs-based electrochemical sensing for pharmaceutical analysis .....	39
	References .....	47
2	Objectives .....	63
3	Experimental .....	67
3.1	Reagents and instruments .....	69
3.1.1	Chemicals and buffers .....	69
3.1.2	Instruments .....	72
3.2	Protocols for MIPs-based sensors and ETs .....	72
3.2.1	Fabrication of graphite epoxy composite electrode .....	72
3.2.2	Preparation of <i>p</i> TS/PPy MIPs/GEC sensors .....	73
3.2.3	Preparation of MIP(FQs)@Au-fMWCNTs/GEC sensors .....	74

3.2.4 Construction of MIPs-based electronic tongues.....	76
3.3 Preparation of samples .....	77
3.4 Electrochemical measurements .....	80
3.5 Data analysis.....	81
4 Results and discussion .....	85
4.1 A novel electronic tongue using electropolymerized molecularly im- printed polymers for the simultaneous determination of active pharmaceutical ingredients.....	91
4.1.1 Synthesis of <i>p</i> TS <sup>-</sup> /PPy MIPs.....	91
4.1.2 <i>p</i> TS <sup>-</sup> /PPy MIPs-based sensors .....	93
4.1.3 <i>p</i> TS <sup>-</sup> /PPy MIPs-based ET .....	100
4.2 A sensor array based on molecularly imprinted polymers and machine learning for the analysis of fluoroquinolone antibiotics .....	105
4.2.1 MIP(FQs)@Au-fMWCNTs based sensors.....	107
4.2.2 MIP(FQs)@Au-fMWCNTs based ET.....	113
5 Conclusions and prospects.....	117
5.1 Conclusions .....	119
5.2 Prospects of MIPs-based ET .....	121
ANNEX.....	123

## ***ABBREVIATIONS***



## Abbreviations

<i>AA</i>	Ascorbic acid
<i>AAB</i>	Acetate buffer
<i>ANN</i>	Artificial neural network
<i>API</i>	Active pharmaceutical ingredient
<i>AuNP</i>	Gold nanoparticle
<i>CFX</i>	Ciprofloxacin
<i>CV</i>	Cyclic voltammetry
<i>CVA</i>	Canonical variate analysis
<i>DCT</i>	Discrete cosine transform
<i>DPV</i>	Differential pulse voltammetry
<i>DWT</i>	Discrete wavelet transform
<i>ECS</i>	Electrochemical sensor
<i>EDOT</i>	3,4-ethylenedioxythiophene
<i>EDX</i>	Energy-dispersive X-ray spectrometry
<i>EIS</i>	Electrochemical impedance spectroscopy
<i>eMIP</i>	Electropolymerized molecularly imprinted polymer

<b><i>EN</i></b>	Electronic nose
<b><i>ET</i></b>	Electronic tongue
<b><i>EtOH</i></b>	Ethanol
<b><i>FFT</i></b>	Fast Fourier transform
<b><i>FLQ</i></b>	Flumequine
<b><i>FQ</i></b>	Fluoroquinolone
<b><i>GEC</i></b>	Graphite epoxy composite
<b><i>IUPAC</i></b>	International Union of Pure and Applied Chemistry
<b><i>LDA</i></b>	Linear discriminant analysis
<b><i>LVX</i></b>	Levofloxacin
<b><i>LOD</i></b>	Limit of detection
<b><i>LSV</i></b>	Linear sweep voltammetry
<b><i>LVX</i></b>	Moxifloxacin
<b><i>MIP</i></b>	Molecularly imprinted polymer
<b><i>MIT</i></b>	Molecularly imprinted technology
<b><i>MLR</i></b>	Multiple linear regression
<b><i>MWCNT</i></b>	Muli-wall carbon nanotube
<b><i>NA</i></b>	Nalidixic acid
<b><i>NIP</i></b>	Non-imprinted polymer
<b><i>NP</i></b>	Nanoparticle
<b><i>nPLS</i></b>	Multiway partial least-squares regression
<b><i>PA</i></b>	Paracetamol
<b><i>PANI</i></b>	Poly aniline
<b><i>PBS</i></b>	Phosphate buffer saline
<b><i>PC</i></b>	Principal component
<b><i>PCA</i></b>	Principle component analysis
<b><i>PCR</i></b>	Principal component regression
<b><i>PEDOT</i></b>	Poly(3,4-ethylenedioxythiophene)

<b><i>PLS</i></b>	Partial least-squares regression
<b><i>PPy</i></b>	Poly pyrrole
<b><i>PSS</i></b>	Poly (styrene sulfonate)
<b><i>pTS<sup>-</sup></i></b>	<i>para</i> -toluenesulfonate anion
<b><i>Py</i></b>	Pyrrole
<b><i>RMSE</i></b>	Root mean square error
<b><i>RSD</i></b>	Relative standard deviation
<b><i>SEM</i></b>	Scanning electron microscopy
<b><i>SPE</i></b>	Screen-printed electrode
<b><i>SVMs</i></b>	Support vector machines
<b><i>SWV</i></b>	Square wave voltammetry
<b><i>TEM</i></b>	Transmission electron microscope
<b><i>TM</i></b>	Template molecule
<b><i>TR</i></b>	Taste receptor
<b><i>TRC</i></b>	Taste receptor cell
<b><i>UA</i></b>	Uric acid





## ***CHAPTER 1 INTRODUCTION***



# **1 Introduction**

## **1.1 Chemical sensors and sensor arrays**

### **1.1.1 Chemical sensors**

#### **1.1.1.1 Definition and composition**

According to the definition proposed by IUPAC commission, chemical sensors are devices that can transform chemical information extending from the concentration of a specific sample component to total composition analysis, which originates from a chemical reaction of the analyte or from a physical property of the investigated system, into an analytically useful signal [1, 2].

As shown in Figure 1.1, a chemical sensor is essentially composed by two important parts: the receptor and the transducer [1]. In the most cases of chemical sensors, the receptor has interaction with target analyte but no interaction with other

compounds. When the target analyte interacts with the receptor part, the physical properties could be changed, such as light, heat, electrons, etc., contributing to an intermediate signal. Afterwards, the intermediate signal would be further transformed into an electrical signal to be output in the transducer part, which can be in the form of a charge, current, voltage, resistance, capacitance, or inductance. By such an analytical system, the goals of the qualitative and (or) quantitative analysis could be attained.

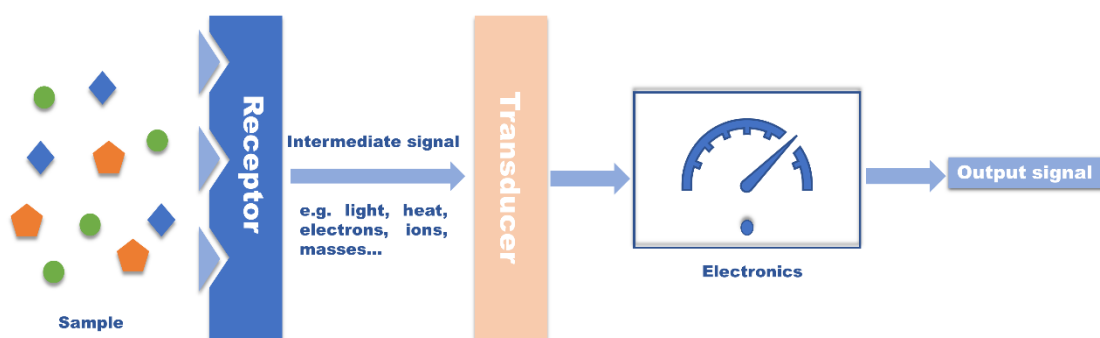


Figure 1.1 General scheme of a chemical sensor.

### 1.1.1.2 Classification

Chemical sensors can be classified in term of the receptor and the transducer. Generally speaking, based on the different operating principle of transducer, chemical sensors are classified into four groups including optical sensors, thermal sensors, mass sensors, and electrochemical sensors.

**Optical sensors:** its fundamental principle is on the basis of the change in optical properties result from absorption, scattering, refraction, or reflection [3]. Currently, according to the type of the optical signal, there are several typical optical sensing strategies: fluorescence, colorimetric, surface enhanced Raman scattering, surface plasmon resonance and chemiluminescence [1, 4, 5].

**Mass sensors:** its fundamental principle is on the basis of mass change result from absorption, evaporation, deposition, or erosion during chemical reactions. For the purpose of detecting mass change, some sensing devices have been exploited, such as

the thickness shear mode resonator, quartz crystal microbalance, and surface acoustic wave device [1, 3].

**Thermal sensors:** its fundamental principle is to obtain output signals depending on the thermal change associated to chemical interaction, generally in the forms of resistance, voltage or current. And it is divided into four types, i.e., resistance temperature detectors, thermally sensitive resistors, silicon sensors, and thermocouples [1, 6].

**Electrochemical sensors:** it transforms the interaction between the analyte and the receptor of an electrode into a measurable electrical analytical signal [1].

### 1.1.1.3 Recognition elements in chemical sensors

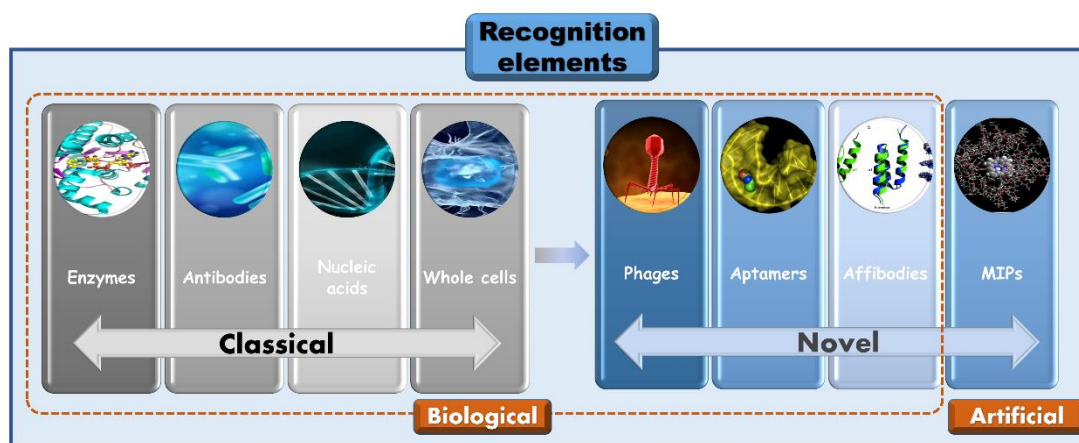


Figure 1.2 The graphical illustration of various recognition elements in sensors.

Considering the constantly increasing demands for the rapid and accurate sensing in various fields, more and more strategies have been adopted to improve the sensing performance in terms of sensitivity, selectivity, stability, and reproducibility in chemical sensing [7]. As previously introduced in *Section 1.1.1.1*, the receptor is one of crucially fundamental compositions of chemical sensors and the recognition mechanism of receptor is important for improving the performance of chemical sensors, especially for selectivity. In general, recognition elements can be biological elements in vitro or artificially fabricated elements, whose selection largely depends on the target analytes

and its affinity with sensor [8].

Various recognition elements used in sensors are shown in Figure 1.2. Enzymes are the earliest and most commonly used ones [9]. Besides, some other classically biological recognition elements also are applied in different types of sensors, such as antibodies for immunosensors [10], nucleic acids for genosensors [11], whole cells for whole-cell biosensors [12]. In recent years, some novel recognition elements, for instance, phages, aptamers and affibodies have been developed with improved stability, cost-efficiency, customizable structures and long shelf-life [8]. Although a variety of prototypes of biosensors have been designed in laboratory based on biological recognition elements, it is still hard to reach a wide application due to their deficient stability.

Molecularly imprinted polymers (MIPs), a class of bio-mimetically synthetic recognition elements, have aroused the interests of researchers [13, 14]. Compared with biological ones, they can be more easily tailored depending on the target compound. More importantly, MIPs compensate the drawbacks in the context of thermal, chemical and mechanical intolerance, and non-reusability, thus having great potential as alternatives to biological elements.

Additionally, with the rapid development of nanomaterials and their substantially application in sensors, the incorporation of recognition elements and nanomaterials is trending. Many literatures reported chemical sensors utilizing recognition elements and carbon materials, metal nanoparticles together to boost sensing performance [15, 16].

## **1.1.2 Electrochemical sensors**

Among the above-mentioned types of chemical sensors commented in *Section 1.1.1.2*, electrochemical sensors (ECSs) are the oldest and widest class. In contrast to the others, the ECSs can convert the interaction between the receptors and targets into electrical signals directly, without any other intermediate signals, which contributes to the simpler requirements for the associated instrumentation. Moreover, by comparison,

ECSs have the merits of robustness, lower-cost, reduced limit of detection and less or negligible sample consumption [17].

### 1.1.2.1 Classification

There are various measurable changes of physical properties in the system that may happen during the electrochemical reactions in electrochemical sensors, such as, current, potential or charge accumulation, and conductive properties. Therefore, the ECSs could be sorted, as shown in Figure 1.3.

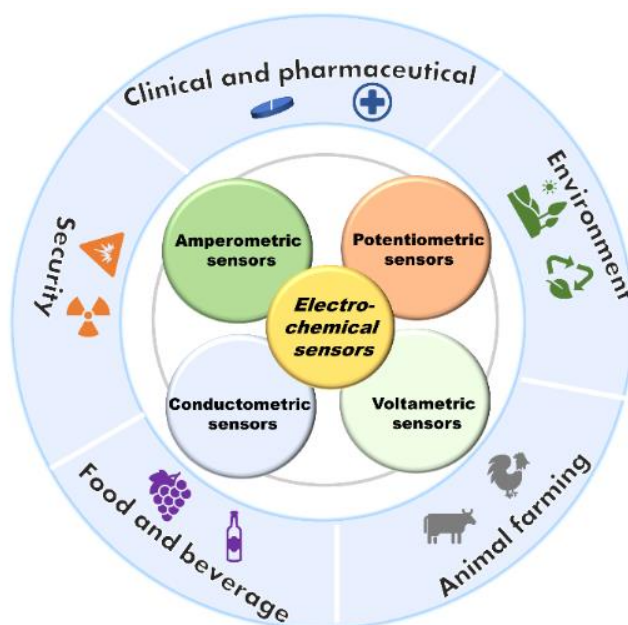


Figure 1.3 Graph of the classification and application of electrochemical sensors.

**Potentiometric sensors:** they are ion-based sensors where a change of potential or charge accumulation could be measured. There are three main types of potentiometric sensors that based on ion-selective electrodes, coated wire electrodes and field effect transistors, respectively.

**Amperometric sensors:** they literally and generally refer to a kind of sensors, in which the current changes with potential. However, the potential could be constant or controlled by a certain variation. Here, the narrow sense was taken, that means the



applied potential is fixed.

**Voltammetric sensors:** as described above, if the current varies with the potential that controlled by a certain variation, this kind of sensors are coined as voltammetric. There are two ways of determining analytes, i.e., a direct way when the target analyte is electroactive and an indirect way when the target analyte is non-electroactive, in which a redox probe is needed. No matter what way is employed, the measured current values is from electrochemical reactions and have an analyzable relationship with the concentration of the corresponding analyte.

**Conductometric/Impedimetric sensors:** they realize the goal of analysis by evaluating the change of conductive properties, such as capacitance and impedance. Although not as common as the previous ones, they are also indispensable. For instance, the most common conductometric sensors based on electrochemical impedance spectroscopy are often used to the analysis of non-electroactive analytes.

### **1.1.2.2 Application and development**

As illustrated in Figure 1.3, due to the incomparable advantages, ECSs have been widely applied in many sectors, for example, detecting metabolites, biomarkers and drug formulations in clinical and pharmaceutical industry, sensing explosives in security, resolving pollutants in environment, detecting the veterinary drug residues in animal husbandry, and monitoring the safety of food and beverage, etc.

A representatively tangible example for proving both practicability and general developing trend of ECSs is glucose sensor. Figure 1.4 graphically illustrates the evolution of glucose sensor. Since the initial concept of glucose enzyme electrodes was firstly proposed in 1962, glucose sensors have gone through four generations of upgrading from the earliest colorimetric sensors to the latest non-invasive ECSs, with less set-up complexity, less demanded amount of blood sample, easier operation procedure, increasingly improved accuracy [18]. More importantly, as the emerging of the novel wearable glucose sensors, continuous glucose monitoring has been achieved

and already commercialized, which proves such a great boon to so many diabetics. Nevertheless, the exploration of non-invasive glucose sensors is still going on and its' full commercialization are widely anticipated with large expectation [19-21].

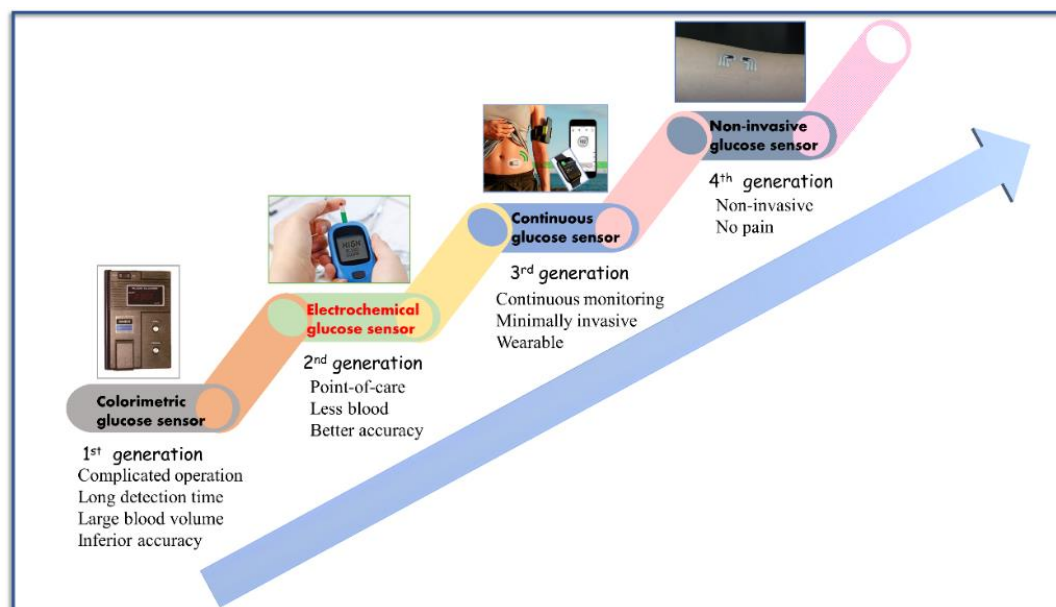


**Figure 1.4** The graphical illustration of the evolution of glucose sensor.

By investigating the evolution of glucose sensor, several important aspects in the upgrading process of ECSs could be concluded. First, the use of various recognition elements facilitates the improved performance of detection. Second, the development of electrode materials provides the better platforms for electrochemical reactions. Last but not least, the advancement of microelectronics makes it possible that devices are handheld, communication-enabled, flexible, and even non-invasive. However, even though the great breakthroughs have been witnessed in the development of ECSs, the drawback that the conventional ECSs are always singly targeted in most cases cannot be neglected.

### 1.1.3 Chemical sensor arrays

For conventional chemical sensors, there are two approaches of achieving its selectivity. The one is choosing a specific receptor for the target analyte, while the other is through a specific transduction process, for instance that the ionic effects lay the foundation for the selectivity of pH electrodes [22]. These specific approaches are well fit on the condition that the background and interferences can be controlled. However, it is not the case in real scenarios, so that conventional chemical sensors have limitations in practical use [23-26]. First of all, due to the non-ideal specificity of receptors, sensors may suffer from low-efficiency for targeting single analyte and hardly achieving simultaneous multi-analysis. Indeed, there is another potential possibility: the specific recognition mechanism could be degraded due to the presence of coexisting competing species that have chemical and structural similarity to the target analyte. Besides, certain matrices such as biological and medical samples have highly complex compositions, where the above situations may occur. Moreover, designing recognition elements for unknown compounds or analytes with uncharted structures might be unattainable. An alternative for solving these issues is the array-based approach.

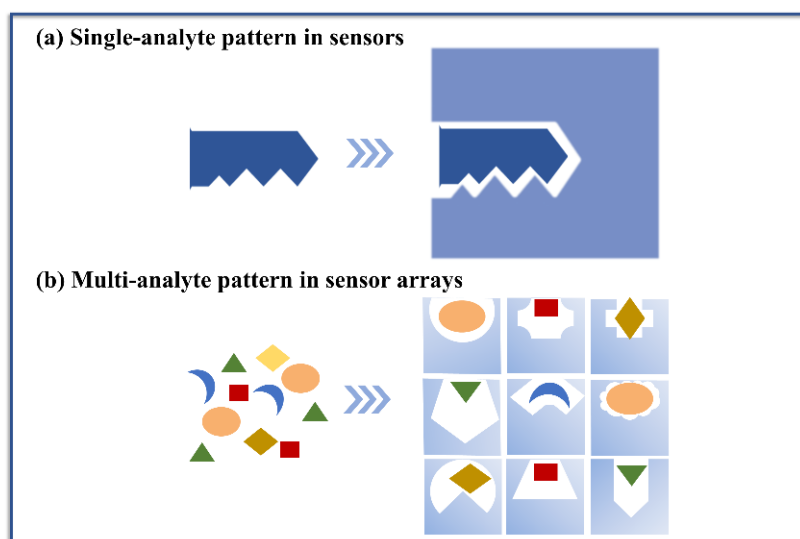


**Figure 1.5 (a) Single-analyte recognition pattern in conventional specific sensors, and (b) multi-analyte recognition pattern with cross-reactivity in sensor arrays.**

Chemical sensor arrays are composed by a collection of chemical sensors with partially selective or non-selective receptors that produce cross-reactive responses to a group of analytes. In conjunction with multivariate statistical techniques, a unique fingerprint response for particular analytes can be provided. The emerging sensing arrays are complementary to conventional chemical sensors in following aspects. Above all, it is not subject to the constraint of high specificity when designing or selecting receptors. Secondly, the array-sensing methods could distinguish minor changes in complex mixtures, facilitating simultaneous multi-analysis of structurally similar compounds. Thirdly, it could largely overcome the impacts of interferences and matrix effect.

Over the past decades, various chemical sensor arrays have been exploited for the applications in various areas, among which optical and electrochemical sensing array are the most common ones [23, 26-29]. For example, Lin and his co-workers reported the identification of volatile organic compounds (VOCs) by a colorimetric sensor array [30]. Elizabeth New's group detected toxic heavy metal in environmental water sources and platinum-based anticancer drug in blood plasma samples using fluorescent sensor arrays [28, 31]. As mentioned in *Section 1.1.2*, electrochemical methods have the merits of easier operation, lower-cost and less time-consuming, that are also popular for building sensor arrays. For example, as early as 1986, there was a report about the detection of hazardous gases and vapors by an electrochemical sensor array [32]. More recently, Alam et al. developed a fully integrated electrochemical sensor array for water quality monitoring [33]. In addition, the existing research line in our laboratory has made some contributions in the field of electrochemical sensor arrays [34-39].

## 1.2 Electronic tongues

### 1.2.1 Taste system: from biological to artificial

#### 1.2.1.1 Biological taste system of mammals

Feeding behavior is the ultimately survival base of almost all live forms. As a dominant regulator and driver of feeding behavior, gustatory system is responsible for the detection of nutrient and harmful substance in food and drink, and then triggers the decision making if they can be accepted or rejected. After the endeavor of researchers, the recognition mechanism of gustatory system of mammals has been well studied.

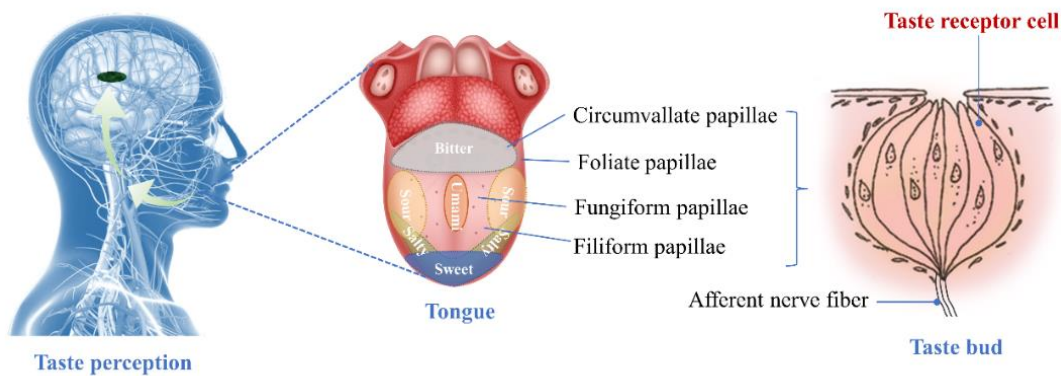


**Figure 1.6 The structure and work principle of gustatory system.**

Taste buds, housed in the various papillae of tongue epithelium, are the crucial units for recognizing a battery of different tastes primarily including sweet, salty, sour, bitter and umami, each of which consists of 50-100 tightly packed taste receptor cells (TRCs) [40, 41]. TRCs could be classified into three types (namely types I, II, and III cells) and since each of them has such distinct structural features, protein markers and function respectively, that they can get involved into different tastes' recognition [42]. Concretely, types I and III TRCs take part in the detection of salty and sour taste while types II TRCs play role in detecting sweet, bitter and umami taste. There are taste receptors (TRs) on TRCs sharing structural features and transduction principle that

involves ionic channels, such as  $\text{Na}^+$  and  $\text{K}^+$  channels, and metabotropic receptors mainly containing membrane proteins. It is TRs that make the recognition of tastes possible because of the unique interaction between receptor and taste molecules, and offer the unique selectivity for mammals' tongue. As shown in Figure 1.6, when the interactions between receptors and taste molecules occur on the tongue, the generated signals are transduced to the brain where the signals are processed and interpreted by nets of neurons to originate the taste perceptions.

### **1.2.1.2 Electronic tongues**

Being inspired by biological gustatory system and benefiting from modern achievements of neural computing, an artificial tongue was proposed and presented by Vlasov, as electronic tongue (ET) [43, 44]. According to a technical report from IUPAC, an ET refers to an analytical tool that integrates an array of a certain number of nonspecific, low-selective, chemical sensors with high stability and cross-sensitivity to different species in solutions, and chemometric methods of pattern recognition and/or multivariate calibration for qualitative and/or quantitative analysis [43]. As crucial as the role that TRCs play in mammals' taste system, sensor arrays are also significant centers in ETs. As it has been discussed in *Section 1.1.3*, in comparison with single sensor, sensor array could provide wide and complete response to targeted analytes that doesn't need to be high selective, but be reproductive and cross-sensitive. Mimicking the signal processing by brain, using chemometric method could reduce the complexity of original data produced by sensor array effectively, plus extract and interpret meaningful information from the recorded responses.

There are various measuring methodologies used in ETs that mainly includes optical methods, such as fluorescent and colorimetry, electrochemical methods, such as potentiometry, amperometry and voltammetry, and mass-change sensing methods [45]. For different measuring methodologies, sensing materials for constructing ETs may be different. For example, in the earlier stage, chalcogenides and oxides were used in

potentiometric ETs while noble metals were used in amperometric ETs [43]. With the development of nanomaterials, more and more novel sensing materials were exploited. Among them, there are some biological elements (such as, enzymes) to build bio-ETs that have specific binding activities, which is not identical to the initially proposed concept of ETs but improves the performance [46-48]. Besides, other elements with specificity also were fruitfully applied to construct applicable ETs, such as MIPs [49-52].

Compared with conventional sensors, ETs not only allow simultaneously qualitative and quantitative multi-analysis for several targeted components, but also improve the detecting abilities in the terms of decreasing LOD and enhancing reproducibility [53]. By providing fingerprints for analytes, ETs achieve the qualitative goals of distinguishing, identification and classification. Besides, ETs can distinguish unknown components even if there is no preliminary information. On the other hand, by building the proper response models, ETs can quantitatively analyze the concentration of targeted components.

## **1.2.2 Data processing and chemometric tools**

### **1.2.2.1 Data processing**

As it has been mentioned, given the sensors in ETs show cross-sensitivity to more than one analyte, sensor arrays tend to produce large and complex readings that need to be processed by appropriate chemometric methods. Generally speaking, there are three concrete steps in data processing, i.e., weighting, data pre-processing and modeling [54].

First, the purpose of weighting is to ensure the quality of the recorded data. To this end, a data-centering and/or normalization should be conducted before modeling, using the strategies including centering, standardization, normalization or auto-scaling of the data. Second, data pre-processing is for the purpose of data compression and reducing the high dimensionality of data, which may involve methods, such as Principal

component analysis (PCA), fast Fourier transform (FFT), discrete wavelet transform (DWT) and so forth. Third, chemometric tools vary from qualitative aim to quantitative aim, and each of them has their own pros and cons, that decides if they can be selected or combining used properly. Methods including PCA, linear discriminant analysis (LDA), canonical variate analysis (CVA), support vector machines (SVMs) have been attempted for qualitative analysis while others containing ANN, multiple linear regression (MLR), principal component regression (PCR), partial least-squares regression (PLS) and multiway partial least-squares regression (nPLS) are mainly applied for quantitative analysis. PCA and ANN are used as main modeling tools in this thesis, which will be introduced in details as following, respectively.

### 1.2.2.2 Principal component analysis

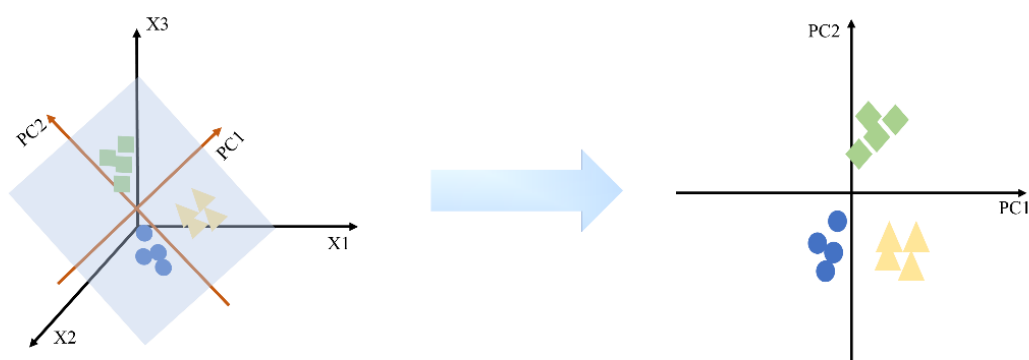


**Figure 1.7 Schematic diagram of data transformation in PCA method.**

PCA is a static method that transforms a set of potentially correlated variables into linearly uncorrelated variables. The obtained new variables are named as principal components (PCs). By PCA, the dimensionality of dataset can be reduced and its interpretability increases with the minimum information loss and the maximum variability [55].

PCA is related to matrix in mathematics. For an original matrix  $X$ , it can be recalculated by two new matrices with lower dimensionality as  $X=TP^T$ , where  $P$  is about



the transformation in the direction and  $T$  is about the coordinate in a new direction. Therefore, essentially, PCA is the operation of changing the direction of axis and setting the variable with maximum variation as the first axis [56]. As can be seen in Figure 1.7, the original data can be summarized in PC1 and PC2 with PCA, by which several distinguished clusters are obtained. PCA is a simple tool that allows the evaluation and visualization of (dis)similarity, but it cannot provide classification if without using a modeling tool, such as LDA, SVM or ANNs [54].

### 1.2.2.3 Artificial neural network

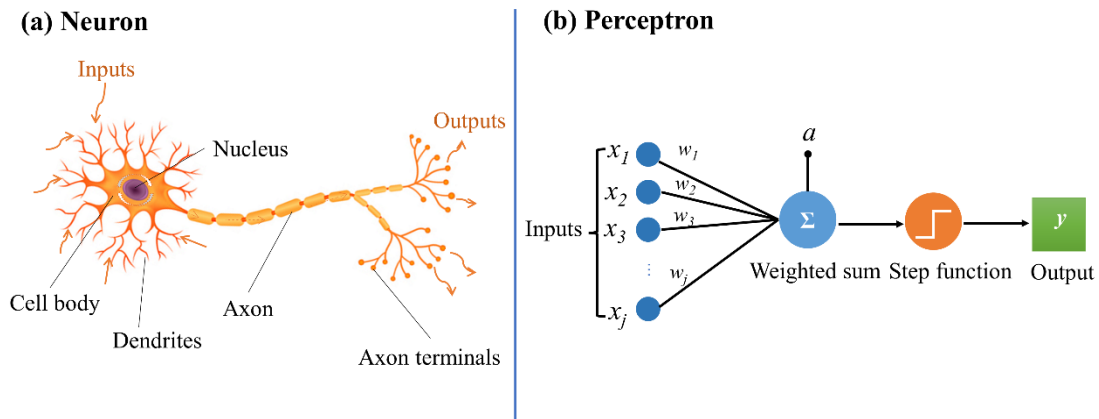


**Figure 1.8** The comparative juxtaposition of the structures and signal processing of (a) a neuron and (b) a perceptron.

It is known that the work principle of biological nervous system has been revealed. In short, as shown in Figure 1.8a, the input signals are transmitted through the dendrite to the cell body where the input signals can be processed, and then transmitted to other neurons through the synapse at the front of the axon. It is through synaptic associations that neurons build neural networks.

Artificial neural network (ANN) is such a chemometric tool that simulates the signal processing of the biological nervous system. As an analogy to neuron, perceptron is seen as the basic unite in ANNs, and Figure 1.8b describes the construction and signal processing of perceptron. Above all, several inputs from  $x_1$  to  $x_j$  are multiplied by their

respective weights from  $w_i$  to  $w_j$ , leading to the weighted values. Then, with a bias  $a$  introduced, a total weighted sum can be calculated by adding those weighted values up. Subsequently, a proper step function is required to produce output  $y$ . It is the association of perceptrons shapes the final configuration of ANNs (Figure 1.9a) in a way that neighboring perceptrons form layers including input layer that provides input information, hidden layer that computes the model, and output layer gives results.

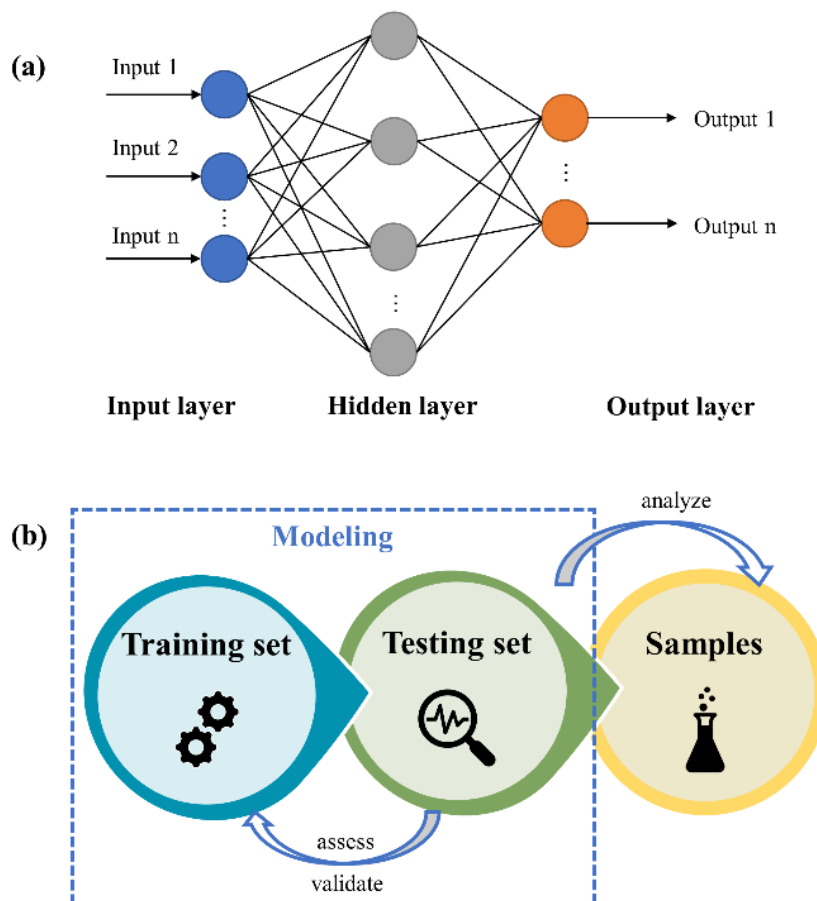


**Figure 1.9 (a) The scheme of the configuration of ANN made up of multi-layered perceptrons, (b) different datasets in ANN's modeling.**

The well-training of ANN actually requires some necessary steps. First is the data preprocessing for input data to overcome the imbalance among them. Then, on the condition that the number of input and output perceptron are known, trial and error can be attempted in order to confirm the amount of perceptrons in the hidden layer, which means decreasing from a large number gradually until a best model is obtained. Besides,

the transfer functions in these layers are vital for adjusting model that keep the same in one layer but differ between layers. For example, the input layer can use *purelin* while the saturated linear function (*satlins*) tends to be used in the output layer due to its linear correspondence. Compared to the input and output layers, the hidden layer is more complicated and sigmoidal transfer functions are recommended, such as, *logsig* and *tansig*.

As a modeling tool, the modeling process of ANN is commonly performed with two datasets: training subset and testing subset. The former generates a model, and the latter is for assessing and validating the model's performance. The well-constructed ANN model could be applied to the determination of samples, so being widely considered as a promising tool in usage of sensor arrays (Figure 1.9b).

### **1.3 Molecularly imprinted polymers**

Molecular imprinting refers to “the construction of ligand selective recognition sites in synthetic polymers where a template (atom, ion, molecule, complex or a molecular, ionic or macromolecular assembly) is employed in order to facilitate recognition site formation during the covalent assembly of the bulk phase by a polymerization or polycondensation process, with subsequent removal of some or all of the template being necessary for recognition to occur in the spaces vacated by the templating species” [57]. Since Polyakov serendipitously utilized molecular imprinting technology (MIT) in silica-based matrices in 1931, the concept of the molecular imprinting was firstly proposed. Afterwards, the theory about the formation of antibodies and the mechanism of its selectivity were put forward by Linus Pauling and other scientists in 1940s. It was suggested that antibody forms in the presence of antigen that acts as a template and it is the template-induced conformational effect that facilitates the amazing selectivity for antibodies, which is also regarded as the instructional theory for molecular imprinting [58]. By 1972, Wulff and Klotz pioneeringly shifted MIT from silica to organic polymers, respectively, so that

molecularly imprinted polymers (MIPs) were produced [59, 60].

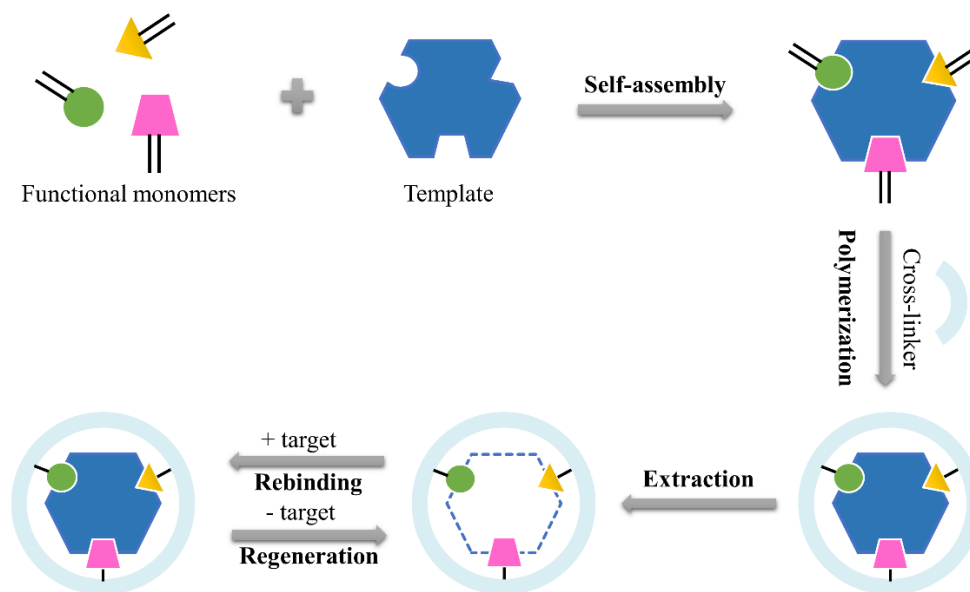


**Figure 1.10 Graphical representation of the formation of MIP.**

By mimicking the specific recognition mechanism between antibody and antigen, MIPs are figuratively called as “plastic antibodies”. On the one hand, MIPs are known as a kind of artificially tailor-made polymeric matrix comparable to natural antibodies because of the specific binding sites that are complementary to the size, shape, and functional groups of the template molecules, as shown in Figure 1.10, which are obtained via copolymerizing the functional monomers in presence of templates and then removing them, resulting in imprinted sites [61, 62]. On the other hand, MIPs not only have some attractive advantages that avoid some inevitable limitations of natural antibody, such as chemical and thermal stability, physical robustness and remarkable reusability, but also can be easily synthesized with low-cost.

After the continuously ongoing endeavor of scientists in the past decades, the full-blown development of MIP’s design, synthesis and application has been witnessed [57, 61-65].

## 1.3.1 Synthesis and polymerization

### 1.3.1.1 Elements in polymerization

#### ○ Templates

Templates in MIPs can be the targeted compound or structural analogues of the targeted compound. Combining the existing theoretic and practical knowledge, it can be concluded that the templates that can be effectively imprinted into polymers should meet following basic conditions. First, the template itself is required to be stable enough during the polymerization reactions that may undergo a longstanding high temperature. Second, the template cannot impede the process of polymerization reaction. Third, it has to structurally contain one or more groups that can assemble with functional monomers.

So far, various templates have been used for MIPs synthesis, from small molecules and inorganic ions to macromolecules, such as proteins, even to living cells. Several critical reviews discussed and summarized different imprinted templates in details [63, 66-71].

#### ○ Functional monomers

Functional monomers play an important role in offering functional groups, interacting with templates, and forming an imprinted polymeric complex. Therefore, selecting an appropriate functional monomer is a crucially key step. Besides, the optimal molar ratio of function monomer to template has impacts on the performance of MIPs. In this regard, trial-and-error method is frequently committed. Compared with tedious and laboratory trial-and-error tests, computer simulation might be a good alternative, that has been regarded as a promising tool for designing and selecting proper type and amount of functional monomer.

There are some typically used functional monomers for molecular imprinting including some mainly for radical polymerization, such as methacrylic acid, acrylic acid,

2- or 4-vinylpyridine, acrylamide, trifluoromethacrylic acid and 2-hydroxyethyl methacrylate, and the others mainly for electropolymerization, such as pyrrole, aniline, phenol, and their derivatives. In recent years, efforts have been made for the purpose of seeking some new functional monomers and improving traditional monomers. For instance,  $\beta$ -cyclodextrins has attracted attention as a novel promising monomer due to its special structural characteristics with a hydrophilic exterior and a hydrophobic inner cavity [72]. And bio-sourced chitosan is also innovatively used for imprinting polymers due to its excellent properties [73].

### ○ Crosslinkers

Crosslinkers help to form extremely cross-linked rigid polymer in three terms [74]. First, it immobilizes the imprinted templates with the functional groups of monomers, which results in stable binding sites. Second, it plays important role in controlling the morphology of MIPs. Third, it can enhance the stability of the synthesized polymer. Thus, similar to functional monomers, both the kind and amount of crosslinker need to be optimized due to their profound impacts on MIPs' selectivity and binding capacity. Examples of widely used crosslinkers include divinylbenzene, ethylene glycol dimethacrylate, N, N-methylenebisacrylamide and trimethylolpropane trimethacrylate. The amount of crosslinkers should be enough for ensuring the structural stability of MIPs. Conversely, the excessive amount of crosslinker may lead to the decrease of binding sites. Nevertheless, it is noted that as the exploitation of novel synthesis methods and functional monomers, crosslinker may be not mandatory during the polymerization, which saves the reagents and some optimization steps.

### ○ Initiators

In free radical polymerization, initiators are used as the radical source with a relative low amount compared with monomers [74]. By means of heat, light or chemical/electrochemical way, initiators can be decomposed to radicals with the controlled rate and mode. One of typical example of initiators is azobisisobutyronitrile, which is often used for initiating the polymerization vinyl monomers.

### ○ Porogenic solvents

Porogenic solvents serve as dispersion media and pore forming agents in the polymerization reactions [62]. The polarity of solvents has an impact on the interactions between templates and monomers, especially for non-covalent interactions. Particularly, to obtain a better imprinting efficiency in non-covalent imprinting, the solvents with non-polarity and less polarity are usually utilized. Acetonitrile, chloroform, dichloroethane, N, N-dimethylformamide, 2-methoxyethanol, methanol, tetrahydrofuran, toluene and so forth are popular to be used in polymerization.

#### 1.3.1.2 Imprinting approaches

Between functional monomers and templates, there might be one or more interactions, graphically introduced as Figure 1.11. According to the type of interaction, imprinting can be categorized into covalent imprinting, non-covalent imprinting, semi-covalent imprinting and ionic imprinting.

Covalent imprinting was introduced by Wuff, representing that templates are covalently anchored in polymeric matrix followed the production of recognition site by the cleavage of covalent bond, and templates rebind with binding sites also via the reestablishment of covalent bonds. In this approach, the functional groups only strongly interact with the template sites and homogeneously distributed binding sites are produce. However, it is only applicable to imprint confined compounds that can form covalent linkages, such as carboxylic acids imprinted by carboxylic esters linkage, amine or aldehyde imprinted by using Schiff's base, and diols and carbonyl compounds imprinted by reversible ketal bonds. Besides, the drawbacks that the formation of covalent bonds needs high formation kinetics and the rebinding process by reestablishment covalent bonds is time-consuming hinder its wide application.

Non-covalent imprinting was proposed by Mosbach [75], in which both the formation and reestablishment of the interactions between templates and monomers are non-covalent including Van der Waals' force, hydrogen bond, ion-paring and dipole-

dipole interactions. The removal of templates does not need the destruction of chemical bonds, which is easy to be operated and prevents the structural collapse of MIPs. Compared with covalent imprinting, the non-covalent imprinting is more flexible, more universal and easier. Therefore, it is the widest method for imprinting.

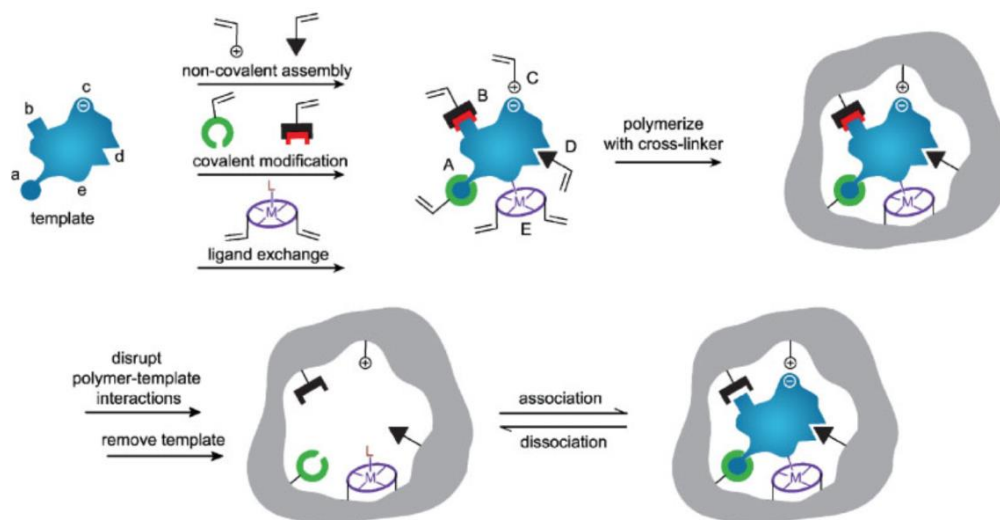


**Figure 1.11** Schematic representation of different interactions between functional monomers and templates [57].

Except for the former mentioned imprinting approaches, there is a mixed one combining covalent and non-covalent interactions, namely, semi-covalent imprinting introduced by the group of Whitcombe. The templates are covalently associated with monomers' functional groups and rebound with binding sites by non-covalent interactions, which contributes to the higher affinity, the more uniform distribution of sites and the easier rebinding process without kinetic restrictions. What's more, as an imprinting approach for imprinting metal ions, that ionic imprinting allows that the cross-linking of polymers containing functional groups with metals [57].

### 1.3.1.3 Polymerization methods and imprinting strategies

Generally speaking, according to the mechanism of MIPs' formation, polymerization methods can be mainly grouped into two broad categories: free radical polymerization and sol-gel polymerization [61]. Free radical polymerization methods



are widely popular and include bulk polymerization, suspension and emulsion polymerization, and precipitation polymerization. Bulk polymerization is a conventional and common method for synthesizing monolithic MIPs, properly appreciated for the simplicity in operation and the low production cost. However, the resulting bulk polymers need to undergo the mechanical grinding and sieve to obtain the desired MIPs particles, which can give rise to the loss of binding sites and low yield [76]. Precipitation polymerization, suspension and emulsion polymerization are similar to bulk polymerization, but produce spherical MIPs. Since the posttreatment of grinding and sieving are not required, precipitation polymerization reduces the likelihood of tampering with the binding sites. Besides, in precipitation polymerization, the uniform size of MIPs particles can be adjusted and controlled by changing the reacting conditions. Compared with other methods, suspension and emulsion polymerization have the merit of increasing the dispersity of polymers by utilizing surfactants, but concurrently introduce the problem of surfactants remnants.

Although the aforementioned polymerization methods of synthesizing MIPs have been constantly studied and greatly improved, the limitations of these classical methods are still inevitable. For instance, there is a typical problem related to the incomplete removal of template in classical polymerization methods, shown in Figure 1.12a. In addition, template leakage and the resultant MIPs' irregular shape and incompatibility with aqueous media also happen on occasion. These issues impede the potential application of MIPs, thus more smart and advanced imprinting strategies have been attempted, including surface imprinting, nanoimprinting, multi-template and multi-functional monomer imprinting, dummy imprinting strategy, etc. [62, 77-80]. Among them, surface imprinting is attractive for allowing the MIP's direct combination with various nanomaterials, extensively improving MIP's performance. For example, comparing with Figure 1.12a, Figure 1.12b presents the more thorough extraction of templates and more efficient sites binding via surface imprinting. Electropolymerization is one of the frequently used methods based on surface

imprinting strategy. To provide a more detailed insight, electropolymerization method will be later introduced in depth. For the purpose of comparing, it is contained in the summary of various polymerization method, as shown in Table 1.1.

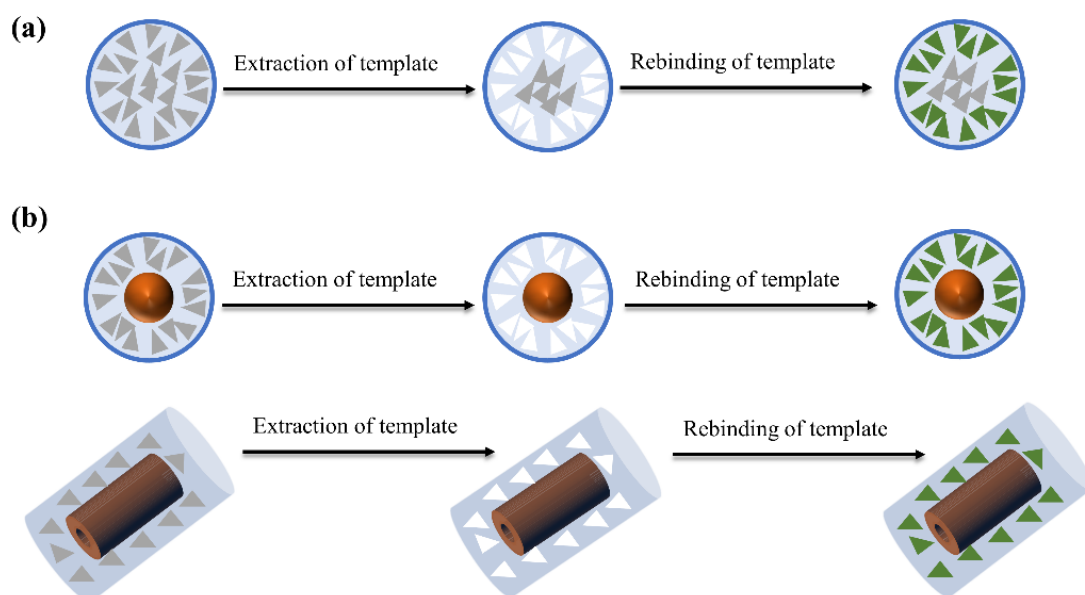


**Figure 1.12** The representative comparison of the extraction and rebinding of template in (a) classical polymerization methods and (b) surface imprinting strategy.

**Table 1.1** Summary of various MIP's polymerization method.

Polymerization methods	Advantages	Disadvantages
Bulk polymerization	universality, operation simplicity, low production cost	tedious posttreatment procedure, irregular MIPs particle, low yield, loss of binding sites
Suspension and emulsion polymerization	increase mono-dispersity, high yield, water-soluble polymers	surfactant polymers required, surfactant remnant, big particle size
Precipitation polymerization	free of surfactant, uniform and controllable MIPs size	irregular MIPs shape, high dilution factor
Electro-polymerization	simple and fast, controllable polymeric films, high reproducibility, easier removal of template	unsuitable for large applications

## 1.3.2 Electropolymerization of MIPs

### 1.3.2.1 Electropolymerization method

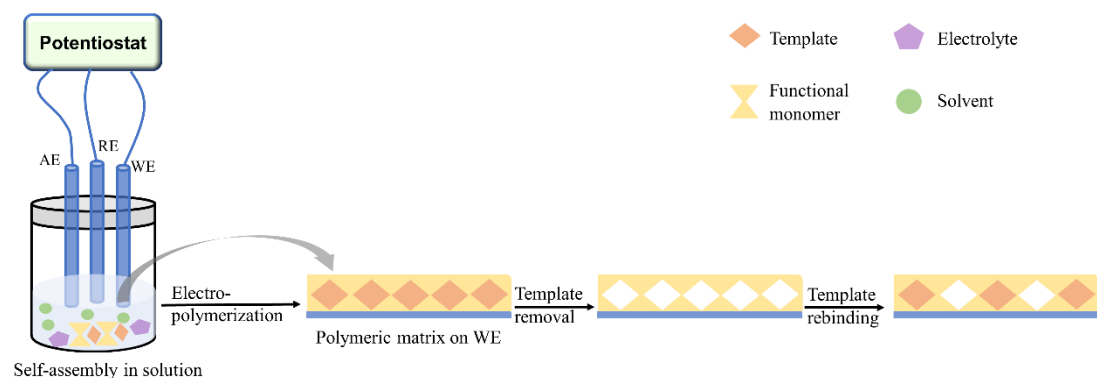


**Figure 1.13 Schematic illustration of the formation of MIPs film using electropolymerization method.**

Obtaining MIPs by electropolymerization allows a direct deposition of polymeric films onto electrode surface, facilitating constructing chemosensors and biosensors. Most of electropolymerization process involves anodic oxidation reaction, which is carried out in a classical three-electrode system in the presence of functional monomer, template, supporting electrolyte and solvent [81]. Figure 1.13 demonstrates how the MIPs film forms using electropolymerization method. First, the template and functional monomer self-assemble in solution via the non-covalent interactions. And the self-assembling complex not only can be remained in the electropolymerization process, but also further form a thin film of polymeric matrix due to the copolymerization of template and functional monomer on the surface of work electrode. Then, the specific sites are obtained by the removal of template, which can be performed by electrochemical or chemical means. In order to achieve electropolymerization, there are three primary optional techniques, i.e., potentiostatic, voltammetric and galvanostatic [82]. Chief among them is cyclically voltammetric electropolymerization, in which the

functional monomer goes through the redox reaction and produce a polymeric film with trapped template. By setting proper parameters including potential range, scan rate and cycle number, the thickness and morphology of MIPs film can be well controlled. In contrast, potentiostatic and galvanostatic induce electropolymerization via imposing a fixed potential or a constant current on the electrode, respectively, and the MIPs film can be tuned by changing potential or current.

Compared with conventional polymerization methods of synthesizing MIPs, for instance free radical polymerization, it can be seen that electropolymerization method doesn't require initiators and crosslinkers, even no need for organic solvents, allowing the easier and faster preparation in aqueous and producing cleaner electropolymerized MIPs (eMIPs) [81, 82]. In addition to the controllable thickness and morphology of MIPs film, its structural rigidity and porosity also can be adjusted by changing supporting electrolyte or entrapped counterions [82]. When there is the requirement of building sensors, the eMIPs are superior because of its direct and robust adherence to the surface of transducers rather than post drop casting or spin coating, as needed by conventional synthetic protocols.

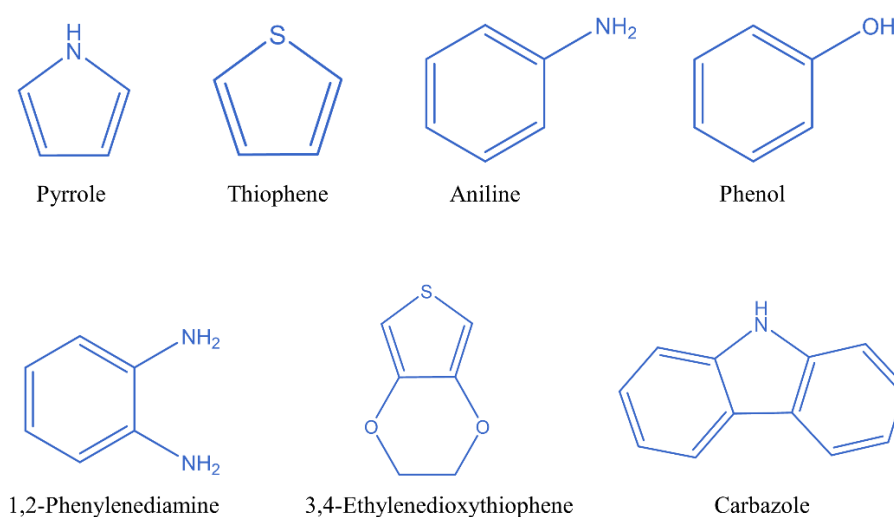


**Figure 1.14 Molecular Structures of the most commonly used functional monomers for eMIPs.**

As previously introduced in *Section 1.3.1.1*, functional monomers should meet some generally necessary requirements. In terms of the selection of functional monomer, in addition to meeting the necessary conditions, electropolymerization methods are more inclined to electroactive functional monomers than non-electroactive ones. In Figure 1.14, it exhibits the molecular structures of the most frequently used functional monomers in electropolymerization methods. Pyrrole, thiophene, aniline and phenol are all the basic functional monomers that extensively reported [83-93]. Except for themselves, their various derivatives with specially functional groups have been also explored [94]. For instance, based on the structure of thiophene, 3,4-ethylenedioxythiophene (EDOT) has been proved to be suitable for large and small molecular imprinting, especially doping with poly (styrene sulfonate) (PSS) [95-98]. In order to optimize the morphology and improve the performance of eMIPs, great efforts have been made in the aspect of functional monomers. Apart from introducing new functional groups, the strategy of structural hybridization of different monomers also was attempted. Take carbazole as a typical example, itself is regarded as the combined derivative of pyrrole and aniline, but it also can be integrated with other monomers [99-101]. In addition, the use of dual monomers also acts as an effective means to improve the performance of eMIPs [78, 102].

Herein, it would not go into details about all kinds of functional monomers, and the introduction of the polypyrrole (PPy)-based eMIPs would be exclusively focused, as PPy is mainly used in this research work.

### **1.3.2.2 PPy-based eMIPs**

Among a number of various functional monomers, pyrrole (Py) is the most extensively studied one because of its remarkable intrinsic properties. Compared with other functional monomers, Py has superior advantages of the relatively low oxidation potential allowing the easier oxidation, the possibility to offer highly electrical conductivity and good solubility in both aqueous and organic solvents. The

electropolymerization of Py is the oxidation process on the surface of an electrode induced by an anodic potential. Although the mechanism of Py electropolymerization is intricate and still controversial to date, the mechanism proposed by Diaz is the most often cited that has been theoretically confirmed by Waltman and Bargon, which is described as Figure 1.15a. In short, it goes through a set of steps including the oxidation of monomer to obtain cation radical, the coupling of two cation radical to form dihydromer dication, the formation of aromatic dimer by the deprotonation of losing two protons, and the polymerization reaction by repeating the former three steps to produce PPy chain [103]. However, it is worthy to mention that the final produced PPy polymer is not electrically neutral, but averagely carrying a positive charge in every 3 to 4 pyrrole units. Therefore, as shown in Figure 1.15b, PPy is actually doped with counter-ions that come from the supporting electrolyte in order to keep its electrical neutrality [103].

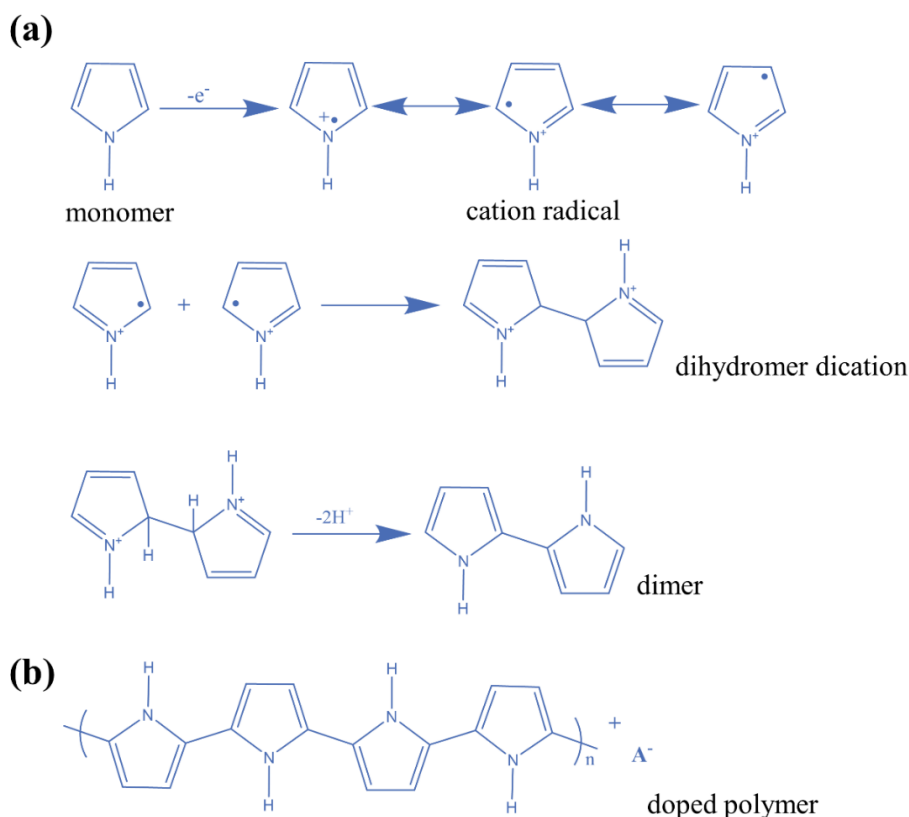


**Figure 1.15 (a) The different stages in the polymerization of pyrrole, (b) the structure of the doped PPy where A represents the doping anion.**

The intrinsic properties of PPy-based eMIPs (e.g., conductivity and morphology) are not only influenced by the parameters of electrochemical techniques, but also depend on the electropolymerization conditions, such as the kind of supporting electrolyte, solvent, the ratio of Py monomer to template, etc.

As described in the introduction of the mechanism of pyrrole polymerization, it is essential that the anions are doped into polypyrrole chains. Thus, the supporting electrolyte plays a vital role in the electropolymerization of pyrrole. Both inorganic and organic anions can be used as doping counter-ions, but its anionic potential must be higher than that of pyrrole. Typically, the anions doped into PPy-based eMIP are some small-sized inorganic anions, for instance, the most frequently used perchlorate anion. However, according to the reported literatures, anions with different sizes have different impacts on the polymerization of pyrrole [104-106]. There are also organic anions doped into PPy with a large size, such as polystyrene sulfonate ( $\text{PSS}^-$ ) and dodecylbenzenesulfonate ( $\text{DBS}^-$ ), and with a medium size, such as benzenesulfonate ( $\text{DS}^-$ ) and *p*-toluenesulfonate ( $\text{pTS}^-$ ). In contrast with inorganic anions, organic anions with an appropriate size such as  $\text{pTS}^-$ , favor the generation of more stable PPy with higher mechanical strength and conductivity in aqueous solution [107, 108]. Due to their surfactant properties, these organic anions have hydrophobic interactions with water so that they can be ordered along the polymer chain, which in turn increases structural order of polymers [107]. Besides, with benzene ring, some organic anions may be conjugated to the template, thereby enhancing the link between the polymers and the templates that leads to more imprinted sites. What's more, the solubility and nucleophilicity of supporting electrolyte also should be taken into account.

Solvent is another important factor that affects the performance of PPy-based eMIPs, which is dominated by the interaction between solvent and cation radicals[109]. First of all, solvents for pyrrole's electropolymerization should minimize the nucleophilic reactions, so aprotic solvents are preferred, for example, acetonitrile is frequently used [103]. Considering the dual characteristics of nucleophilic and

electrophilic nature, in order to obtain the desired mechanical properties and conductivity, aqueous solution can be suitable by adjusting the type and concentration of the added salt. The pH of the solution also has an influence on the performance of PPy-based eMIPs, which has been studied in the literatures [110, 111]. Although the electropolymerization can be improved in the low pH solutions, the over low pH may lead to low conductivity. Notably, the optimization of pH should be combined with the acid-base properties of the analyte templates [111].

In order to better visualize the conditions of MIPs prepared via electropolymerization using pyrrole as functional monomer, some parameters in recent literatures were summarized including template, the type of electrode, electropolymerization technique, supporting electrolyte, solvent, as shown in Table 1.2. From Table 1.2, it can be seen that PPy-based eMIPs are appropriated for the integration with different nanomaterials for imprinting a number of various templates, facilitating its potential applicability in many areas.

**Table 1.2 Summary of the parameters of MIPs prepared via electropolymerization using pyrrole as the functional monomer in recent publications.**

Template	Electrode material	Technique	Electrolyte /solvent	Ref.
<b>paracetamol</b>	PGE	CV	LiClO <sub>4</sub> /aqueous	[112]
<b>bisphenol A</b>	laser scribed graphene	CV	PBS/aqueous	[113]
<b>dibutyl phthalate</b>	PGE	CV	LiClO <sub>4</sub> /acetonitrile	[114]
<b>tramadol</b>	f-MWCNT/GCE	CV	LiClO <sub>4</sub> /aqueous	[115]
<b>butanethiol</b>	GCE	CV	PBS/aqueous	[116]
<b>nevirapine</b>	ERGO/ GCE	CV	PBS/aqueous	[117]
<b>gastrodin</b>	rGO/AgNPs/Ni foam	CV	PBS+KCl/aqueous	[64]
<b>dopamine</b>	MWCNT/GCE	CV	LiClO <sub>4</sub> /aqueous	[118]
<b>dopamine</b>	GQDs/TiO <sub>2</sub>	CV	LiClO <sub>4</sub> /aqueous	[119]
<b>domperidone</b>	ERGO/GCE	CV	LiClO <sub>4</sub> /methanol+water	[120]
<b>fisetin</b>	MXene/NH <sub>2</sub> -CNTs	CV	PBS+LiClO <sub>4</sub>	[121]



			/aqueous	
<b>methimazole</b>	PGE	CV	NaClO <sub>4</sub> /aqueous	[122]
<b>1,4-dihydroxy-anthraquinone</b>	MWCNT/GCE	CV	Britton–Robinson buffer+NaClO <sub>4</sub> /aqueous	[123]
<b>ascorbic acid</b>	exfoliated graphene/GCE	CV	LiClO <sub>4</sub> /aqueous	[124]
<b>bisphenol S</b>	hNiNS/GQDs/GCE	CV	LiClO <sub>4</sub> /acetonitrile	[125]
<b>dopamine</b>	ZnO nanotube/FTO	CV	LiClO <sub>4</sub> /aqueous	[126]
<b>sulfadiazine and acetaminophen</b>	GO@COF/GCE	CV	TBAP/ acetonitrile	[127]
<b>glyphosate</b>	PB-AuNP-ITO	CV	PBS/aqueous	[128]
<b>dopamine</b>	carbon aerogel electrode	CV	PBS/aqueous	[129]
<b>quercetin</b>	MIL-101 (Cr)/MoS <sub>2</sub> /GCE	Chrono-coulometry	H <sub>2</sub> SO <sub>4</sub> /aqueous	[130]

*CV*: cyclic voltammetry, *PGE*: pencil graphite electrode, *f-MWCNT/GCE*: functionalized multi-wall carbon nanotube/glassy carbon electrode, *ERGO*: electrochemically reduced graphene oxides, *rGO*: reduced graphene oxides, *AgNPs*: silver nanoparticles, *GQDs*: graphene quantum dots, *hNiNS*: hollow nickel nanospheres, *FTO*: fluorine doped tin oxide, *PB-AuNP-ITO*: Prussian Blue-gold nanoparticle-indium doped tin oxide

## 1.4 Electrochemical sensing based on MIPs

### 1.4.1 MIPs-based electrochemical sensors

From the description in *Section 1.3.1* and the summarized milestones in the development of MIPs in Figure 1.16, it is known that after conceptual foundation of MIT in 1931, MIPs were firstly synthesized in 1972 after the establishment of the guiding theory in 1940s. At the earlier stage, the application of MIPs-based materials was mainly focused on the field of separation and extraction. In recent decades, with the rapid development of the synthesis technology that greatly improved the performance of MIPs, MIPs were found to be fit for chemical sensing. The Mosbach's group in Lund pioneered the use of MIPs for electrochemical sensing in the 1990's. The bar chart in Figure 1.17 compares the number of publications regarding MIPs-based

sensors and MIPs-based electrochemical sensors from 2012 and 2021, which shows how both of them have been kept rising. Besides, especially in the recent years, the number of MIPs-based electrochemical sensors accounts for almost half of the total number of all kind of MIPs-based sensors, proving the superiority of electrochemical sensors and the vital importance of combining MIPs with electrochemical sensing.

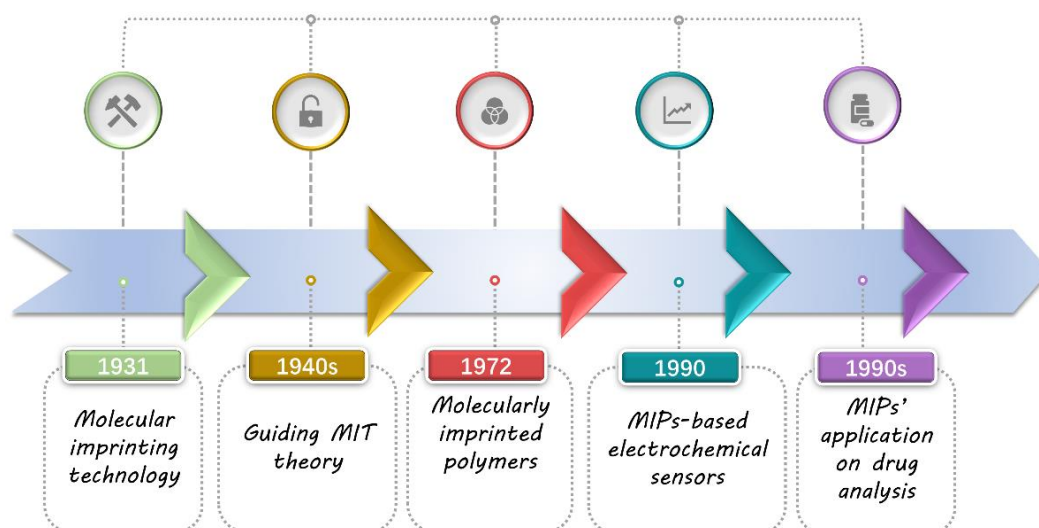


**Figure 1.16** Milestones during the development of MIPs and their application in electrochemical sensing.

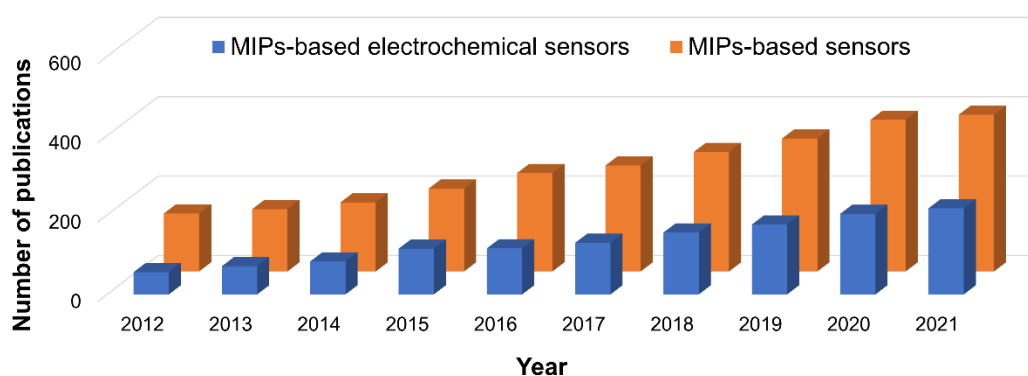


**Figure 1.17** Histogram representing the number of the reported publications during the last decade in the field of MIPs-based sensors and MIPs-based electrochemical sensors. (Data was taken from Scopus)

As previously introduced in *Section 1.1.2*, one of key points of electrochemical sensors (ECSs) is the successful integration of transducer and proper recognition element. Compared with natural recognition elements, such as antibodies, MIPs not only can be flexibly and artificially designed and synthesized, but also bear the good stability in harsh environments. In contrast with other nanomaterials, MIPs have the advantages of higher selectivity, simpler preparation at lower-cost. Particularly worth mentioning is the direct and stable adhesion of eMIP that may be accomplished on the surface of the transducer, which provides the possibility of the easier preparation and wider application of MIPs-based ECSs.

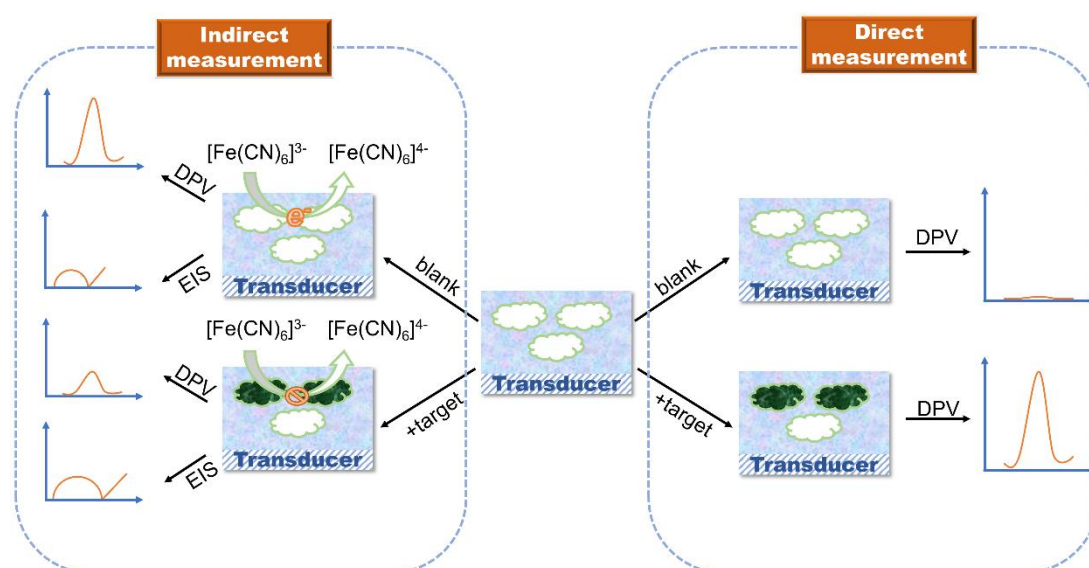


**Figure 1.18** Schematic graph of the detection mechanism of MIPs-based electrochemical sensors through direct and indirect ways.

The theoretical detection mechanism of MIPs-based ECSs is based on the change of electrical signals including current, potential and impedance that may be related to the concentration of analyte. For the practical measurement, MIPs-based ECSs mainly adopt voltammetry and electrochemical impedance spectroscopy (EIS), and the former includes cyclic voltammetry (CV), linear sweep voltammetry (LSV), differential pulse voltammetry (DPV) and square wave voltammetry (SWV). There are the direct way for electroactive compounds and the indirect way for non-electroactive compounds (Figure

1.18). In the indirect way, it relies on a “gate-controlled” mechanism and redox probes are needed, e.g.  $[\text{Fe}(\text{CN})_6]^{3-/4-}$ . As the entrapment of target in the imprinted sites, the mass and charge transfer impedance increase, showing the lower current peak in voltammetry and larger semi-circle in Nyquist plot. In the direct way, the rebinding of the electroactive analyte increases the electroactive signal in voltammetry.

## 1.4.2 Strategies to improve MIPs-based electrochemical sensors

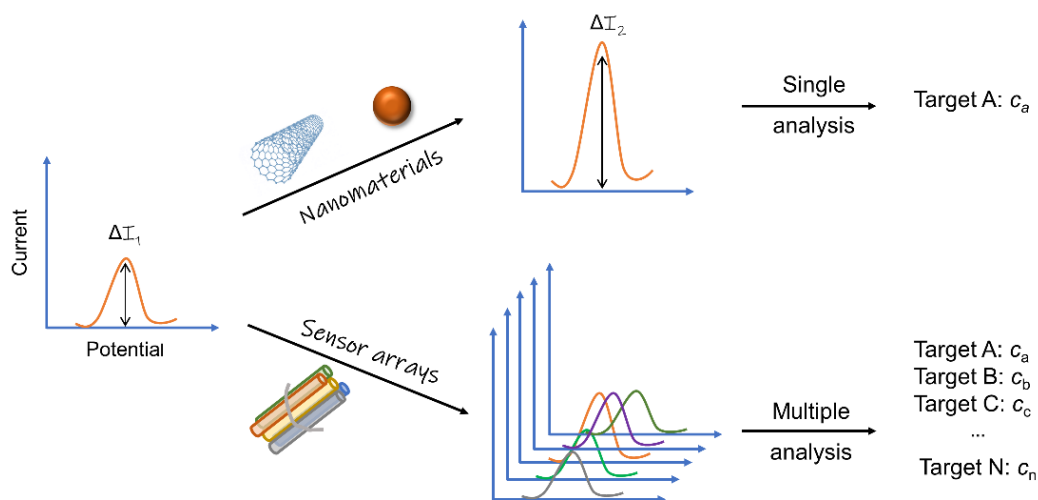


**Figure 1.19** A sketch of the two practical strategies to improve the performance of MIPs-based electrochemical sensors.

Indeed, MIPs are good candidates as recognition elements in ECSs, playing an important role in terms of selectivity. However, it is difficult for MIPs-based ECSs to transform the recognition events into analytical signals efficiently [131], due to the limitations in intrinsic properties including the poor conductivity and inferior electrocatalytic activity. In addition, the improper morphology of MIPs can lead to the problem of uneven distribution of imprinting sites and poor site accessibility for analyte. The sensitivity of MIPs-based ECSs bears the brunt of the described disadvantages. Thus, in order to improve the performance of MIPs-based ECSs, it is imperative to

propose some effective strategies. As presented in Figure 1.19, two practical routes are available, namely, coupling MIPs with nanomaterials from the standpoint of improving the electrode and integrating multiple MIPs-based ECSs into a MIPs-based sensor array, both of which would be discussed as follow.

### 1.4.2.1 MIPs' combination with nanomaterials

#### ○ MIPs' combination with carbon nanomaterials

In the past decades, carbon nanomaterials are at the forefront in the field of advanced materials research for their attractive merits of high conductivity, good mechanical and electronic properties, and low cost [132]. There are different types of carbon nanomaterials from zero-dimension to three-dimension (Figure 1.20), allowing the widespread applications in improving the performance of MIPs-based ECSs, such as carbon quantum dots (0D), carbon fibers (1D), carbon nanotubes (1D), graphene (2D), mesoporous carbon (3D), so forth [16].

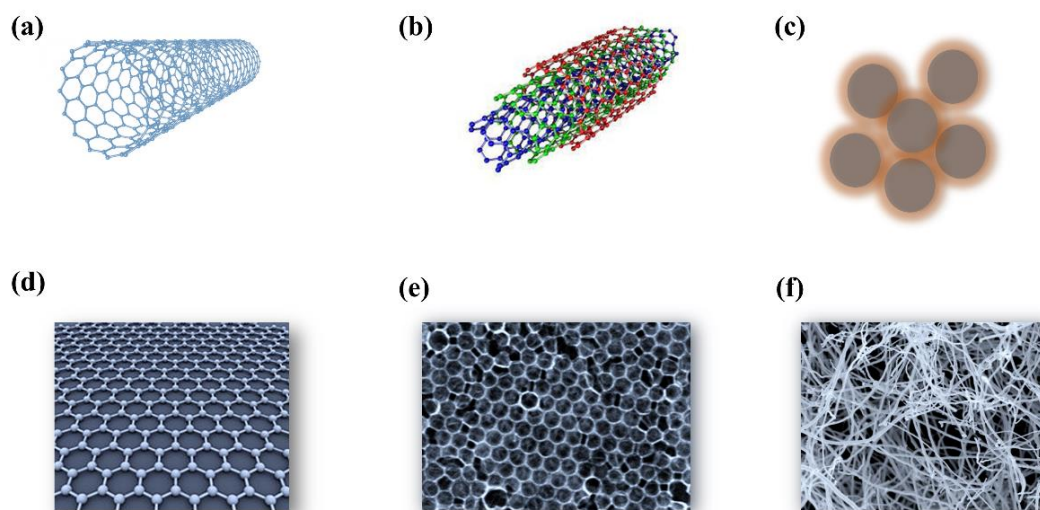


**Figure 1.20** The pictures of different types of carbon nanomaterials. (a) single wall carbon nanotube, (b) multi-wall carbon nanotube, (c) carbon quantum dot, (d) graphene, (e) mesoporous carbon, (f) carbon fiber.

Particularly, carbon nanotubes (CNTs) have unique physiochemical properties, fast electron transfer kinetics and large surface area, which may complement the disadvantages of MIPs. CNTs are classified into single wall carbon nanotubes (SWCNTs) and multi-wall carbon nanotubes (MWCNTs), whose structures can be observed in Figure 1.20a and b. The former is regarded as a cylinder of seamless  $sp^2$  carbon sheets, while the latter is made up of unstacked multiple layers of rolled carbon. The functionalization with amide or carboxyl groups endows MWCNTs unique features, making them have easier conjugation with MIPs and higher affinity to analytes. The incorporation of MIPs and MWCNTs in ECSs can involve three routines: polymerizing MIPs on MWCNTs, co-polymerizing MIPs with MWCNTs, and drop-casting or spin-coating MIPs on MWCNTs. In contrast with drop-casting or spin-coating, the other two ways may go through surface imprinting, in which the growth of MIPs occur upon the MWCNTs and produces the core-shell structures with more even imprinting sites, high efficiency for templates' removal, and much easier site accessibility for analytes. There are substantial reports regarding the use of MWCNTs in MIPs-based ECSs. For example, very recently, it was reported that the incorporation of MIP and the thiophene functionalized MWCNTs (MWCNTs-Th) has been attempted and used for the ultrasensitive detection of Chlorpyrifos in vegetables [133].

#### ○ MIPs' combination with metal-based nanomaterials

Diverse metal-based nanomaterials have been coupled with MIPs in ECSs because of excellent conductivity and catalytic properties. For instance, some typical metal oxides, sulfides and hydroxides were reported, such as ZnO [126],  $TiO_2$  [134],  $Ni(OH)_2$  [135]. Moreover, noble metal nanoparticles (e.g., AgNPs and AuNPs) are also included. Compared with many other metal-based nanomaterials, AuNPs could be prepared in a relatively facile and simple way, and the remarkable catalytic activity presented by AuNPs can compensate for MIPs. Besides, other characteristics of AuNPs are also attractive in ECSs, including chemical inertness, the fast electron transfer and good biocompatibility [15].

Except for carbon or metal-based nanomaterials, their multi-hybrid nanocomposites are also popular. It can be the hybrid of the same type of nanomaterials like CNTs and graphene, or different kinds like CNTs and AuNPs. In a word, the reasonable designs of MIPs combining with nanomaterials can effectively improve the performance of MIPs-based ECSs.

#### **1.4.2.2 Integration into MIPs-based electrochemical sensor array**

Although the sensitivity of MIPs-based ECSs can be boosted by improving electrode materials through the combination of MIPs and nanomaterials, there are still some issues to be dealt with in real world scenario. For one aspect, it is generally acknowledged that MIPs have distinguished specificity to the template or the species that are structurally similar to the template. When it is used in real applications, the complex detecting matrices may contain some interferences that cannot be differentiated from target analyte by MIPs, which has negative impacts on the analyzed results. For another, the advantages of specificity can be a double-edged sword, that hinders the multiple analysis of a family of structural analogues [136]. In order to solve the above two problems, another strategy was proposed, that is, integrating MIPs-based ECSs into a sensor array and linking with chemometric methods. Even if there are a few literatures has been reported on this strategy, the previous works of our group has demonstrated its feasibility, suitability and effectiveness so far [49-52].

## 1.4.3 MIPs-based electrochemical sensing for pharmaceutical analysis

### 1.4.3.1 State of the art

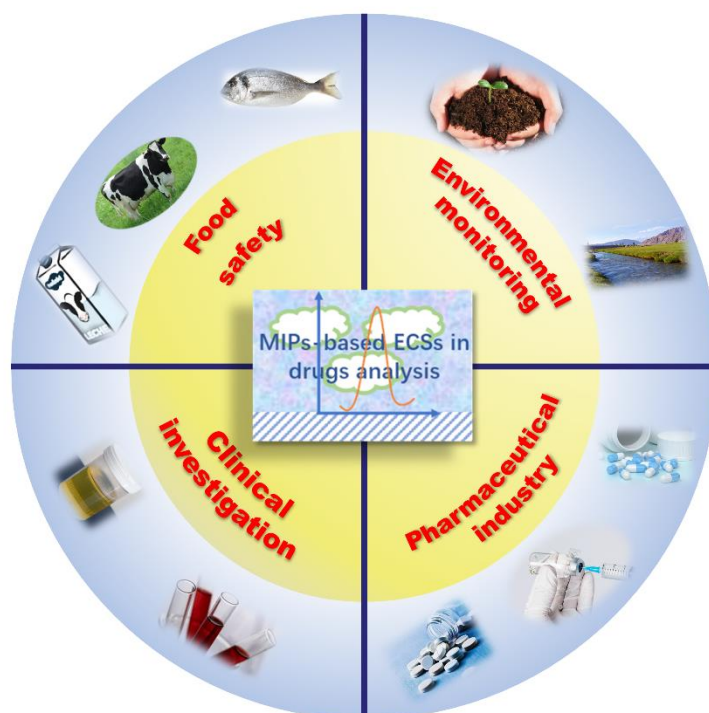


**Figure 1.21** Graphical presentation of the pharmaceutical analysis using MIPs-based ECSs in various fields.

Like various applications of general ECSs (Figure 1.3), as presented in Figure 1.21, MIPs-based ECSs also have promising potentials in the fields of security [51], environment [136, 137], food and beverage sectors [50, 138-140]. Another outstanding aspect in MIPs-based ECSs' application is pharmaceutical analysis. As we all know, the discovery and usage of drugs treating various diseases are vital for improving human being life quality and extension. Pharmaceutical analysis plays key roles of therapeutic drug monitoring in clinical investigation and drug component assessment in pharmaceutical industrial. What's more, drugs abusing can lead to the issues of bioconcentration in animals and drug residues in ecosystem. Therefore, the detected



matrices of MIPs-based ECSs can cover the range of commercial pharmaceutical formulations, human or animal body fluids including urine, serum and plasma, environmental samples including water and soil, and animal food including milk and meats, involving also a very diverse range of concentrations, from percentage range to ultratrace level. Herein, illustrative reports on MIPs-based ECSs' application for pharmaceutical analysis in various matrices are summarized in Table 1.3.

### **1.4.3.2 Classification of the analyzed drugs**

#### **○ Antibiotics**

Antibiotics are widely used for treating specific illnesses and or infections in human beings and animals. Although many countries have made special rules for monitoring the use of antibiotics, when it comes to the issues of drug abusing, antibiotics have to be mentioned. According to the reported literatures (summarized in Table 1.3), it can be deduced that MIPs-based ECSs are fit for the detection of different kinds of antibiotics in various matrices.

Particularly, fluoroquinolones (FQs) are an important class of antibiotics sharing similar structure. In the past decades, there have been various variants from the first to fourth generation through continuous evolution and development, such as nalidixic acid, ciprofloxacin, levofloxacin, moxifloxacin, and so on. There are a number of MIPs-based ECSs that were exploited to detect FQs [141]. For example, Liu and coworkers fabricated a copolymer complex made up of the MIP decorating 3D functionalized multi-walled carbon nanotubes (fMWCNTs-MIP) through precipitation polymerization [142]. Due to the synergic effects of fMWCNTs and MIP, the produced fMWCNTs-MIP presented wide linear detection ranges, low limit of determination (LOD), and excellent selectivity in ultrasensitive electrochemical detecting norfloxacin.

#### **○ Catecholamines**

Catecholamines are vital neurological substances that play important physiological roles in stimulating nerve receptors and vasoconstriction, increasing

cardiac output and heart rate. The frequently used catecholamine drugs in clinical mainly involve dopamine, norepinephrine, epinephrine, etc. Parkinson's disease is known as a great threat to the elderly that is proved to be closely related to the lack of dopamine in the body. Therefore, the detection of dopamine using MIPs-based ECSs has been extensively studied in human's or animals' body fluids.

#### ○ **Psychotropic drugs**

In recent years, mental illness has received more and more attentions, such as anxiety and depression, thus increasingly use of psychotropic drugs has been witnessed. Some groups detected psychotropic drugs based on MIPs-based ECSs, e.g., chlorpromazine and trimipramine. Motaharian et al. synthesized the nanocomposite of MIP and MWCNT by suspension polymerization method using chlorpromazine as template, that was used to modify screen printed carbon electrodes (SPCE). The built MIP-MWCNTs-SPCE sensor was successfully applied to detect chlorpromazine drug in tablet and spiked human urine samples [143].

#### ○ **Others**

There are some active pharmaceutical ingredients (APIs) that are quite common in daily life. Paracetamol (PA) is the typical one, that is widely used as analgesic and antipyretic drug due to the effective relief of fevers and pains. However, PA could lead to the accumulation of its toxic metabolites in the cases of overdose that has fatal hepato- and nephro-toxic effects on health. Ascorbic acid (AA) is a valuable vitamin of great biological significance for human being and widely used to combined with other medicines in the treatment of the common cold because of the positive effect on the immune system. It has been proved that the deficiency of AA is closely related to scurvy, the disturbances in the collagen metabolism and the reduced women's fertility. On the contrary, AA's abuse can also cause a deep vein thrombosis. Hence, the detection of PA and AA based on MIPs-based ECSs were attempted. In addition to PA and AA, other APIs are also detected, such as tramadol painkiller.

Although all kinds of pharmaceuticals cannot be described in details, the reported

MIPs-based ECSs in the application of pharmaceutical analysis were summarized in Table 1.3.

Table 1.3 Summary of the reported MIPs-based ECSs in the application of pharmaceutical analysis.

Analyte	Category	Electrode materials	Method	Linear range	LOD	Matrix	Ref.
<b>amoxicillin</b>	antibiotic (cephalosporin)	MWCNTs@MIP/GCE	DPV	1-1000 nM 1000-6000 nM	0.89 nM	milk and honey	[144]
<b>avibactam</b>	antibiotic ( $\beta$ - lactamase)	MIP/N-Mo <sub>2</sub> C/SPE	SWV	1-1000 $\mu$ M	0.5 $\mu$ M	human serum	[145]
<b>ceftazidime</b>	antibiotic (cephalosporin)	MIP/N-Mo <sub>2</sub> C/SPE	SWV	50-1000 $\mu$ M	35 $\mu$ M	human serum	[145]
<b>sulfapyridine</b>	antibiotic (sulfonamide)	MIP/Ni(OH) <sub>2</sub> / Ni foam	DPV	0.59-1340 $\mu$ M	0.357 $\mu$ M	fish	[135]
<b>ceftizoxime</b>	antibiotic (cephalosporin)	MIP/MWCNT/GCE	DPV	0.001-0.1 $\mu$ M 0.2-100 $\mu$ M	0.1 nM	human serum and urine	[146]
<b>ciprofloxacin</b>	antibiotic (fluoroquinolone)	Ch-AuMIP	DPV	1-100 $\mu$ M	210 nM	water, milk, and pharmaceutical	[147]
<b>enrofloxacin</b>	antibiotic (fluoroquinolone)	MIP/graphite	SWV	10 <sup>-4</sup> -100 M	0.657 pM	pharmaceutical	[148]
<b>levofloxacin</b>	antibiotic (fluoroquinolone)	MIP/ graphene–Au/GCE	DPV	1-100 $\mu$ M	0.53 $\mu$ M	pharmaceutical	[149]
<b>lomefloxacin</b>	antibiotic (fluoroquinolone)	MIP/Fe-doped porous carbon	DPV	1-120 nM	0.2 nM	water and milk	[150]
<b>moxifloxacin</b>	antibiotic (fluoroquinolone)	MIP/GR/GCE	DPV	1-10 nM 10-50000 nM	0.512 nM	human urine and pharmaceutical	[151]
<b>norfloxacin</b>	antibiotic	fMWCNTs-NIP/GCE	DPV	0.003-0.391 $\mu$ M	1.58 nM	pharmaceutical	[142]

	(fluoroquinolone)			0.391-3.125 $\mu$ M		and rat plasma	
<b>norfloxacin</b>	antibiotic (fluoroquinolone)	MIP/CoFe-MOFs/AuNPs/GCE	DPV	5-100 pM 100-1000 pM 1000-6000 pM	0.131 pM	Milk	[152]
<b>norfloxacin</b>	antibiotic (fluoroquinolone)	MIP/MWCNT/GCE	SWV	0.1-8.0 $\mu$ M	0.46 nM	human urine	[153]
<b>methimazole</b>	antibiotic (nitroimidazole)	MIP-PGE	DPV	0.007-6 mM	3.0 $\mu$ M	human serum	[122]
<b>metronidazole</b>	antibiotic (nitroimidazole)	MIP/NPNi/ GCE.	CV	0.06-0.4 pM 0.4-4.0 pM	0.05 pM	pharmaceutical and fish tissue	[84]
<b>sulfadiazine</b>	antibiotic (sulfonamide)	MIP/GO@COF/GCE	DPV	0.5-200 $\mu$ M	0.16 $\mu$ M	beef and fodder	[127]
<b>nevirapine</b>	anti-HIV drug	MIP/ErGO/GCE	DPV	0.005-400 $\mu$ M	2.0 nM	human serum and pharmaceutical	[117]
<b>paracetamol</b>	antipyretic, analgesic	MIP/pABSA/GCE	DPV	0.05-100 $\mu$ M	0.043 $\mu$ M	human tablets and urine	[93]
<b>paracetamol</b>	antipyretic, analgesic	MIP-PGE	DPV	1.25-4.5mM	0.79 $\mu$ M	commercial tablets	[112]
<b>paracetamol</b>	antipyretic, analgesic	MIP/GO@COF/GCE	DPV	0.05-20 $\mu$ M	0.032 $\mu$ M	beef and fodder	[127]
<b>paracetamol</b>	antipyretic, analgesic	nanoMIPs- SPCE	DPV	0.1-1.0 mM	167 $\mu$ M	human plasma	[154]
<b>dipyridamole</b>	cardiovascular drug	MIP/ Fe <sub>3</sub> O <sub>4</sub> @Au-MWCNT/ GCE	DPV	0.5-1900 ng/mL	0.03 ng/mL	human serum	[155]
<b>dopamine</b>	catecholamine	MIP/ZIF-67/Nafion/	DPV	0.08-100 $\mu$ M	30.8 nM	human serum	[156]

		GCE		100-500 $\mu\text{M}$			
<b>dopamine</b>	catecholamine	MIP/ZnO/FTO	DPV	0.02-5 $\mu\text{M}$ 10-800 $\mu\text{M}$	-	human urine	[126]
<b>dopamine</b>	catecholamine	Au/N-GOQDs/ NiS <sub>2</sub> /BC/GCE	DPV	0.05-8.0 $\mu\text{M}$	2.8 nM	human serum, urine and pharmaceutical	[79]
<b>dopamine</b>	catecholamine	MIP-MWCNTs/GCE	DPV	0.04 $\mu\text{M}$ -70 $\mu\text{M}$	0.015 $\mu\text{M}$	rat plasma sample	[157]
<b>dopamine</b>	catecholamine	MIP/Au/GCE	DPV	2.0-180 $\mu\text{M}$	0.3 $\mu\text{M}$	bovine serum	[88]
<b>epinephrine</b>	catecholamine and hormone	MIP-MWCNTs/GCE	DPV	0.04 $\mu\text{M}$ -70 $\mu\text{M}$	0.023 $\mu\text{M}$	rat plasma sample	[157]
<b>sofosbuvir</b>	nucleotide polymerase inhibitor	MIP-AuNPs/ N, S@GQDs/PGE	DPV	1-400 nM	0.36 nM	human plasma	[158]
<b>tramadol</b>	painkiller	MIP/f-MWCNT/GCE	SWV	0.2-2.0 nM 2.0-20.0 nM	0.03 nM	tablet and urine	[115]
<b>chlorpromazine</b>	psychotropic drug	Au/N-GOQDs/ NiS <sub>2</sub> /BC/GCE	DPV	0.005-2.0 $\mu\text{M}$	0.25 nM	human serum, urine and pharmaceutical	[79]
<b>chlorpromazine</b>	psychotropic drug	MIP/Pt/Co <sub>3</sub> O <sub>4</sub>	DPV	0.005-9 $\mu\text{M}$	2.6 nM	human serum, and pharmaceutical	[102]
<b>chlorpromazine</b>	psychotropic drug	MIP-MWCNTs/SPCE	SWV	0.75-250 nM	0.296 nM	human urine	[143]
<b>trimipramine</b>	psychotropic drug	MIP-MWCNTs-carbon paste	SWV	0.1-2.5 nM	0.045 nM	human serum, urine and pharmaceutical	[159]

<b>ecstasy</b>	recreational drug	MIP-SPCE	SWV	2.5-200 $\mu\text{M}$	2.6 $\mu\text{M}$	human blood serum and urine	[85]
<b>gastrodin</b>	traditional Chinese medicine	MIPs/rGO-AgNPs/Ni foam	DPV	0.01-1 $\mu\text{M}$	1 nM	human serum	[64]
<b>ascorbic acid</b>	vitamin	MIP/ZIF-67/CC	amperometric	0.057-11.4 $\mu\text{M}$	0.019 $\mu\text{M}$	-	[89]
<b>ascorbic acid</b>	vitamin	PPy-BPQDs-MIPs /PEDOT nanorods /GCE	DPV	0.01-4 mM	3.3 nM	soft drink	[91]
<b>ascorbic acid</b>	vitamin	MIP-EG -GCE	DPV	0.1-8.0 mM	0.10 mM	-	[124]

*SPE*: screen-printed electrode, *Ch*: chitosan, *GR*: graphene, *MOF*: metal organic frameworks, *PGE*: pencil graphite electrode, *NPNi*: nanoporous nickel, *GO*: graphene oxide, *COF*: covalent organic framework, *ErGO*: electrochemically reduced graphene oxide, *pABSA*: poly(p-aminobenzenesulfonic acid), *SPCE*: screen-printed carbon electrodes, *FTO*: fluorine-doped tin oxide, *N-GOQDs*: N-doped graphene oxide quantum dots, *BC*: biomass carbon, *N, S@ GQDs*: N, S co-doped graphene quantum dots, *CC*: carbon cloth, *BPQDs*: black phosphorene quantum dots, *EG*: exfoliated graphene

## **References**

- [1] A. Hulanicki., S. Glab., F. Ingman., Chemical sensors: definitions and classification, *Pure and Applied Chemistry*, 63(1991) 1247-1250.
- [2] J. Janata., Chemical Sensors, *Analytical Chemistry*, 64(1992) 196R-219R.
- [3] S. Joo., R.B. Brown., Chemical Sensors with Integrated Electronics, *Chemical Reviews* (Washington, DC, United States), 108(2008) 638–651.
- [4] M. Pirzada, Z. Altintas, Recent Progress in Optical Sensors for Biomedical Diagnostics, *Micromachines* (Basel), 11(2020) 356-387.
- [5] X. Yan, H. Li, X. Su, Review of optical sensors for pesticides, *TRAC Trends in Analytical Chemistry*, 103(2018) 1-20.
- [6] F. Reverter, A Tutorial on Thermal Sensors in the 200th Anniversary of the Seebeck Effect, *IEEE Sensors Journal*, 21(2021) 22122-22132.
- [7] C.I.L. Justino, T.A.P. Rocha-Santos, S. Cardoso, A.C. Duarte, Strategies for enhancing the analytical performance of nanomaterial-based sensors, *Trends Analyt Chem*, 47(2013) 27-36.
- [8] C.I.L. Justino, A.C. Freitas, R. Pereira, A.C. Duarte, T.A.P. Rocha Santos, Recent developments in recognition elements for chemical sensors and biosensors, *TRAC Trends in Analytical Chemistry*, 68(2015) 2-17.
- [9] H.H. Nguyen, S.H. Lee, U.J. Lee, C.D. Fermin, M. Kim, Immobilized Enzymes in Biosensor Applications, *Materials* (Basel), 12(2019) 121.
- [10] H. Zhang, B.L. Miller, Immunosensor-based label-free and multiplex detection of influenza viruses: State of the art, *Biosensors and Bioelectronics*, 141(2019) 111476.
- [11] C.L. Manzanares-Palenzuela, B. Martín-Fernández, M. Sánchez-Paniagua López, B. López-Ruiz, Electrochemical genosensors as innovative tools for detection of genetically modified organisms, *TRAC Trends in Analytical Chemistry*, 66(2015) 19-31.
- [12] M. Moraskie, M.H.O. Roshid, G. O'Connor, E. Dikici, J.M. Zingg, S. Deo, et al., Microbial whole-cell biosensors: Current applications, challenges, and future perspectives, *Biosensors and Bioelectronics*, 191(2021) 113359.
- [13] C. Algieri, E. Drioli, L. Guzzo, L. Donato, Bio-mimetic sensors based on molecularly imprinted



membranes, *Sensors (Basel)*, 14(2014) 13863-13912.

[14] Y. Cao, T. Feng, J. Xu, C. Xue, Recent advances of molecularly imprinted polymer-based sensors in the detection of food safety hazard factors, *Biosens Bioelectron*, 141(2019) 111447.

[15] R. Ahmad, N. Griffete, A. Lamouri, N. Felidj, M.M. Chehimi, C. Mangeney, Nanocomposites of Gold Nanoparticles@Molecularly Imprinted Polymers: Chemistry, Processing, and Applications in Sensors, *Chemistry of Materials*, 27(2015) 5464-5478.

[16] S. Ansari, Combination of molecularly imprinted polymers and carbon nanomaterials as a versatile biosensing tool in sample analysis: Recent applications and challenges, *TRAC Trends in Analytical Chemistry*, 93(2017) 134-151.

[17] D. Grieshaber, R. MacKenzie, J. Voros, E. Reimhult, Electrochemical Biosensor-Sensor Principles and Architectures, *Sensors*, 8(2008) 1400-1458.

[18] W. Joseph, Glucose Biosensors: 40 Years of Advances and Challenges, *Electroanalysis* 13(2001) 983-988.

[19] J. Kim, A.S. Campbell, J. Wang, Wearable non-invasive epidermal glucose sensors: A review, *Talanta*, 177(2018) 163-170.

[20] H. Lee, Y.J. Hong, S. Baik, T. Hyeon, D.H. Kim, Enzyme-Based Glucose Sensor: From Invasive to Wearable Device, *Advanced Healthcare Materials*, 7(2018) 1701150.

[21] Y. Yao, J. Chen, Y. Guo, T. Lv, Z. Chen, N. Li, et al., Integration of interstitial fluid extraction and glucose detection in one device for wearable non-invasive blood glucose sensors, *Biosensors and Bioelectronics*, 179(2021) 113078.

[22] K.J. Albert, N.S. Lewis, C.L. Schauer, G.A. Sotzing, S.E. Stitzel, T.P. Vaid, et al., Cross-Reactive Chemical Sensor Arrays, *Chemical Reviews (Washington, DC, United States)*, 100(2000) 2595-2626.

[23] P. Anzenbacher, Jr., P. Lubal, P. Bucek, M.A. Palacios, M.E. Kozelkova, A practical approach to optical cross-reactive sensor arrays, *Chemical Society Reviews*, 39(2010) 3954-3979.

[24] Z.-H. Chen, Q.-X. Fan, X.-Y. Han, G. Shi, M. Zhang, Design of smart chemical ‘tongue’ sensor arrays for pattern-recognition-based biochemical sensing applications, *TrAC Trends in Analytical Chemistry*, 124(2020).

[25] J.J. Lavigne, E.V. Anslyn, Sensing A Paradigm Shift in the Field of Molecular Recognition: From Selective to Differential Receptors, *Angewandte Chemie International Edition*, 40(2001) 3118-

3130.

[26] D.G. Smith, I.L. Topolnicki, V.E. Zwicker, K.A. Jolliffe, E.J. New, Fluorescent sensing arrays for cations and anions, *Analyst*, 142(2017) 3549-3563.

[27] J.R. Askim, M. Mahmoudi, K.S. Suslick, Optical sensor arrays for chemical sensing: the optoelectronic nose, *Chemical Society Reviews*, 42(2013) 8649-8682.

[28] A.A. Bowyer, C. Shen, E.J. New, A fluorescent three-sensor array for heavy metals in environmental water sources, *Analyst*, 145(2020) 1195-1201.

[29] K.L. Diehl, E.V. Anslyn, Array sensing using optical methods for detection of chemical and biological hazards, *Chemical Society Reviews*, 42(2013) 8596-8611.

[30] H. Lin, M. Jang, K.S. Suslick, Preoxidation for colorimetric sensor array detection of VOCs, *Journal of the American Chemical Society*, 133(2011) 16786-16789.

[31] L. Mitchell, C. Shen, H.C. Timmins, S.B. Park, E.J. New, A Versatile Fluorescent Sensor Array for Platinum Anticancer Drug Detection in Biological Fluids, *ACS Sensors*, 6(2021) 1261-1269.

[32] J.R. Stetter, P.C. Jurs, S.L. Rose, Detection of Hazardous Gases and Vapors: Pattern Recognition Analysis of Data from an Electrochemical Sensor Array, *Analytical Chemistry*, 58(1986) 860-866.

[33] A.U. Alam, D. Clyne, H. Jin, N.X. Hu, M.J. Deen, Fully Integrated, Simple, and Low-Cost Electrochemical Sensor Array for in Situ Water Quality Monitoring, *ACS Sens*, 5(2020) 412-422.

[34] X. Cetó, F. Céspedes, M. Del Valle, Comparison of methods for the processing of voltammetric electronic tongues data, *Microchimica Acta*, 180(2013) 319-330.

[35] X. Cetó, A. Gutés, M. Del Valle, Simple data preprocessing for voltammetric Electronic Tongues using Artificial Neural Networks, *Acta Manilana*, 61(2013) 39-49.

[36] M. Del Valle, *Electronic Tongues Employing Electrochemical Sensors*, *Electroanalysis*, (2010) 1539-1555.

[37] A. Gutés, D. Calvo, F. Céspedes, M. Del Valle, Automatic sequential injection analysis electronic tongue with integrated reference electrode for the determination of ascorbic acid, uric acid and paracetamol, *Microchimica Acta*, 157(2007) 1-6.

[38] D. Ortiz-Aguayo, M. Bonet-San-Emeterio, M. Del Valle, Simultaneous Voltammetric Determination of Acetaminophen, Ascorbic Acid and Uric Acid by Use of Integrated Array of Screen-Printed Electrodes and Chemometric Tools, *Sensors (Basel)*, 19(2019) 3286.

- [39] M. Sarma, N. Romero, X. Cetó, M. Del Valle, Optimization of Sensors to be Used in a Voltammetric Electronic Tongue Based on Clustering Metrics, *Sensors (Basel)*, 20(2020) 4798.
- [40] D.A. Yarmolinsky, C.S. Zuker, N.J. Ryba, Common sense about taste: from mammals to insects, *Cell*, 139(2009) 234-244.
- [41] B. Lindemann, Receptors and transduction in taste, *Nature*, 413(2001) 219-225.
- [42] T. Wasilewski, W. Kamysz, J. Gebicki, Bioelectronic tongue: Current status and perspectives, *Biosens Bioelectron*, 150(2020) 111923.
- [43] Y. Vlasov, A. Legin, A. Rudnitskaya, C. Di Natale, A. D'Amico, Nonspecific sensor arrays ("electronic tongue") for chemical analysis of liquids (IUPAC Technical Report), *Pure and Applied Chemistry*, 77(2005) 1965-1983.
- [44] Y. Vlasov, A. Legin, Non-selective chemical sensors in analytical chemistry: from "electronic nose" to "electronic tongue", *Fresenius Journal of Analytical Chemistry*, 361(1998) 255–260.
- [45] D. Ha, Q. Sun, K. Su, H. Wan, H. Li, N. Xu, et al., Recent achievements in electronic tongue and bioelectronic tongue as taste sensors, *Sensors and Actuators B: Chemical*, 207(2015) 1136-1146.
- [46] X. Cetó, F. Cespedes, M.I. Pividori, J.M. Gutierrez, M. del Valle, Resolution of phenolic antioxidant mixtures employing a voltammetric bio-electronic tongue, *Analyst*, 137(2012) 349-356.
- [47] A. Gutes, F. Cespedes, S. Alegret, M. del Valle, Determination of phenolic compounds by a polyphenol oxidase amperometric biosensor and artificial neural network analysis, *Biosensors and Bioelectronics*, 20(2005) 1668-1673.
- [48] A. Cipri, C. Schulz, R. Ludwig, L. Gorton, M. Del Valle, A novel bio-electronic tongue using different cellobiose dehydrogenases to resolve mixtures of various sugars and interfering analytes, *Biosens Bioelectron*, 79(2016) 515-521.
- [49] A. Herrera-Chacon, S. Dinc-Zor, M. del Valle, Integrating molecularly imprinted polymer beads in graphite-epoxy electrodes for the voltammetric biosensing of histamine in wines, *Talanta*, 208(2020) 120348.
- [50] A. Herrera-Chacon, A. González-Calabuig, I. Campos, M. del Valle, Bioelectronic tongue using MIP sensors for the resolution of volatile phenolic compounds, *Sensors and Actuators B: Chemical*, 258(2018) 665-671.
- [51] A. Herrera-Chacon, A. Gonzalez-Calabuig, M. del Valle, Dummy Molecularly Imprinted Polymers Using DNP as a Template Molecule for Explosive Sensing and Nitroaromatic Compound

Discrimination, *Chemosensors*, 9(2021) 255.

[52] M. Wang, X. Cetó, M. Del Valle, A novel electronic tongue using electropolymerized molecularly imprinted polymers for the simultaneous determination of active pharmaceutical ingredients, *Biosens Bioelectron*, 198(2022) 113807.

[53] Y.G. Vlasov, A.V. Legin, A.M. Rudnitskaya, Electronic tongue: Chemical sensor systems for analysis of aquatic media, *Russian Journal of General Chemistry*, 78(2009) 2532-2544.

[54] X. Cetó, N.H. Voelcker, B. Prieto-Simon, Bioelectronic tongues: New trends and applications in water and food analysis, *Biosensors and Bioelectronics*, 79(2016) 608-626.

[55] I.T. Jolliffe, J. Cadima, Principal component analysis: a review and recent developments, *Philosophical transactions of the Royal Society A*, 374(2016) 20150202.

[56] M. del Valle, Sensor Arrays and Electronic Tongue Systems, *International Journal of Electrochemistry*, 2012(2012) 1-11.

[57] C. Alexander, H.S. Andersson, L.I. Andersson, R.J. Ansell, N. Kirsch, I.A. Nicholls, et al., Molecular imprinting science and technology: a survey of the literature for the years up to and including 2003, *Journal of Molecular Recognition* 19(2006) 106-180.

[58] L. Pauling, A Theory of the Structure and Process of Formation of Antibodies, *Journal of the American Chemical Society*, 62(1940) 2643-2657.

[59] W. G., S. A., The use of polymers with enzyme-analogous structures for the resolution of racemates, *Angewandte Chemie International Edition*, 11(1972) 341.

[60] T. T., K. IM., Macromolecule-small molecule interactions; introduction of additional binding sites in polyethyleneimine by disulfide cross-linkages, *Biopolymers*, 11(1972) 483-491.

[61] L. Chen, S. Xu, J. Li, Recent advances in molecular imprinting technology: current status, challenges and highlighted applications, *Chemical Society Reviews*, 40(2011) 2922-2942.

[62] L. Chen, X. Wang, W. Lu, X. Wu, J. Li, Molecular imprinting: perspectives and applications, *Chemical Society Reviews*, 45(2016) 2137-2211.

[63] M. Dabrowski, P. Lach, M. Cieplak, W. Kutner, Nanostructured molecularly imprinted polymers for protein chemosensing, *Biosensors and Bioelectronics*, 102(2018) 17-26.

[64] R. Gui, H. Jin, H. Guo, Z. Wang, Recent advances and future prospects in molecularly imprinted polymers-based electrochemical biosensors, *Biosensors and Bioelectronics*, 100(2018) 56-70.

[65] J.J. BelBruno, *Molecularly Imprinted Polymers*, Chemical Reviews (Washington, DC, United

States), 119(2019) 94-119.

[66] S. Xu, L. Wang, Z. Liu, Molecularly Imprinted Polymer Nanoparticles: An Emerging Versatile Platform for Cancer Therapy, *Angewandte Chemie, International Edition in English*, 60(2021) 3858-3869.

[67] S. Ansari, S. Masoum, Molecularly imprinted polymers for capturing and sensing proteins: Current progress and future implications, *TRAC Trends in Analytical Chemistry*, 114(2019) 29-47.

[68] M.J. Whitcombe, I. Chianella, L. Larcombe, S.A. Piletsky, J. Noble, R. Porter, et al., The rational development of molecularly imprinted polymer-based sensors for protein detection, *Chemical Society Reviews*, 40(2011) 1547-1571.

[69] S. Piletsky, F. Canfarotta, A. Poma, A.M. Bossi, S. Piletsky, Molecularly Imprinted Polymers for Cell Recognition, *Trends in Biotechnology*, 38(2020) 368-387.

[70] J. Pan, W. Chen, Y. Ma, G. Pan, Molecularly imprinted polymers as receptor mimics for selective cell recognition, *Chemical Society Reviews*, 47(2018) 5574-5587.

[71] T.P. Rao, R. Kala, S. Daniel, Metal ion-imprinted polymers—novel materials for selective recognition of inorganics, *Analytica Chimica Acta*, 578(2006) 105-116.

[72] S.M. Ng, R. Narayanaswamy, Molecularly imprinted  $\beta$ -cyclodextrin polymer as potential optical receptor for the detection of organic compound, *Sensors and Actuators B: Chemical*, 139(2009) 156-165.

[73] F. Zouaoui, S. Bourouina-Bacha, M. Bourouina, N. Jaffrezic-Renault, N. Zine, A. Errachid, Electrochemical sensors based on molecularly imprinted chitosan: A review, *TRAC Trends in Analytical Chemistry*, 130(2020) 115982.

[74] H. Yan, K.H. Row, Characteristic and Synthetic Approach of MIP, *International Journal of Molecular Sciences*, 7(2006) 155-178.

[75] R. Arshady, K. Mosbach, Synthesis of substrate-selective polymers by host-guest polymerization, *Die Makromolekulare Chemie*, 182(1981) 687-692.

[76] S. Farooq, J. Nie, Y. Cheng, Z. Yan, J. Li, S.A.S. Bacha, et al., Molecularly imprinted polymers' application in pesticide residue detection, *Analyst*, 143(2018) 3971-3989.

[77] X. Hu, Y. Xia, Y. Liu, F. Zhao, B. Zeng, Determination of patulin using dual-dummy templates imprinted electrochemical sensor with PtPd decorated N-doped porous carbon for amplification, *Mikrochimica Acta*, 188(2021) 148.

[78] Y. Li, L. Zhang, Y. Dang, Z. Chen, R. Zhang, Y. Li, et al., A robust electrochemical sensing of molecularly imprinted polymer prepared by using bifunctional monomer and its application in detection of cypermethrin, *Biosens Bioelectron*, 127(2019) 207-214.

[79] Z. Lu, Y. Li, T. Liu, G. Wang, M. Sun, Y. Jiang, et al., A dual-template imprinted polymer electrochemical sensor based on AuNPs and nitrogen-doped graphene oxide quantum dots coated on NiS<sub>2</sub>/biomass carbon for simultaneous determination of dopamine and chlorpromazine, *Chemical Engineering Journal*, 389(2020) 124417.

[80] C. Dong, H. Shi, Y. Han, Y. Yang, R. Wang, J. Men, Molecularly imprinted polymers by the surface imprinting technique, *European Polymer Journal*, 145(2021) 110231.

[81] R.D. Crapnell, A. Hudson, C.W. Foster, K. Eersels, B.V. Grinsven, T.J. Cleij, et al., Recent Advances in Electrosynthesized Molecularly Imprinted Polymer Sensing Platforms for Bioanalyte Detection, *Sensors (Basel)*, 19(2019) 1204.

[82] P.S. Sharma, A. Pietrzyk-Le, F. D'Souza, W. Kutner, Electrochemically synthesized polymers in molecular imprinting for chemical sensing, *Analytical and Bioanalytical Chemistry*, 402(2012) 3177-3204.

[83] A. Sanati, R. Siavash Moakhar, I.H. I, K. Raeissi, F. Karimzadeh, M. Jalali, et al., Gold Nano/Micro-Islands Overcome the Molecularly Imprinted Polymer Limitations to Achieve Ultrasensitive Protein Detection, *ACS Sensors*, (2021) 797-807.

[84] Y. Li, Y. Liu, Y. Yang, F. Yu, J. Liu, H. Song, et al., Novel electrochemical sensing platform based on a molecularly imprinted polymer decorated 3D nanoporous nickel skeleton for ultrasensitive and selective determination of metronidazole, *ACS Applied Materials & Interfaces*, 7(2015) 15474-15480.

[85] R.A.S. Couto, S.S. Costa, B. Mounsef, J.G. Pacheco, E. Fernandes, F. Carvalho, et al., Electrochemical sensing of ecstasy with electropolymerized molecularly imprinted poly(o-phenylenediamine) polymer on the surface of disposable screen-printed carbon electrodes, *Sensors and Actuators B: Chemical*, 290(2019) 378-386.

[86] E. Buffon, N.R. Stradiotto, A molecularly imprinted polymer on reduced graphene oxide-gold nanoparticles modified screen-printed electrode for selective determination of ferulic acid in orange peels, *Microchemical Journal*, 167(2021) 106339.

[87] K. Phonklam, R. Wannapob, W. Sriwimol, P. Thavarungkul, T. Phairatana, A novel molecularly

imprinted polymer PMB/MWCNTs sensor for highly-sensitive cardiac troponin T detection, *Sensors and Actuators B: Chemical*, 308(2020) 127630.

[88] N. Li, C. Nan, X. Mei, Y. Sun, H. Feng, Y. Li, Electrochemical sensor based on dual-template molecularly imprinted polymer and nanoporous gold leaf modified electrode for simultaneous determination of dopamine and uric acid, *Microchimica Acta*, 187(2020) 496.

[89] Y. Guo, L. Wang, L. Xu, C. Peng, Y. Song, A ascorbic acid-imprinted poly(o-phenylenediamine)/zeolite imidazole frameworks-67/carbon cloth for electrochemical sensing ascorbic acid, *Journal of Materials Science*, 55(2020) 9425-9435.

[90] B. Chen, Y. Zhang, L. Lin, H. Chen, M. Zhao, Au nanoparticles@metal organic framework/polythionine loaded with molecularly imprinted polymer sensor: Preparation, characterization, and electrochemical detection of tyrosine, *Journal of Electroanalytical Chemistry*, 863(2020) 114052.

[91] Z. Zhang, Y. Li, J. Xu, Y. Wen, Electropolymerized molecularly imprinted polypyrrole decorated with black phosphorene quantum dots onto poly(3,4-ethylenedioxythiophene) nanorods and its voltammetric sensing of vitamin C, *Journal of Electroanalytical Chemistry*, 814(2018) 153-160.

[92] Y. Li, X. Chen, H. Ren, X. Li, S. Chen, B.-C. Ye, A novel electrochemical sensor based on molecularly imprinted polymer-modified C-ZIF67@Ni for highly sensitive and selective determination of carbendazim, *Talanta*, 237(2022) 122909.

[93] Y. Teng, L. Fan, Y. Dai, M. Zhong, X. Lu, X. Kan, Electrochemical sensor for paracetamol recognition and detection based on catalytic and imprinted composite film, *Biosens Bioelectron*, 71(2015) 137-142.

[94] T.-P. Huynh, P.S. Sharma, M. Sosnowska, F. D'Souza, W. Kutner, Functionalized polythiophenes: Recognition materials for chemosensors and biosensors of superior sensitivity, selectivity, and detectability, *Progress in Polymer Science*, 47(2015) 1-25.

[95] D. Dechtrirat, P. Yingyuad, P. Prajongtat, L. Chuenchom, C. Sriprachuabwong, A. Tuantranont, et al., A screen-printed carbon electrode modified with gold nanoparticles, poly(3,4-ethylenedioxythiophene), poly(styrene sulfonate) and a molecular imprint for voltammetric determination of nitrofurantoin, *Microchimica Acta*, 185(2018) 261-269.

[96] S. Khumngern, P. Thavarungkul, P. Kanatharana, T. Bejrananda, A. Numnuam, Molecularly imprinted electrochemical sensor based on poly(o-phenylenediamine-co-o-aminophenol) incorporated

with poly(styrenesulfonate) doped poly(3,4-ethylenedioxythiophene) ferrocene composite modified screen-printed carbon electrode for highly sensitive and selective detection of prostate cancer biomarker, *Microchemical Journal*, 177(2022) 107311.

[97] A. Menaker, V. Syritski, J. Reut, A. Öpik, V. Horváth, R.E. Gyurcsányi, Electrosynthesized Surface-Imprinted Conducting Polymer Microrods for Selective Protein Recognition, *Advanced Materials*, 21(2009) 2271-2275.

[98] A. Maria C G, A. K B, S. Rison, A. Varghese, L. George, Molecularly imprinted PEDOT on carbon fiber paper electrode for the electrochemical determination of 2,4-dichlorophenol, *Synthetic Metals*, 261(2020) 116309.

[99] M. Gajda, R. Rybakiewicz, M. Cieplak, T. Zolek, D. Maciejewska, E. Gilant, et al., Low-oxidation-potential thiophene-carbazole monomers for electro-oxidative molecular imprinting: Selective chemosensing of aripiprazole, *Biosensors and Bioelectronics*, 169(2020) 112589.

[100] J. Luo, Q. Ma, W. Wei, Y. Zhu, R. Liu, X. Liu, Synthesis of Water-Dispersible Molecularly Imprinted Electroactive Nanoparticles for the Sensitive and Selective Paracetamol Detection, *ACS Applied Materials & Interfaces*, 8(2016) 21028-21038.

[101] B. Xu, B. Zhang, L. Yang, F. Zhao, B. Zeng, Electrochemical determination of luteolin using molecularly imprinted poly-carbazole on MoS<sub>2</sub>/graphene-carbon nanotubes nanocomposite modified electrode, *Electrochimica Acta*, 258(2017) 1413-1420.

[102] Y. Liu, X. Hu, Y. Xia, F. Zhao, B. Zeng, A novel ratiometric electrochemical sensor based on dual-monomer molecularly imprinted polymer and Pt/Co<sub>3</sub>O<sub>4</sub> for sensitive detection of chlorpromazine hydrochloride, *Analytica Chimica Acta*, 1190(2022) 339245.

[103] G. Sabouraud, S. Sadki, N. Brodie, The mechanisms of pyrrole electropolymerization, *Chemical Society Reviews*, 29(2000) 283-293.

[104] N.A. Ogurtsov, Y.V. Noskov, O.S. Kruglyak, S.I. Bohvan, V.V. Klepko, M.V. Petrichuk, et al., Effect of the Dopant Anion and Oxidant on the Structure and Properties of Nanocomposites of Polypyrrole and Carbon Nanotubes, *Theoretical and Experimental Chemistry*, 54(2018) 114-121.

[105] X. Zhang, S. Wang, S. Lu, J. Su, T. He, Influence of doping anions on structure and properties of electro-polymerized polypyrrole counter electrodes for use in dye-sensitized solar cells, *Journal of Power Sources*, 246(2014) 491-498.

[106] Y. Wang, Y. Zhang, C. Hou, M. Liu, Ultrasensitive electrochemical sensing of dopamine using



reduced graphene oxide sheets decorated with p-toluenesulfonate-doped polypyrrole/Fe<sub>3</sub>O<sub>4</sub> nanospheres, *Microchimica Acta*, 183(2016) 1145-1152.

[107] T. Raudsepp, M. Marandi, T. Tamm, V. Sammelselg, J. Tamm, Study of the factors determining the mobility of ions in the polypyrrole films doped with aromatic sulfonate anions, *Electrochimica Acta*, 53(2008) 3828-3835.

[108] A. Hallik, A. Alumaa, H. Kurig, A. Jänes, E. Lust, J. Tamm, On the porosity of polypyrrole films, *Synthetic Metals*, 157(2007) 1085-1090.

[109] K. Imanishi, M. Satoh, Y. Yasuda, R. Tsushima, S. Aoki, Solvent effect on electrochemical polymerization of aromatic compounds, *Journal of Electroanalytical Chemistry and Interfacial Electrochemistry*, 242(1988) 203-208.

[110] S. Shimoda, E. Smela, The effect of pH on polymerization and volume change in PPy(DBS), *Electrochimica Acta*, 44(1998) 219-238.

[111] T.F. Otero, J. Rodríguez, Parallel kinetic studies of the electrogeneration of conducting polymers: mixed materials, composition and properties control, *Electrochimica Acta*, 39(1994) 245-253.

[112] L. Özcan, Y. Şahin, Determination of paracetamol based on electropolymerized-molecularly imprinted polypyrrole modified pencil graphite electrode, *Sensors and Actuators B: Chemical*, 127(2007) 362-369.

[113] T. Beduk, A. Ait Lahcen, N. Tashkandi, K.N. Salama, One-step electrosynthesized molecularly imprinted polymer on laser scribed graphene bisphenol a sensor, *Sensors and Actuators B: Chemical*, 314(2020) 128026.

[114] G. Bolat, Y.T. Yaman, S. Abaci, Molecularly imprinted electrochemical impedance sensor for sensitive dibutyl phthalate (DBP) determination, *Sensors and Actuators B: Chemical*, 299(2019) 127000.

[115] B. Deiminiat, G.H. Rounaghi, M.H. Arbab-Zavar, Development of a new electrochemical imprinted sensor based on poly-pyrrole, sol-gel and multiwall carbon nanotubes for determination of tramadol, *Sensors and Actuators B: Chemical*, 238(2017) 651-659.

[116] M.F. Falone, E. Buffon, N.R. Stradiotto, Molecularly imprinted electrochemical sensor for monitoring mercaptan sulfur in aviation biofuel, *Fuel*, 307(2022) 121783.

[117] B. Hassan Pour, N. Haghazari, F. Keshavarzi, E. Ahmadi, B.R. Zarif, A sensitive sensor based on molecularly imprinted polypyrrole on reduced graphene oxide modified glassy carbon electrode for nevirapine analysis, *Analytical Methods*, (2021) 4767-4777.

[118] X. Kan, H. Zhou, C. Li, A. Zhu, Z. Xing, Z. Zhao, Imprinted electrochemical sensor for dopamine recognition and determination based on a carbon nanotube/polypyrrole film, *Electrochimica Acta*, 63(2012) 69-75.

[119] Q. Kang, Q. Zhang, L. Zang, M. Zhao, X. Chen, D. Shen, Enhancement anti-interference ability of photoelectrochemical sensor via differential molecularly imprinting technique demonstrated by dopamine determination, *Anal Chim Acta*, 1125(2020) 201-209.

[120] D.R. Kumar, G. Dhakal, V.Q. Nguyen, J.J. Shim, Molecularly imprinted hornlike polymer@electrochemically reduced graphene oxide electrode for the highly selective determination of an antiemetic drug, *Anal Chim Acta*, 1141(2021) 71-82.

[121] S.E. Elugoke, A.S. Adekunle, O.E. Fayemi, E.D. Akpan, B.B. Mamba, E.S.M. Sherif, et al., Molecularly imprinted polymers (MIPs) based electrochemical sensors for the determination of catecholamine neurotransmitters – Review, *Electrochemical Science Advances*, (2020).

[122] A. Nezhadali, L. Mehri, R. Shadmehri, Determination of methimazole based on electropolymerized-molecularly imprinted polypyrrole modified pencil graphite sensor, *Materials Science and Engineering C*, 85(2018) 225-232.

[123] A. Nezhadali, S. Senobari, M. Mojarab, 1,4-dihydroxyanthraquinone electrochemical sensor based on molecularly imprinted polymer using multi-walled carbon nanotubes and multivariate optimization method, *Talanta*, 146(2016) 525-532.

[124] S.M. Oliveira, J.M. Luzardo, L.A. Silva, D.C. Aguiar, C.A. Senna, R. Verdan, et al., High-performance electrochemical sensor based on molecularly imprinted polypyrrole-graphene modified glassy carbon electrode, *Thin Solid Films*, 699(2020) 137875.

[125] H. Rao, X. Zhao, X. Liu, J. Zhong, Z. Zhang, P. Zou, et al., A novel molecularly imprinted electrochemical sensor based on graphene quantum dots coated on hollow nickel nanospheres with high sensitivity and selectivity for the rapid determination of bisphenol S, *Biosens Bioelectron*, 100(2018) 341-347.

[126] H.H. Wang, X.J. Chen, W.T. Li, W.H. Zhou, X.C. Guo, W.Y. Kang, et al., ZnO nanotubes supported molecularly imprinted polymers arrays as sensing materials for electrochemical detection of dopamine, *Talanta*, 176(2018) 573-581.

[127] Y. Sun, J. He, G.I.N. Waterhouse, L. Xu, H. Zhang, X. Qiao, et al., A selective molecularly imprinted electrochemical sensor with GO@COF signal amplification for the simultaneous

determination of sulfadiazine and acetaminophen, *Sensors and Actuators B: Chemical*, 300(2019) 126993.

[128] J. Xu, Y. Zhang, K. Wu, L. Zhang, S. Ge, J. Yu, A molecularly imprinted polypyrrole for ultrasensitive voltammetric determination of glyphosate, *Microchimica Acta*, 184(2017) 1959-1967.

[129] Z. Yang, X. Liu, Y. Wu, C. Zhang, Modification of carbon aerogel electrode with molecularly imprinted polypyrrole for electrochemical determination of dopamine, *Sensors and Actuators B: Chemical*, 212(2015) 457-463.

[130] W. Zhang, L. Zong, G. Geng, Y. Li, Y. Zhang, Enhancing determination of quercetin in honey samples through electrochemical sensors based on highly porous polypyrrole coupled with nanohybrid modified GCE, *Sensors and Actuators B: Chemical*, 257(2018) 1099-1109.

[131] A.A. Volkert, A.J. Haes, Advancements in nanosensors using plastic antibodies, *Analyst*, 139(2014) 21-31.

[132] R. Gui, H. Guo, H. Jin, Preparation and applications of electrochemical chemosensors based on carbon-nanomaterial-modified molecularly imprinted polymers, *Nanoscale Advances*, 1(2019) 3325-3363.

[133] T.S. Anirudhan, V.S. Athira, S.S. Nair, Detection of chlorpyrifos based on molecular imprinting with a conducting polythiophene copolymer loaded on multi-walled carbon nanotubes, *Food Chemistry*, 381(2022) 132010.

[134] Z. Zhang, L. Huang, S. Sheng, C. Jiang, Y. Wang, MIL-125(Ti)-derived COOH functionalized TiO<sub>2</sub> grafted molecularly imprinted polymers for photoelectrochemical sensing of ofloxacin, *Sensors and Actuators B: Chemical*, 343(2021) 130119.

[135] Z. Liu, Y. Zhang, J. Feng, Q. Han, Q. Wei, Ni(OH)<sub>2</sub> nanoarrays based molecularly imprinted polymer electrochemical sensor for sensitive detection of sulfapyridine, *Sensors and Actuators B: Chemical*, 287(2019) 551-556.

[136] P. Rebelo, E. Costa-Rama, I. Seguro, J.G. Pacheco, H.P.A. Nouws, M. Cordeiro, et al., Molecularly imprinted polymer-based electrochemical sensors for environmental analysis, *Biosens Bioelectron*, 172(2021) 112719.

[137] N. Tarannum, S. Khatoon, B.B. Dzantiev, Perspective and application of molecular imprinting approach for antibiotic detection in food and environmental samples: A critical review, *Food Control*, 118(2020).

[138] H. Wang, S. Yao, Y. Liu, S. Wei, J. Su, G. Hu, Molecularly imprinted electrochemical sensor based on Au nanoparticles in carboxylated multi-walled carbon nanotubes for sensitive determination of olaquinox in food and feedstuffs, *Biosensors and Bioelectronics*, 87(2017) 417-421.

[139] N. Tarannum, S. Khatoon, B.B. Dzantiev, Perspective and application of molecular imprinting approach for antibiotic detection in food and environmental samples: A critical review, *Food Control*, 118(2020) 107381.

[140] Y. Cao, T. Feng, J. Xu, C. Xue, Recent advances of molecularly imprinted polymer-based sensors in the detection of food safety hazard factors, *Biosensors and Bioelectronics*, 141(2019) 111447.

[141] M. Majdinasab, K. Mitsubayashi, J.L. Marty, Optical and Electrochemical Sensors and Biosensors for the Detection of Quinolones, *Trends Biotechnol*, 37(2019) 898-915.

[142] Z. Liu, M. Jin, H. Lu, J. Yao, X. Wang, G. Zhou, et al., Molecularly imprinted polymer decorated 3D-framework of functionalized multi-walled carbon nanotubes for ultrasensitive electrochemical sensing of Norfloxacin in pharmaceutical formulations and rat plasma, *Sensors and Actuators B: Chemical*, 288(2019) 363-372.

[143] A. Motaharian, M.R.M. Hosseini, K. Naseri, Determination of psychotropic drug chlorpromazine using screen printed carbon electrodes modified with novel MIP-MWCNTs nano-composite prepared by suspension polymerization method, *Sensors and Actuators B: Chemical*, 288(2019) 356-362.

[144] G. Yang, F. Zhao, Molecularly imprinted polymer grown on multiwalled carbon nanotube surface for the sensitive electrochemical determination of amoxicillin, *Electrochimica Acta*, 174(2015) 33-40.

[145] X. Wang, Y. Liu, J. Liu, J. Qu, J. Huang, R. Tan, et al., A bifunctional electrochemical sensor for simultaneous determination of electroactive and non-electroactive analytes: A universal yet very effective platform serving therapeutic drug monitoring, *Biosensors and Bioelectronics*, 208(2022) 114233.

[146] M.R. Ali, M.S. Bacchu, M.R. Al-Mamun, M.M. Rahman, M.S. Ahommed, M.A.S. Aly, et al., Sensitive MWCNT/P-Cys@MIP sensor for selective electrochemical detection of ceftizoxime, *Journal of Materials Science*, 56(2021) 12803-12813.

[147] S.G. Surya, S. Khatoon, A. Ait Lahcen, A.T.H. Nguyen, B.B. Dzantiev, N. Tarannum, et al., A chitosan gold nanoparticles molecularly imprinted polymer based ciprofloxacin sensor, *RSC Advances*,

10(2020) 12823-12832.

[148] C. Yan, R. Zhang, Y. Chen, G. Wang, Electrochemical determination of enrofloxacin based on molecularly imprinted polymer via one-step electro-copolymerization of pyrrole and o - phenylenediamine, *Journal of Electroanalytical Chemistry*, 806(2017) 130-135.

[149] F. Wang, L. Zhu, J. Zhang, Electrochemical sensor for levofloxacin based on molecularly imprinted polypyrrole-graphene-gold nanoparticles modified electrode, *Sensors and Actuators B: Chemical*, 192(2014) 642-647.

[150] J. Li, X. Huang, J. Ma, S. Wei, H. Zhang, A novel electrochemical sensor based on molecularly imprinted polymer with binary functional monomers at Fe-doped porous carbon decorated Au electrode for the sensitive detection of lomefloxacin, *Ionics*, 26(2020) 4183-4192.

[151] Z. Jiang, G. Li, M. Zhang, A novel sensor based on bifunctional monomer molecularly imprinted film at graphene modified glassy carbon electrode for detecting traces of moxifloxacin, *RSC Advances*, 6(2016) 32915-32921.

[152] C. Ye, X. Chen, D. Zhang, J. Xu, H. Xi, T. Wu, et al., Study on the properties and reaction mechanism of polypyrrole@norfloxacin molecularly imprinted electrochemical sensor based on three-dimensional CoFe-MOFs/AuNPs, *Electrochimica Acta*, 379(2021).

[153] H. da Silva, J. Pacheco, J. Silva, S. Viswanathan, C. Delerue-Matos, Molecularly imprinted sensor for voltammetric detection of norfloxacin, *Sensors and Actuators B: Chemical*, 219(2015) 301-307.

[154] K. Alanazi, A. Garcia Cruz, S. Di Masi, A. Voorhaar, O.S. Ahmad, T. Cowen, et al., Disposable paracetamol sensor based on electroactive molecularly imprinted polymer nanoparticles for plasma monitoring, *Sensors and Actuators B: Chemical*, 329(2021) 129128.

[155] X. Liu, J. Zhong, H. Rao, Z. Lu, H. Ge, B. Chen, et al., Electrochemical dipyradamole sensor based on molecularly imprinted polymer on electrode modified with Fe<sub>3</sub>O<sub>4</sub>@Au/amine-multi-walled carbon nanotubes, *Journal of Solid State Electrochemistry*, 21(2017) 3071-3082.

[156] A. Pathak, B.D. Gupta, Ultra-selective fiber optic SPR platform for the sensing of dopamine in synthetic cerebrospinal fluid incorporating permselective nafion membrane and surface imprinted MWCNTs-PPy matrix, *Biosensors and Bioelectronics*, 133(2019) 205-214.

[157] W. Liu, F. Cui, H. Li, S. Wang, B. Zhuo, S. Wang, Three-dimensional hybrid networks of molecularly imprinted poly(9-carbazoleacetic acid) and MWCNTs for simultaneous voltammetric

determination of dopamine and epinephrine in plasma sample, *Sensors and Actuators B: Chemical*, 323(2020) 128669.

[158] A.M. Mahmoud, M.M. El-Wakil, M.H. Mahnashi, M.F.B. Ali, S.A. Alkahtani, Modification of N,S co-doped graphene quantum dots with p-aminothiophenol-functionalized gold nanoparticles for molecular imprint-based voltammetric determination of the antiviral drug sofosbuvir, *Microchimica Acta*, 186(2019) 617.

[159] M. Akhoundian, T. Alizadeh, M.R. Ganjali, F. Rafiei, A new carbon paste electrode modified with MWCNTs and nano-structured molecularly imprinted polymer for ultratrace determination of trimipramine: The crucial effect of electrode components mixing on its performance, *Biosensors and Bioelectronics*, 111(2018) 27-33.



## ***CHAPTER 2 OBJECTIVES***





## 2 Objectives

Herein, the general objective of the thesis is to synthesize MIPs materials through electropolymerization using pyrrole as functional monomer that are used to build MIPs-based electrochemical sensors. The prepared voltammetric sensors are intended to be used combined into sensor arrays to form the basis of ET systems. For this purpose, they will be combined with chemometric tools, mainly including PCA and ANN, in order to conduct the qualitative and quantitative analysis of pharmaceutical compounds. The specific objectives were divided into two major modules, described as following in details:

1. To develop an MIPs-based ET for the analysis of paracetamol, ascorbic acid, and uric acid in mixtures.
  - To synthesize three different  $pTS^-/PPy$  MIPs through electropolymerization, using  $pTS^-$  as doping counter ion and paracetamol, ascorbic acid, and uric acid as templates, respectively.

- To characterize the morphology, composition and electrochemical properties of *p*TS<sup>-</sup>/PPy MIPs.
  - To study the performance of *p*TS<sup>-</sup>/PPy MIPs-based sensors in the context of cross-response to the three APIs, stability and repeatability.
  - To build an *p*TS<sup>-</sup>/PPy MIPs-based ET for the qualitative and quantitative analysis of the three compounds.
  - To prove the applicability of *p*TS<sup>-</sup>/PPy MIPs-based ET in real scenarios.
  - To develop the application of the quantitative simultaneous determination, determining paracetamol, ascorbic acid, and uric acid in pharmaceutical products.
2. To develop an improved MIPs-based ETX by the incorporation of MIPs with nanomaterials for the analysis of fluoroquinolone antibiotics, by imprinting different antibiotics in equivalent PPy matrices. In this study case, gold nanoparticles and MWCNTs were incorporated to improve electroanalytical performance of the developed sensors.
- To electrochemically synthesize MIPs on the gold nanoparticles decorated MWCNTs, using ciprofloxacin, levofloxacin and moxifloxacin as templates, respectively.
  - To demonstrate the merits of the incorporation of MIPs with other advanced nanomaterials.
  - To optimize the experimental conditions for the electropolymerization and measuring conditions of analytes by MIPs-based sensors.
  - To investigate the ability of MIPs-based ET to discriminate and determinate different fluoroquinolone antibiotics.
  - To develop simultaneously quantitative application, to determine fluoroquinolone antibiotics in real samples.

## ***CHAPTER 3 EXPERIMENTAL***



## **3 Experimental**

The experimental section in this thesis is mainly related to two kinds of MIPs-based ET systems, that would be described systematically, covering the used reagents and instruments in experiments, the protocols of engineering the MIPs-based sensors, characterization and measuring techniques, the samples under study, and the methods of data analysis.

### **3.1 Reagents and instruments**

#### **3.1.1 Chemicals and buffers**

All solutions in the experiments were prepared using deionized water from a Milli-Q System (Millipore, Billerica, MA, USA). All involved reagents are analytical reagent grade and used directly without any further purification. The reagents' corresponding usage and manufacturers are presented in the Table 3.1.

Different buffer solutions were employed for various purposes in different

experiments. There are two main types of buffer solutions including phosphate-buffered saline solution (PBS) and acetate buffer. Their concentrations and pH values are distinctly set in order to meet the various experimental needs, which can be summarized with more details in Table 3.2. Besides, buffer solutions with a series of gradient pH values were adjusted by KOH and HCl solutions on the basis of PBS1 and acetate buffer1 for optimizing the measuring conditions.

**Table 3.1 Summary of the reagents used in the experiments.**

Usage	Reagent	Manufacturer	Article
GEC	graphite powder <sup>1</sup>	BDH Laboratory Supplies	Art.1 Art.2
	epoxy resin kit	Resineco green composites	Art.1 Art.2
Synthesis	pyrrole	Sigma-Aldrich and Alfa-Aesar	Art.1 Art.2
	<i>p</i> -toluenesulfonic acid ( <i>p</i> TS <sup>-</sup> ) sodium salt	Sigma-Aldrich	Art.1
	multi-wall carbon nanotubes <sup>2</sup>	SES Research Inc	Art.2
	anhydrous trisodium citrate	Alfa-Aesar	Art.2
	Gold (III) chloride solution in hydrochloric acid (HAuCl <sub>4</sub> , 30 wt.%)	Aldrich	Art.2
	sodium borohydride	Panreac	Art.2
	Nafion resin solution	Sigma	Art.2
	Sodium hydroxide	Scharlau	Art.2
	Ethanol, 96 vol. %	Scharlau	Art.2
	paracetamol	Sigma-Aldrich	Art.1
	ascorbic acid	Sigma-Aldrich	Art.1

Analytes	uric acid	Sigma-Aldrich	Art.1
	ciprofloxacin	Sigma	Art.2
	levofloxacin	Sigma	Art.2
	moxifloxacin	Sigma	Art.2
	flumequine	Sigma	Art.2
	nalidixic acid	Sigma	Art.2
Buffer solutions	acetic acid, 96 vol. %	Panreac	Art.2
	sodium acetate trihydrate	Panreac	Art.2
	potassium chloride	Sigma-Aldrich	Art.1 Art.2
	potassium hydrogenphosphate	Sigma-Aldrich	Art.1 Art.2
	potassium dihydrogenphosphate	Sigma-Aldrich	Art.1 Art.2
Probe solutions	potassium hexacyanoferrate (II)	Panreac	Art.1
	trihydrate		Art.2
	potassium hexacyanoferrate (III)	Panreac	Art.1 Art.2

<sup>1</sup> the particle size is less than 50  $\mu\text{m}$ ; <sup>2</sup> the outer diameter is in the range of 10 to 30nm.

**Table 3.2 Summary of the buffer solutions in the experiments.**

Buffer solution	pH	Concentration	Usage	Article
PBS 1	7.0	50 mM PBS 100 mM KCl	Measuring	Art.1
PBS 2	10.0	100 mM PBS	Synthesis	Art.2
Acetate buffer 1	3.5	100 mM acetate buffer	Synthesis	Art.2
Acetate buffer 2	4.5	100 mM acetate buffer	Measuring	Art.2



In addition, ferrocyanide redox pair was used as a probe to investigate the functionalization and electrochemical properties of the prepared electrodes. Particularly, the probe solution were prepared in the PBS1 containing 5.0 mM  $K_3[Fe(CN)_6]/K_4[Fe(CN)_6]$ .

### 3.1.2 Instruments

Autolab PGSTAT30 (Ecochemie, Netherlands) with a multichannel configuration associated with GPES Multichannel and FRA software packages was used for the electropolymerization and electrochemical measurements.

Scanning electron microscopy (SEM) and transmission electron microscopy (TEM) were performed using EVO MA10 (Zeiss, Oberkochen, Germany) operating at 30 kV and JEM1210 (Peabody, MA, USA) operating at 120 kV, respectively, for the morphological characterization.

## 3.2 Protocols for MIPs-based sensors and ETs

### 3.2.1 Fabrication of graphite epoxy composite electrode

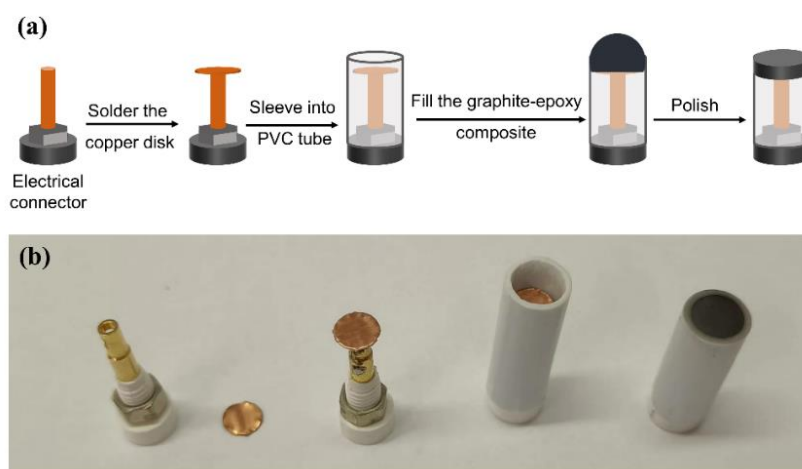


**Figure 3.1 (a) Schematic diagram of GEC's fabrication process, (b) The picture of GEC's components.**

The graphite epoxy composite (GEC) electrodes acted as the substrate for electropolymerization and platform for sensors, that was prepared according to the previous report [1]. The composite was obtained by mixing graphite with epoxy. Concretely, the combination of the hardener and the resin forms epoxy, in which the component ratio is 1/2 (w/w). The graphite was evenly blended with epoxy at a ratio of 42/58 (w/w).

GEC was fabricated through the protocol shown in Figure 3.1. Firstly, the customized electrical connector was soldered with a 5 mm diameter copper disk that was previously cut. Then, it was sleeved into a PVC tube of *ca.* 25 mm of length and 6 mm of inner diameter. Afterwards, filled the fully compacted composite into a PVC tube with a soldered connector. In order to dry the composite in the PVC tube, it was placed in the oven for 2 days at 40 °C. After completely drying, the electrodes were sequentially polished with different grit sandpapers from coarse to fine until the electrode's surface was smooth. Prior to use, the bare GEC electrodes were checked in probe solution by CV test.

### 3.2.2 Preparation of *p*TS<sup>-</sup>/PPy MIPs/GEC sensors

Three different *p*TS<sup>-</sup>/PPy MIPs/GEC sensors imprinted by paracetamol (PA), ascorbic acid (AA) and uric acid (UA) respectively were prepared through a generic routine. As presented in Figure 3.2, the construction of *p*TS<sup>-</sup>/PPy MIPs/ GEC sensor was achieved through the co-electropolymerization of functional monomer with template molecule directly on GEC surface [2].

For PA and AA, 0.02 M of them were mixed with 0.05 M pyrrole and 0.1 M *p*TS<sup>-</sup> in 20 mL aqueous solutions in a straightforward way. But for UA, given its inferior solubility in water, it was firstly dissolved in a 20 mL NaOH solution (pH 10.0) by stirring and sonicating, and then added pyrrole and *p*TS<sup>-</sup> into the filtered UA solution. In order to eliminate the influence of oxygen on the polymerization of pyrrole, the solutions were purged with nitrogen gas for 10 min before using. The

electropolymerization was conducted using CV technique on Autolab PGSTAT30. The cycling potential was set in the range of -0.6 V to +0.8 V vs. Ag/AgCl at a scan rate of 100 mVs<sup>-1</sup>. For the purpose of extracting the template molecules from the polymeric matrix, the electrodes were cycled 35 times in PBS at a scan rate of 50 mV s<sup>-1</sup> in the range of -0.6 V to +1.0 V vs. Ag/AgCl. The prepared electrodes were rinsed with Milli-Q water and kept in the fridge at 4 °C.

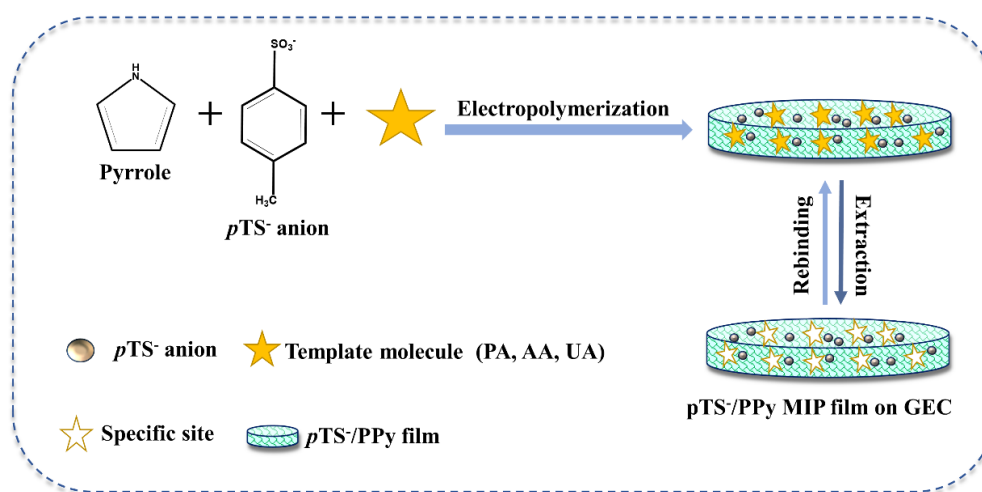


Figure 3.2 The synthesis routine of pTS/PPy MIPs/GEC sensors.

As control, the pTS/PPy NIP/GEC was also synthesized following the same procedure as pTS/PPy MIP/GEC, but without any template in the polymerization solution.

### 3.2.3 Preparation of MIP(FQs)@Au-fMWCNTs/GEC sensors

With the aim of improving the performance of MIPs used in sensors, MIPs were incorporated with MWCNTs and Au nanoparticles to obtain MIPs@Au-fMWCNTs/GEC sensors, that were prepared according to the routine in Figure 3.3.

It is known that the functionalized MWCNTs (fMWCNTs) facilitates the better properties than pristine MWCNTs. In this regard, the pristine MWCNTs were

carbonylated by the ultrasonic bath in an acid mixture of concentrated  $\text{H}_2\text{SO}_4/\text{HNO}_3$  (v/v=3/1) for 6h at 40 °C [3]. Afterwards, washed with Milli-Q water until the pH arrived at neutral. The cleaned fMWCNTs were dried in oven at 40 °C overnight.

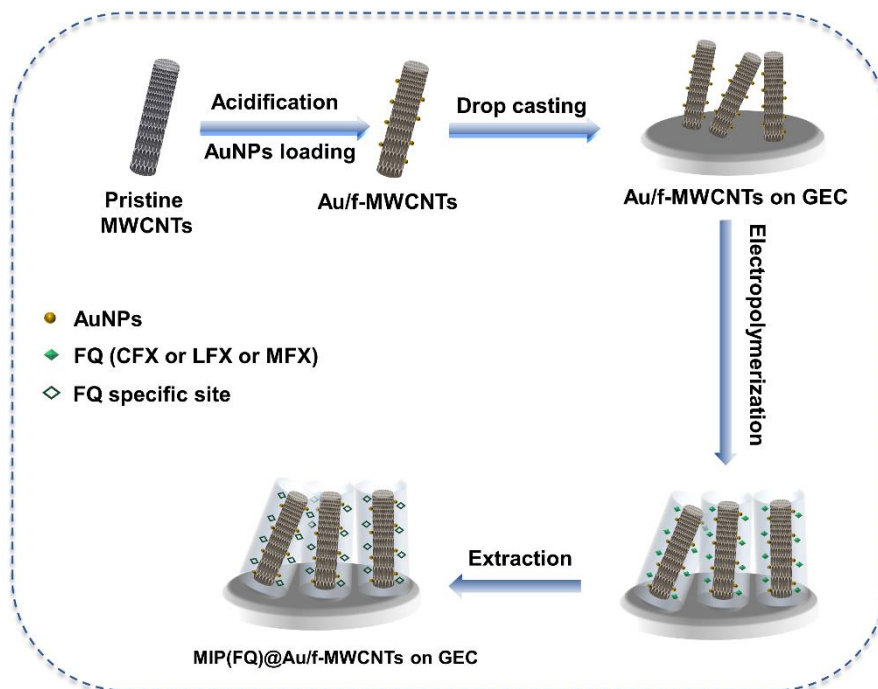


**Figure 3.3** The synthesis routine of MIP(FQs)@Au-fMWCNTs/GEC sensors.

Next, fMWCNTs were decorated with AuNPs based on the literatures [3,4]. Specifically, the mixture of 500  $\mu\text{L}$  of 10 mM  $\text{HAuCl}_4$ , 500  $\mu\text{L}$  of 10 mM tri-sodium citrate and 18.4 mL Milli-Q water was firstly stirred in a round-bottom flask, into which added 20 mg fMWCNTs and 10 mL anhydrous ethanol. After sonicating for 10 min, added 600  $\mu\text{L}$  of 100 mM freshly cold  $\text{NaBH}_4$  into the mixture. The reaction lasted 10h under continuously stirring. The obtained product (denoted as Au-fMWCNTs) was thoroughly washed by Milli-Q water and dried in oven at 40 °C overnight. In order to prepare the Au-fMWCNTs stock solution, 2.0 mg dried Au-fMWCNTs powder was well dispersed in 1 mL dimethyl formamide. To better stabilize Au-fMWCNTs on the surface of electrodes, 100  $\mu\text{L}$  Nafion was added and evenly mixed. Finally, 4  $\mu\text{L}$  of Au-fMWCNTs stock solution was evenly dropped onto the surface of GEC and dried in the

oven at 80 °C for 2h, obtaining Au-fMWCNTs/GEC.

The synthesis of MIPs film on the surface of Au-fMWCNTs/GEC (denoted as MIP(FQs)@ Au-fMWCNTs/GEC) was mainly performed by electrochemical method using FQ (either CFX, LFX, or MFX) as template. The solution containing 0.05 M pyrrole, 0.01M template and 20 mL acetate buffer (pH 3.5) was purged with nitrogen for 10 min. The electropolymerization was conducted by cycling the potential from 0.0 V to +1.3 V vs. Ag/AgCl at a scan rate of 50 mV·s<sup>-1</sup>. Subsequently, two steps were conducted for the purpose of extracting the template molecules from the polymer film. It was cycling the potential from 0.0 V to +1.5 V vs. Ag/AgCl at a scan rate of 100 mV·s<sup>-1</sup> in PBS, then followed the immersion into the mixture solution of EtOH/NaOH (v/v=1/1) for 30 min. The nearly same procedures as above-mentioned were used for the synthesis of non-imprinted polymer on Au-fMWCNTs/GEC as control but not added any FQ templates, denoted as NIP@Au-fMWCNTs/GEC. All produced sensors were kept in fridge at 4°C.

### 3.2.4 Construction of MIPs-based electronic tongues

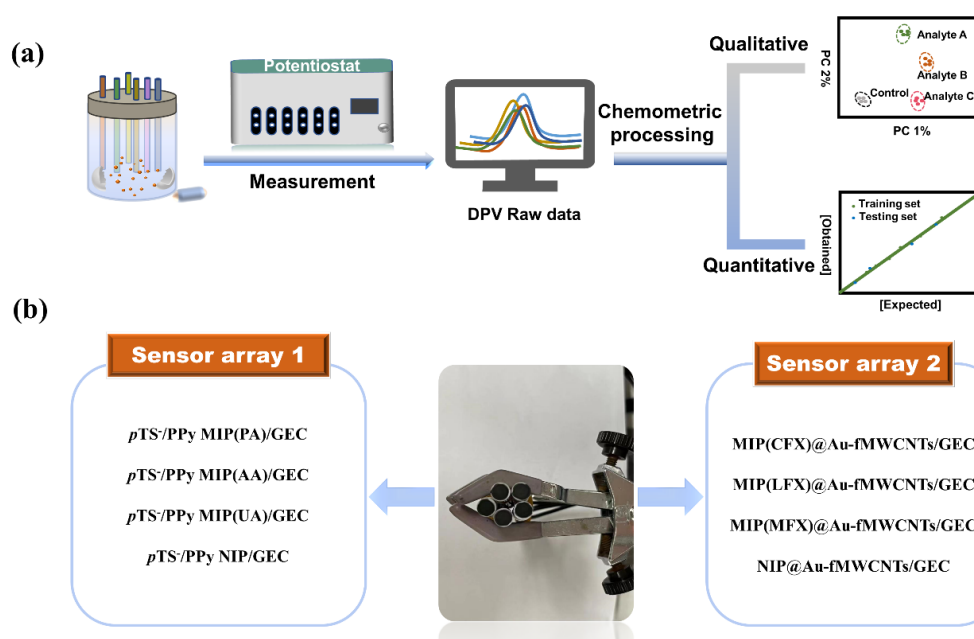


**Figure 3.4** (a) The construction of MIPs-based ETs, (b) the composition of the two sensor arrays in the built MIPs-based ETs.

Based on the above synthesized *p*TS<sup>-</sup>/PPy MIPs/GEC sensors or MIP(FQs)@Au-fMWCNTs/GEC sensors, two kinds of sensor arrays were formulated by the incorporation of sensors, displayed in Figure 3.4.

In order to construct MIPs-based ETs, the chemometric tools were combined with the sensor arrays. PCA and ANN were chosen for the qualification and quantification of pharmaceutical analytes.

### **3.3 Preparation of samples**

#### **○ Samples for characterization**

In the stage that the MIPs-based sensors were characterized in the context of cross-responses, linearity, sensitivity, limit of detection (LOD), stability, repeatability and PCA models building, the fresh stock solutions were prepared using in PBS or acetate buffer, depending on the solubility of different analytes in different media. And then, the intermediate working solutions at different concentrations were obtained by the proper dilution in PBS or acetate buffer. Concretely, the three target analytes in the Article 1, namely, PA, AA and UA were prepared and diluted in PBS, while the three target analytes in the Article 2, namely, CFX, LFX and MFX were prepared and diluted in acetate buffer.

#### **○ Samples for ANN models**

The ANN models were sought to build electronic tongue response models for the simultaneous determination multiple pharmaceuticals. To this end, a 3<sup>3</sup> tilted factorial design was proposed with 3 concentration levels and 3 factors. As exemplified in Figure 3.5, in the coordinate system, the three axes represent the concentrations of three different analytes to be determined. The concentration domains of for each analyte are related to the responding concentration of single sensor, detailed in Table 3.3. A set of samples prepared using the above-mentioned method in the characterization stage were divided into two groups: the training subset and the testing subset. The former is used to establish the response model, containing 27 samples. The latter distributed in the

concentration domains randomly for assessing the capacity of the built model and the sample number in this subset is approximately 10 to 12.

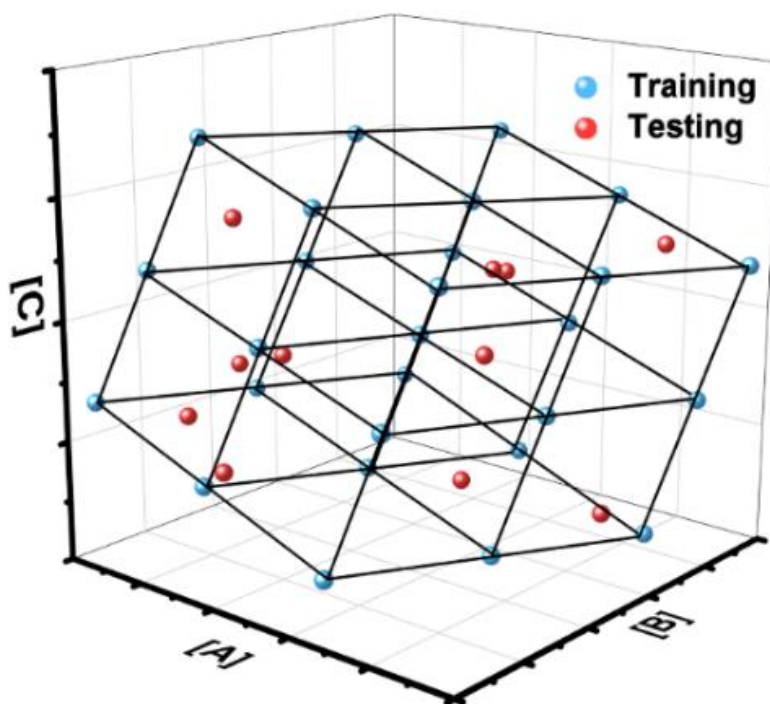


Figure 3.5 The graphical illustration of the training and testing subsets in ANN models.

Table 3.3 The concentration domain of each analyte in ANN models.

Article	Analytes	Concentration domain ( $\mu\text{M}$ )
<b>Art.1</b>	PA	0-50
	AA	0-1000
	UA	50-500
<b>Art.2</b>	CFX	0-300
	LFX	0-300
	MXF	0-300

### ○ Real samples

In order to investigate the applicability of the two built MIPs-based ETs in real-world scenario, the corresponding commercial tablets and spiked human urine samples

were analyzed. All commercial tablets used in the experiments were bought from the local pharmacy with the prescription from doctor if necessary, and human urine samples were collected from volunteers. The detailed information of the commercial samples is presented in Table 3.4.

**Table 3.4 The detailed information of commercial pharmaceuticals used in experiments.**

Article	Commercial sample	Compositions	Supplier
<b>Art.1</b>	<i>Efferaldol</i>	330 mg paracetamol, 200mg ascorbic acid	Bristol Myers Squibb, S.A., Madrid
	<i>Multicentrum</i>	Vitamins and minerals <sup>1</sup>	GlaxoSmithKline, Madrid
	<i>Redoxon</i>	1000 mg vitamin C, 10 mg zinc, 10 µg vitamin D	Bayer Hispania, S.L., Sant Joan Despí
<b>Art.2</b>	<i>Cetraxal plus</i>	3 mg/ml ciprofloxacin, 0.25 mg/ml fluocinolone acetoneide	Laboratorios SALVAT, S.A., Barcelona
	<i>Ciprofloxacin</i> <i>Normon</i>	250 mg ciprofloxacin	Normon Laboratories, S.A., Madrid
	<i>Levofloxacin</i> <i>Aurovitas</i>	500 mg levofloxacin	APL Swift Services Limited, Birzebugia
	<i>Moxifloxacin</i> <i>Qualigen</i>	400 mg moxifloxacin	Pharmathen, S.A., Attiki

<sup>1</sup> 800 µg vitamin A, 15 mg vitamin E, 100 mg vitamin C, 30µg vitamin K, 1.4 mg thiamine (vitamin B1), 1.75 mg riboflavin (vitamin B2), 2 mg vitamin B6, 2.5 µg vitamin B, 12, 5 µg vitamin D, 62.5 µg biotin (vitamin B7), folic acid (vitamin B9), 20 mg niacin (vitamin B3), 7.5 mg pantothenic acid (vitamin B5), 162 mg calcium, 125 mg phosphorous, 100 mg magnesium, 5 mg iron, 100 µg iodine, 500 µg copper, 2 mg manganese, 40 µg chromium, 50 µg molybdenum, 30 µg selenium and 5 mg zinc.



For the  $pTS^-/PPy$  MIPs/GEC ET, it was applied to determine PA, AA and UA in the three commercial tablets. Except that UA was spiked into the samples, the tablets were dissolved directly and diluted in PBS without any pre-treatment, to make sure the expected concentrations fall within the concentration domain of the built models.

Considering the urine excretion rate of FQ antibiotics [5], MIP(FQs)@Au-fMWCNTs/GEC ET was applied to determine CFX, LFX and MFX both in four commercial tablets and human urine samples. The tablets were dissolved directly and diluted without further pre-treatment in acetate buffer. The human urine samples were obtained by diluting the urine 40 times in acetate buffer, and then spiking with the CFX, LFX and (or) MFX.

### 3.4 Electrochemical measurements



**Figure 3.6** The picture of the equipment for the electrochemical measurements.

All electrochemical measurements were conducted in a standard three-electrode cell at room temperature, using an Autolab PGSTAT30 (Figure 3.6). An Ag/AgCl (3 M KCl), a Pt wire and the GECs modified with MIPs-based materials acted as reference electrode, counter electrode and working electrodes, respectively.

To investigate the different modification stages of  $pTS^-/PPy$  MIPs/GEC and MIP(FQs)@Au-fMWCNTs/GEC, stepwise electrochemical characterizations were

carried out through CV and EIS in a solution of 5 mM  $K_3[Fe(CN)_6]/K_4[Fe(CN)_6]$  in PBS [6,7]. Concretely, CV measurements were performed in the potential range from -0.2 V to +0.7 V at a scan rate of  $50\text{ mV s}^{-1}$ , and EIS were recorded in the frequency ranges of 50 kHz to 50 mHz or 100 kHz to 100 mHz with a fixed AC amplitude of 10 mV and an applied potential of +0.23 V or 0.24 V.

The performance of  $pTS^-/PPy$  MIPs/GEC sensors and  $MIP(FQs)@Au-fMWCNTs/GEC$  sensors was studied by DPV. To rebind the analytes with imprinted sites, enough incubation time is necessary before measuring. In addition, the regeneration for the MIPs is important after rebinding that was achieved by electrochemical means. In the case of the analysis of PA, AA and UA with  $pTS^-/PPy$  MIPs/GEC sensors, the potential ranged from -0.4 V to +0.8 V with a step potential of 5 mV and a pulse amplitude of 50 mV. The rebinding was done by immersing the sensors in the solution to be analyzed for 180 s under stirring, while the regeneration was done in PBS by applying a fix potential of +0.8 V on the sensors for 180 s. In the other case of the analysis of FQs with  $MIP(FQs)@Au-fMWCNTs/GEC$  sensors, the potential ranged from +0.6 V to +1.5 V with a step potential of 5 mV and a pulse amplitude of 50 mV. The rebinding was done by immersing the sensors in the solution to be analyzed for 300 s under stirring, while the regeneration was done in PBS by applying a fix potential of +1.2 V on the sensors for 90 s.

For building ETs and analyzing real samples, the measuring conditions were the same as the above-mentioned in the two cases.

### **3.5 Data analysis**

On the one hand, the raw data of characterizing MIPs-based sensors recorded by Autolab PGSTAT30 was converted and presented in Origin 2019b (OriginLab Corporation, Northampton, MA, USA), for final analysis.

On the other hand, the data of MIPs-based ETs was processed in Matlab 7.1 (MathWorks, Natick, MA, USA) with its Neural Network toolbox. Firstly, the complex

recorded voltammograms produced by sensor arrays were compressed to create coefficients using discrete cosine transform (DCT) [8]. The potential of the MIPs-based ETs to qualitative analysis of pharmaceuticals was evaluated by means of PCA, while ANNs acted as the modelling tool for the quantitative analysis.

## **References**

- [1] S. Alegret, J. Alonso, J. Bartoli, F. Cespedes, E. Martinez Fabregas, M. del Valle, Amperometric biosensors based on bulk-modified epoxy graphite biocomposites., *Sensors and Materials*, 8(1996) 147-153.
- [2] M. Wang, X. Cetó, M. Del Valle, A novel electronic tongue using electropolymerized molecularly imprinted polymers for the simultaneous determination of active pharmaceutical ingredients, *Biosensors and Bioelectronics*, 198(2022) 113807.
- [3] A. Cardosode Sá, A. Cipri, A. González-Calabuig, N. Ramos Stradiotto, M. del Valle, Resolution of galactose, glucose, xylose and mannose in sugarcane bagasse employing a voltammetric electronic tongue formed by metals oxy-hydroxide/MWCNT modified electrodes, *Sensors and Actuators B: Chemical*, 222(2016) 645-653.
- [4] Y. Shi, R. Yang, P.K. Yuet, Easy decoration of carbon nanotubes with well dispersed gold nanoparticles and the use of the material as an electrocatalyst, *Carbon*, 47(2009) 1146-1151.
- [5] Keith A. Rodvold, S.C. Piscitelli, New Oral Macrolide and Fluoroquinolone Antibiotics: An Overview of Pharmacokinetics, Interactions, and Safety, *Clinical Infectious Diseases*, 17(1993) S192–S199.
- [6] Z. Jiang, G. Li, M. Zhang, A novel sensor based on bifunctional monomer molecularly imprinted film at graphene modified glassy carbon electrode for detecting traces of moxifloxacin, *RSC Advances*, 6(2016) 32915-32921.
- [7] Z. Liu, M. Jin, H. Lu, J. Yao, X. Wang, G. Zhou, et al., Molecularly imprinted polymer decorated 3D-framework of functionalized multi-walled carbon nanotubes for ultrasensitive electrochemical sensing of Norfloxacin in pharmaceutical formulations and rat plasma, *Sensors and Actuators B: Chemical*, 288(2019) 363-372.
- [8] X. Cetó, S. Pérez, Voltammetric electronic tongue for vinegar fingerprinting, *Talanta*, 219(2020) 121253.



## ***CHAPTER 4 RESULTS AND DISCUSSION***



## 4 Results and discussion

As described in *Chapter 3*, a series of synthesis, characterization and measuring experiments were conducted, from which the experimental results were obtained. For the clearer analysis and presentation of all experimental data, it would be organized and discussed in two individual parts that correspond to two articles, respectively.

**Article 1:** M. Wang, X. Cetó, M. del Valle, A novel electronic tongue using electropolymerized molecularly imprinted polymers for the simultaneous determination of active pharmaceutical ingredients, *Biosensors and Bioelectronics*, 198 (2022) 113807.

**Article 2:** M. Wang, X. Cetó, M. del Valle, A sensor array based on molecularly imprinted polymers and machine learning for the analysis of fluoroquinolone antibiotics, *ACS Sensors*, submitted.





---

# Article 1

---

**A novel electronic tongue using electropolymerized molecularly imprinted polymers for the simultaneous determination of active pharmaceutical ingredients**

Mingyue Wang, Xavier Cetó, Manel del Valle

Biosensors and Bioelectronics 198 (2022) 113807



## **4.1 A novel electronic tongue using electropolymerized molecularly imprinted polymers for the simultaneous determination of active pharmaceutical ingredients**

As introduced in *Section 1.4.3.2*, PA and AA are the most common APIs in our daily life, and often they are used in combination to treat the common cold. However, their abuse and the deficiency of AA can pose threats to human health. Besides, as an important biomarker related to various diseases including gout, hyperuricemia, cardiovascular and kidney diseases, etc., UA's concentration in body fluids can be affected by the intake of AA. Due to the association between PA, AA and UA, in this article, the simultaneous determination of them is targeted through the strategy of incorporating *pTS*<sup>-</sup>/PPy MIPs sensors with chemometric models involving PCA and ANN, which constitutes an electronic tongue approach.

### **4.1.1 Synthesis of *pTS*<sup>-</sup>/PPy MIPs**

#### **4.1.1.1 Electropolymerization and extraction**

The synthesis of *pTS*<sup>-</sup>/PPy MIPs and NIP went through the electropolymerization of Py on the surface of GEC using CV technique in the presence of PA, AA, or UA, respectively, or in the absence of template. In Figure 4.1, from the left column, compared with *pTS*<sup>-</sup>/PPy NIP, it can be observed that PA, AA and UA take part in the electropolymerization process and show different characteristic shapes of CV curves. In order to produce imprinted sites, the templates trapped in polymeric matrix need to be removed by the electrochemical extraction also using CV method. From the right column, we can see that as the overoxidation of PPy happens, the characteristic shapes of *pTS*<sup>-</sup>/PPy MIPs attributed to the template molecules disappear gradually with the consecutive scans, until these resemble the *pTS*<sup>-</sup>/PPy NIP profiles, proving the

successful extraction of templates.

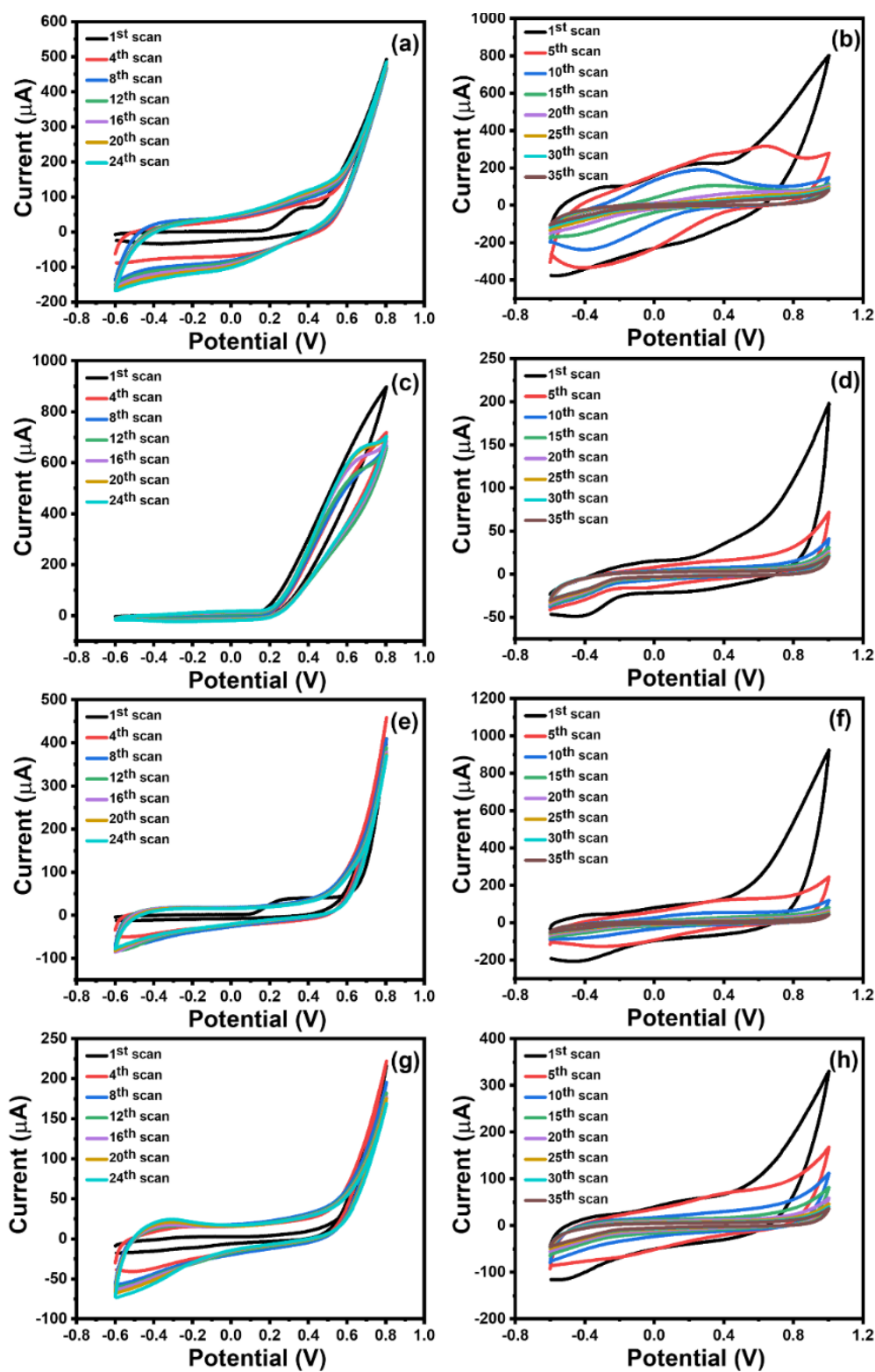


Figure 4.1 (Left) CV curves recorded during electropolymerization, (Right) CV curves recorded during template extraction.

#### 4.1.1.2 Optimization of scan number

The thickness of generated MIPs, that has an impact on the mass and charge transport, can be controlled by adjusting the scan number during electropolymerization. In this regard, the *p*TS<sup>-</sup>/PPy MIP(PA) and *p*TS<sup>-</sup>/PPy NIP with different scan numbers ranging from 8 to 40 cycles were attempted and their response to 30  $\mu$ M PA solution in PBS were measured. From Figure 4.2, it can be deduced that 24 cycles is the optimal number because of the ratio between the MIP and NIP is the highest under this condition.

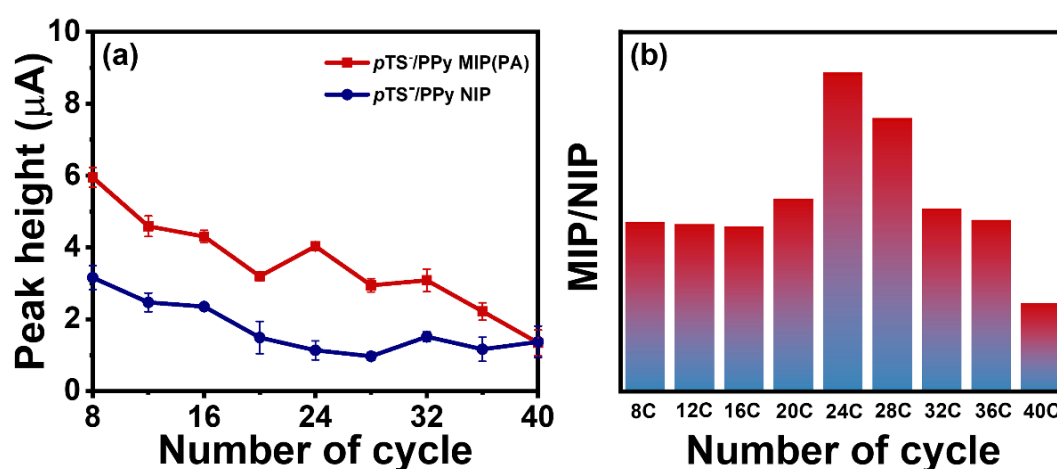


Figure 4.2 Optimization of scan number during the electropolymerization. (a) The comparison of the peak heights of *p*TS<sup>-</sup>/PPy MIP(PA) and *p*TS<sup>-</sup>/PPy NIP. (b) The peak height ratio of *p*TS<sup>-</sup>/PPy MIP(PA) to *p*TS<sup>-</sup>/PPy NIP.

### 4.1.2 *p*TS<sup>-</sup>/PPy MIPs-based sensors

#### 4.1.2.1 Morphological and electrochemical characterization

Taking *p*TS<sup>-</sup>/PPy MIP(PA) and *p*TS<sup>-</sup>/PPy NIP as the first two basic materials in this study, they were morphologically and electrochemically characterized. On the one side, to investigate the morphology of the sensors, the top and cross-section images of *p*TS<sup>-</sup>/PPy MIP(PA) and *p*TS<sup>-</sup>/PPy NIP were observed by SEM, shown in Figure 4.3. Both *p*TS<sup>-</sup>/PPy MIP(PA) and *p*TS<sup>-</sup>/PPy NIP films grew evenly on the surface of GEC,

but  $pTS^-/PPy$  MIP(PA) film is much rougher, which represents a larger specific surface area that is benefit for mass and charge transfer. Energy-dispersive X-ray spectrometry (EDX) was used to analyze the elemental composition, in which oxygen, nitrogen and sulfur were targeted, presented in Figure 4.3c and 4.3f.

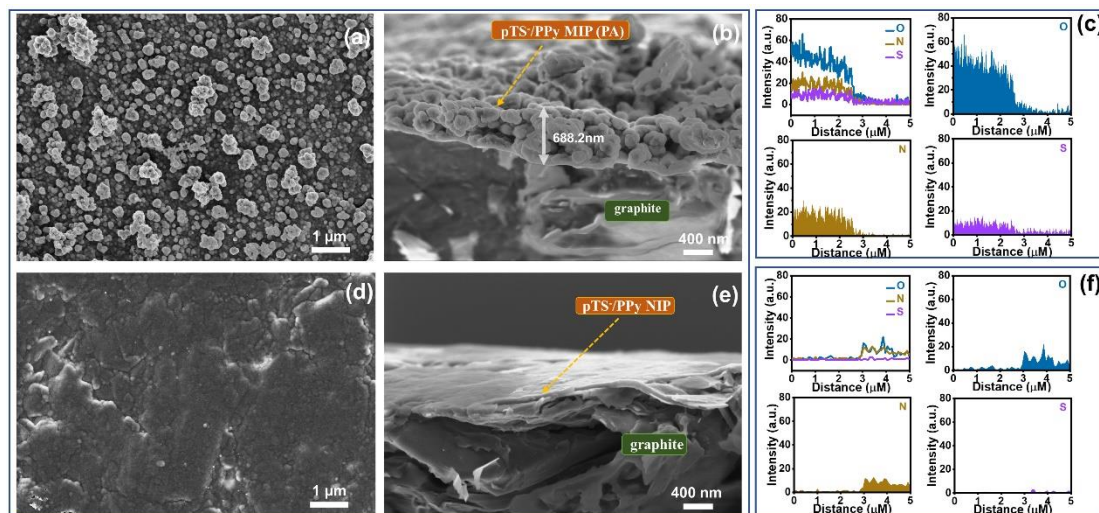


**Figure 4.3** SEM images of (a, b)  $pTS^-/PPy$  MIP(PA) and (d, e)  $pTS^-/PPy$  NIP. EDX data graphs of (c)  $pTS^-/PPy$  MIP(PA) and (f)  $pTS^-/PPy$  NIP.

On the other side, the modification process of  $pTS^-/PPy$  MIPs-based sensor was studied step by step through CV and EIS methods, using  $[Fe(CN)_6]^{3-/4-}$  solution as probe. As can be seen in Figure 4.4, comparing with bare GEC, the current in CV increases and  $R_{ct}$  in EIS decreases after the electropolymerization step, indicating the better electrochemical behavior. However, after the extraction of the template, the conductivity of  $pTS^-/PPy$  MIP(PA) and  $pTS^-/PPy$  NIP decreases probably due to the overoxidation of PPy. Notably,  $pTS^-/PPy$  MIP(PA) shows lower  $R_{ct}$  than  $pTS^-/PPy$  NIP, which can be attributed to the left cavities after the removal of PA. After rebinding with PA, the conductivity of  $pTS^-/PPy$  MIP(PA) further decreases because of the occupancy of the recognition cavities.

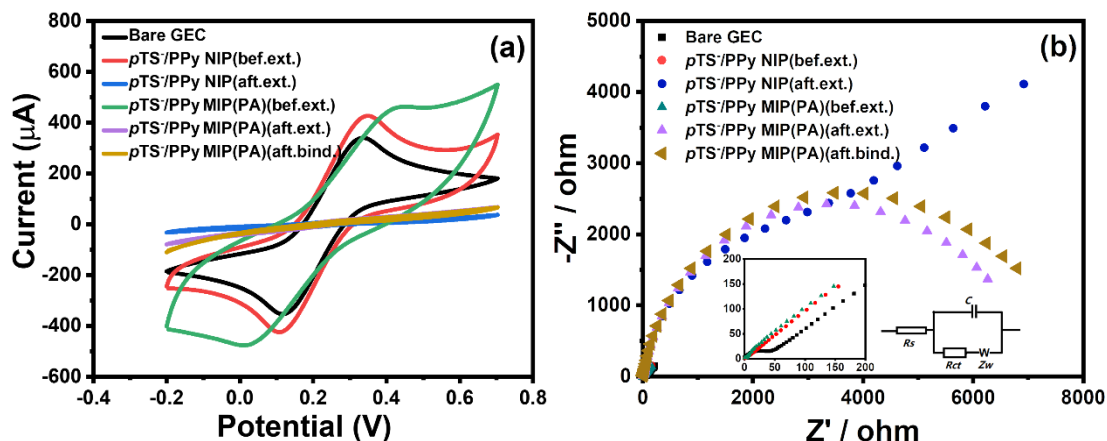


Figure 4.4 Stepwise measurements in a 5 mM  $[\text{Fe}(\text{CN})_6]^{3-/4-}$ , (a) CV and (b) EIS.

#### 4.1.2.2 Voltammetric response

The fully rebinding of analytes with the specific sites is important, where an incubation time has to be fixed. Therefore, before the voltammetric characterization, the condition of incubation time was optimized. As shown in Figure 4.5, the peak height of *p*TS/PPy MIP(PA) and *p*TS/PPy NIP gradually increases with the increase of incubation time until they almost arrive at the relatively steady value at 180s. Thus, the incubation time was set as 180s for following voltammetric measurements.

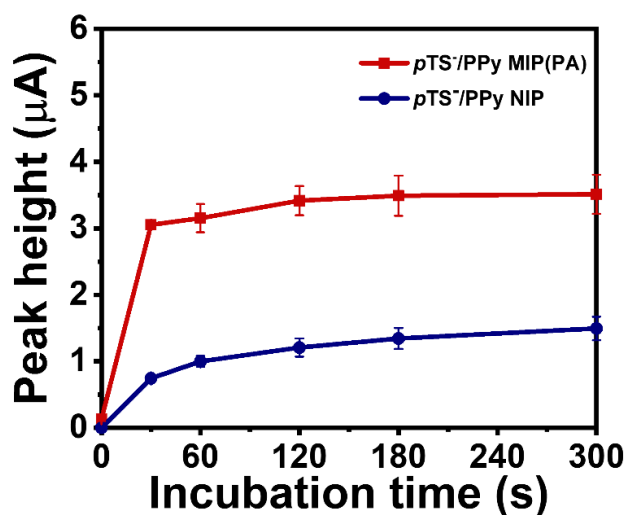


Figure 4.5 Optimization of incubation time.

The respective voltammetric responses of the three *p*TS/PPy MIPs and *p*TS/PPy NIP sensors to PA, AA and UA were measured using DPV method. From Figure 4.6, it



is obvious that the current peaks increase as the analytes' concentration increases. And based on the calculated peak height, the calibration plots were built. Figure 4.7 proves that each of *p*TS<sup>-</sup>/PPy MIPs and *p*TS<sup>-</sup>/PPy NIP sensors show good linear trends to PA, AA and UA with satisfactory correlation coefficients. Moreover, from Figure 4.8a and 4.8b, it can be observed that in the response to PA, *p*TS<sup>-</sup>/PPy MIP(PA) shows highest sensitivity among all sensors, while in the response to AA, *p*TS<sup>-</sup>/PPy MIP(AA) shows highest sensitivity. Nevertheless, this is not the case for UA, may due to the lower solubility of UA in the electrolyte solution of electropolymerization that ultimately leads to fewer specific sites in *p*TS<sup>-</sup>/PPy MIP(UA). Totally, except for the specificity of MIPs, there is still some degree of cross-response, which is fit for the ET approach.

In addition, according to the experimental results of the DPV measurements, a set of analytical parameters including specific details of LOD, sensitivity, linear range and correlation value are summarized, as presented in Table 4.1.

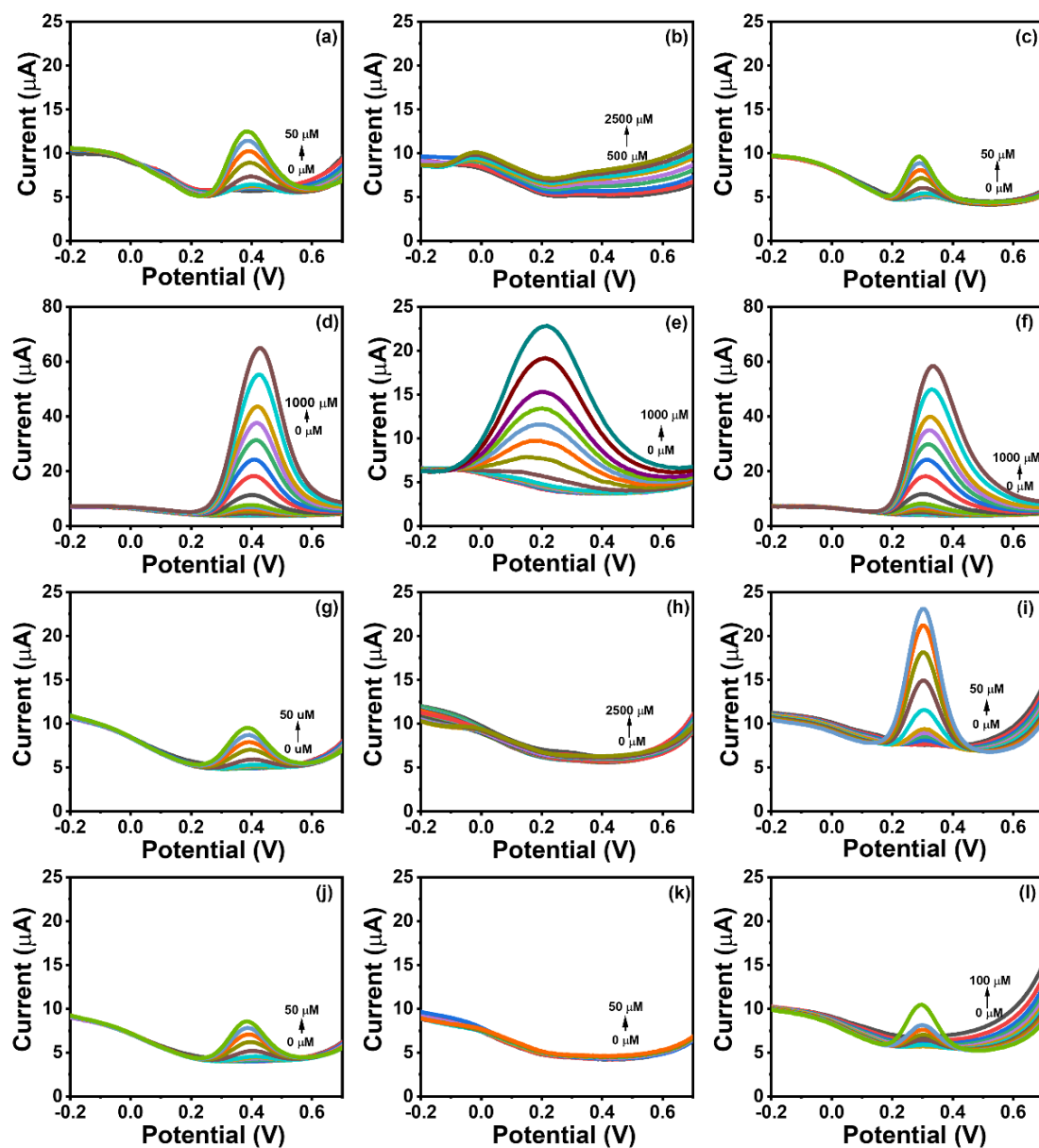


Figure 4.6 DPV curves of the three *pTS*/*PPy* MIPs and *pTS*/*PPy* NIP sensors to the three analytes. (a-c) *pTS*/*PPy* MIP(PA) to PA, AA and UA, (d-f) *pTS*/*PPy* MIP(AA) to PA, AA and UA, (g-i) *pTS*/*PPy* MIP(UA) to PA, AA and UA, (j-l) *pTS*/*PPy* NIP to PA, AA and UA.

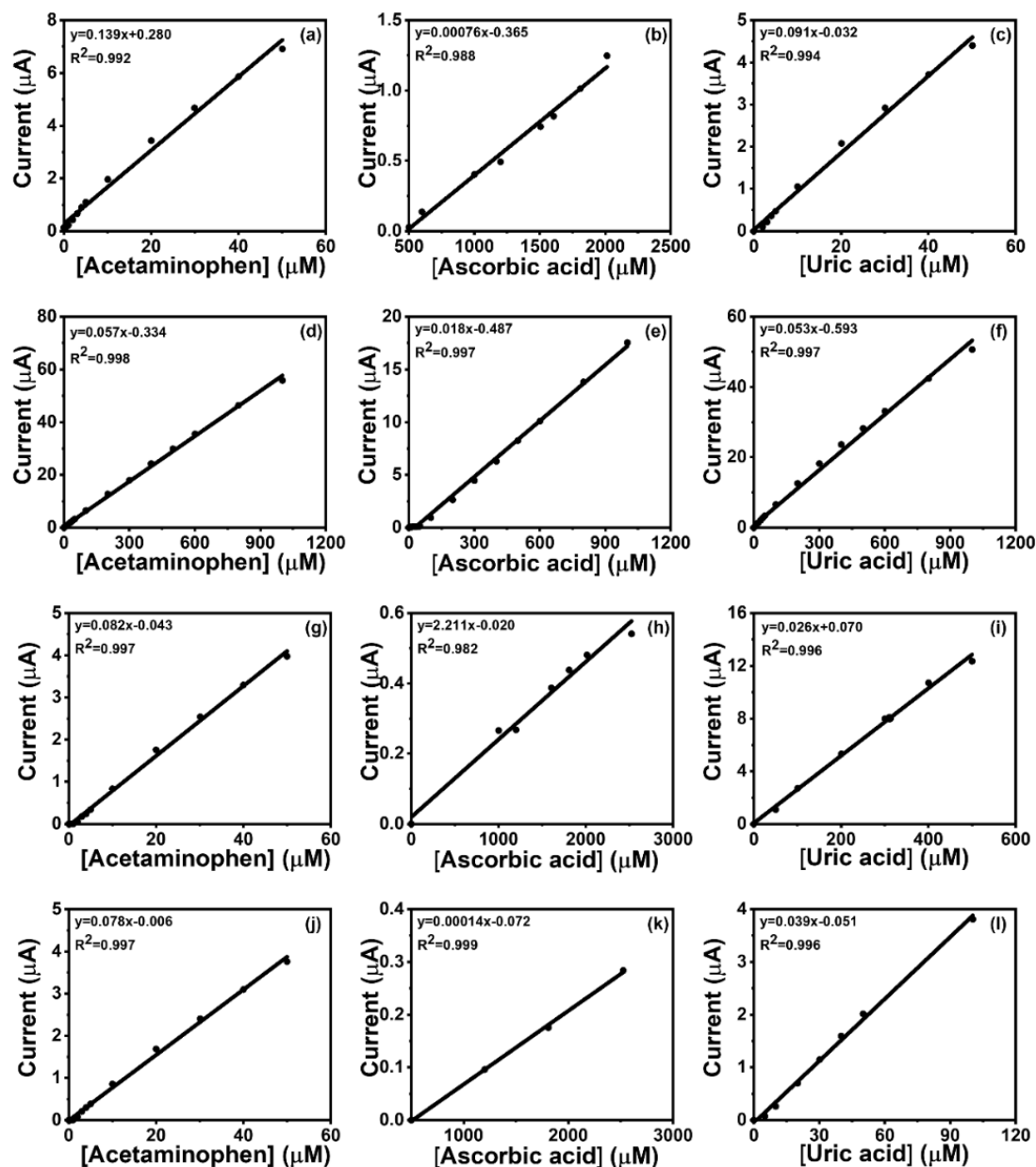


Figure 4.7 Calibration graphs of the three  $p\text{TS}/\text{PPy}$  MIPs and  $p\text{TS}/\text{PPy}$  NIP sensors to the three analytes. (a-c)  $p\text{TS}/\text{PPy}$  MIP(PA) to PA, AA and UA, (d-f)  $p\text{TS}/\text{PPy}$  MIP(AA) to PA, AA and UA, (g-i)  $p\text{TS}/\text{PPy}$  MIP(UA) to PA, AA and UA, (j-l)  $p\text{TS}/\text{PPy}$  NIP to PA, AA and UA.

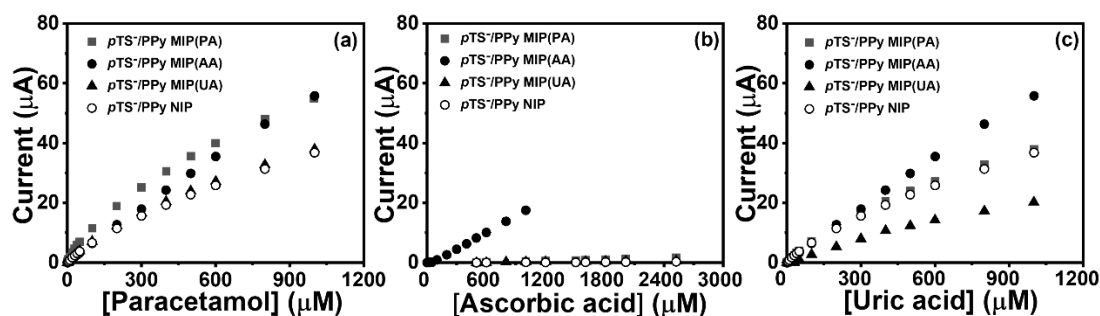


Figure 4.8 Calibration graphs of the three *pTS*/PPy MIPs and *pTS*/PPy NIP sensors to the three analytes. (a) paracetamol, (b) ascorbic acid and (c) uric acid.

Table 4.1 Analytical parameters of the different *pTS*/PPy MIPs and NIP sensors towards PA, AA and UA.

Sensor and Analyte	LOD ( $\mu\text{M}$ )	Sensitivity ( $\text{nA}\cdot\mu\text{M}^{-1}$ )	Linear range ( $\mu\text{M}$ )	Coefficient of determination ( $R^2$ )
<b><i>pTS</i>/PPy MIP(PA)/GEC</b>				
Paracetamol	1.828	139	0.5-50	0.992
Ascorbic acid	177	0.8	500-2000	0.988
Uric acid	1.9	91	2-50	0.994
<b><i>pTS</i>/PPy MIP(AA)/GEC</b>				
Paracetamol	177	57	1-1000	0.999
Ascorbic acid	19	18	5-1000	0.997
Uric acid	17	53	0.5-1000	0.997
<b><i>pTS</i>/PPy MIP(UA)/GEC</b>				
Paracetamol	1.3	82	0-50	0.997
Ascorbic acid	320	0.2	100-2500	0.983
Uric acid	24	26	50-500	0.996
<b><i>pTS</i>/PPy NIP/GEC</b>				
Paracetamol	1.1	78	0.5-50	0.997
Ascorbic acid	157	0.1	500-2500	0.999
Uric acid	3.1	39	5-100	0.996

### 4.1.2.3 Study of repeatability

Repeatability is a substantial feature of sensors, especially important for constructing an ET. To this end, the intra-day repeatability and inter-day repeatability were assessed for the developed sensors. Concretely, the intra-day repeatability was checked by consecutively measuring the responses of sensors to their corresponding template solutions for 30 times, while the inter-day repeatability was checked by measuring the same sensor in three consecutive days. It should be pointed out here that the sensors were cleaned after each measurement, as described in *Section 3.4*. In Table 4.2, all of values of RSD% are below 6.5% that demonstrates all of *pTS*<sup>-</sup>/*PPy* MIPs and *pTS*<sup>-</sup>/*PPy* NIP sensors have excellent repeatability.

**Table 4.2 Intra-day repeatability and inter-day repeatability of *pTS*<sup>-</sup>/*PPy* MIPs and *pTS*<sup>-</sup>/*PPy* NIP sensors.**

Sensor	intra-day (RSD%)	inter-day (RSD%)
<i>pTS</i> <sup>-</sup> / <i>PPy</i> MIP(PA)	3.5	4.1
<i>pTS</i> <sup>-</sup> / <i>PPy</i> MIP(AA)	3.3	4.6
<i>pTS</i> <sup>-</sup> / <i>PPy</i> MIP(UA)	5.9	6.2
<i>pTS</i> <sup>-</sup> / <i>PPy</i> NIP	6.1	6.5

### 4.1.3 *pTS*<sup>-</sup>/*PPy* MIPs-based ET

After characterizing the features and performance of the developed *pTS*<sup>-</sup>/*PPy* MIPs and *pTS*<sup>-</sup>/*PPy* NIP sensors, *pTS*<sup>-</sup>/*PPy* MIPs-based ET was built by integrating them into a sensor array to be combined with chemometric models. For the qualitative and quantitative analysis of APIs, PCA and ANN models were attempted respectively, before which a set of samples were measured by the sensor array and all registered voltammograms were compressed into 16 coefficients using DCT for the purpose of

reducing the complexity of the original signals.

#### 4.1.3.1 Qualitative analysis

First, a set of samples including PBS solution and five replicate 50  $\mu$ M solutions of PA, AA and UA were measured employing the sensor array under the optimized conditions. Then, the obtained voltammograms were dealt with DCT-PCA. Figure 4.9 shows the score plot for the analysis of the three APIs, and the cumulative variance accounts to 91.2% that proves almost all the variance in the original data is compressed into only the first two principal components. Furthermore, it is obvious that the different clusters related to different analytes are separated with each other either in PC1 or PC2, which means they can be clearly distinguished.

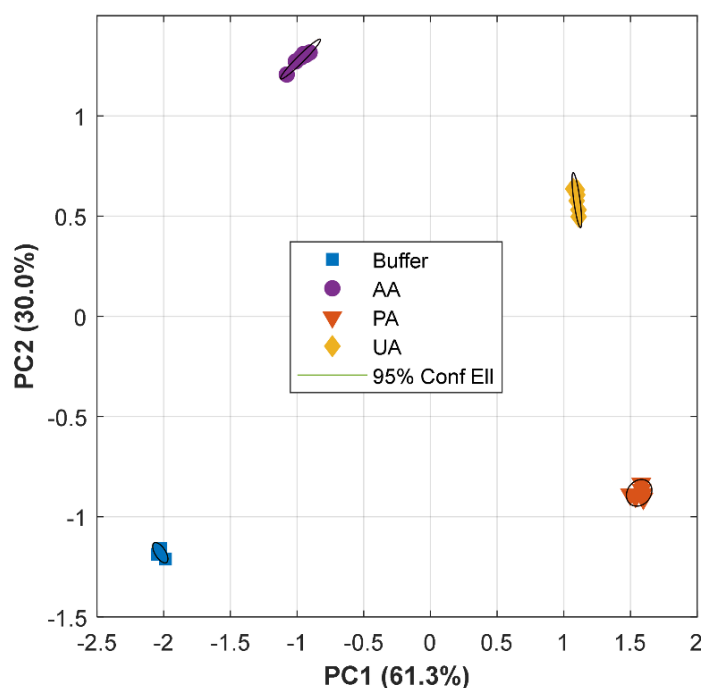
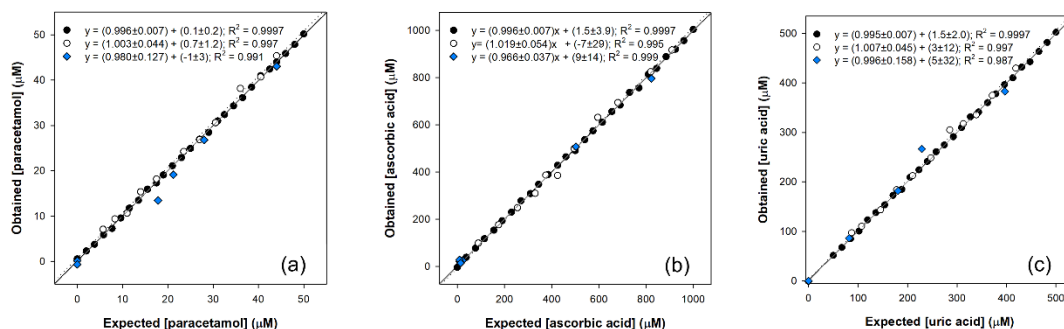


Figure 4.9 Score plot of the first two principal components for the analysis of PA, AA, UA.

#### 4.1.3.2 Quantitative analysis

As described in *Section 3.3*, in order to build the ANN model for the simultaneous determination of the three compounds, 38 samples were split into two subset and

measured in the optimized conditions. 27 samples were used for training the model, while the other 11 samples were used for assessing the ability of the model. The detailed modelling process can be seen in ANNEX, Article 1. Figure 4.10 and Table 4.3 illustrate the excellent performance of the built model.



**Figure 4.10 Modeling ability of the DWT-ANN. (a) PA, (b) AA and (c) UA. (●, solid line) training subsets, (○, dotted line) testing subsets, (◆) pharmaceutical samples and (dashed line) theoretical line:  $y = x$ .**

### 4.1.3.3 Real sample analysis

**Table 4.3 Analytical parameters of the three compounds in the pharmaceutical samples. Intervals are calculated at the 95% confidence level.**

Compound	Slope	Intercept (μM)	$R^2$	RMSE (μM)	Total NRMSE
PA	$0.980 \pm 0.127$	$-1 \pm 3$	0.991	2.28	
AA	$0.966 \pm 0.037$	$9 \pm 14$	0.999	15.2	0.0363
UA	$0.996 \pm 0.158$	$5 \pm 32$	0.987	18.2	

In order to demonstrate the applicability of the built ET, a series of commercial drugs were analyzed for evaluating the concentration of PA, AA, and spiked UA. The results are showed in the Table 4.3 that presents a satisfactory agreement between obtained and expected concentration values of the three compounds.

---

# Article 2

---

**A sensor array based on molecularly imprinted polymers and machine learning for the analysis of fluoroquinolone antibiotics**

Mingyue Wang, Xavier Cetó, Manel del Valle

**ACS Sensors, submitte**





## 4.2 A sensor array based on molecularly imprinted polymers and machine learning for the analysis of fluoroquinolone antibiotics

Fluoroquinolone (FQs) is one of important kinds of antibiotics in the clinical, poultry and aquaculture industries. For example, LFX and MFX are considered as respiratory quinolones that have good bactericidal activity against most of respiratory pathogens, while CFX is used to treat the infections of urinary tract and intestine. Nevertheless, the abuse of FQs has led to severe issues, such as antibiotic residues in food and/or antimicrobial resistance. Thus, FQs monitoring is demanded in different stages, such as in pharmaceutical factories when produced, in hospitals during its administration to the patients or in the environment for the treatment of wastewater. However, as shown in Figure 4.11, different FQs are derived from nalidixic acid (NA), sharing the same quinoline ring, but having different substitutions made to it, which begets the structural similarity of FQs that makes the simultaneous analysis more difficult. Therefore, this article mainly works on developing a voltammetric ET for the simultaneous analysis of FQs.

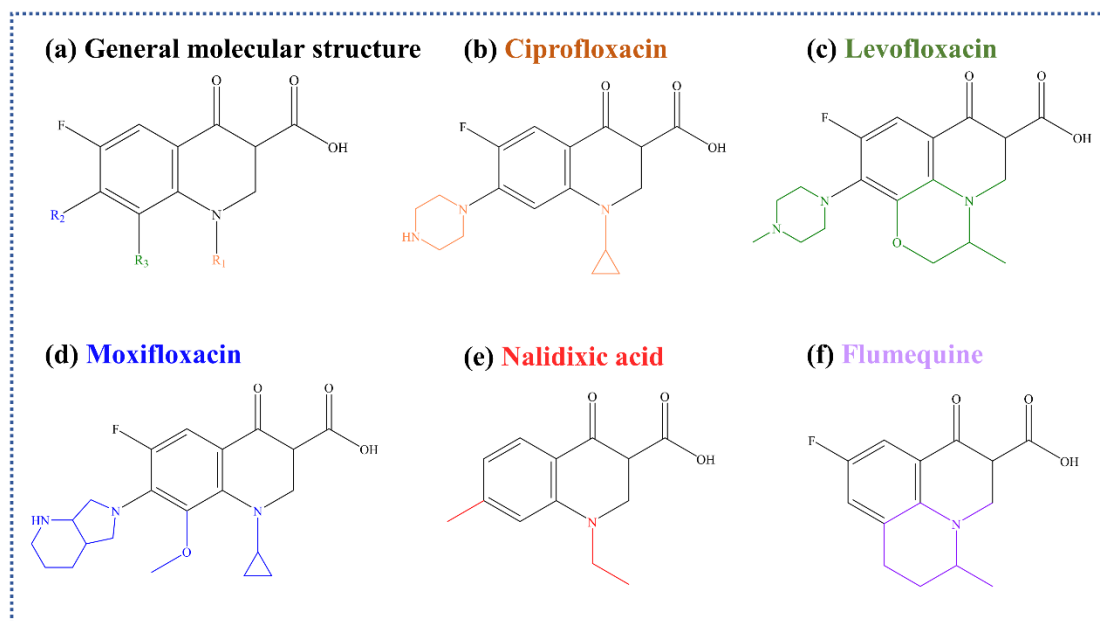


**Figure 4.11 Molecular structure of different FQs antibiotics.**

As described in *Section 3.2.3*, after the drop casting of Au-fMWCNTs onto the surface of GEC, the MIP (FQs) films were obtained by electropolymerizing Py on Au-fMWCNTs/GEC in the presence of each of the different FQs. Take the formation of MIP(CFX) as the studied case, the effects of different factors on MIP (FQs) films were investigated in terms of the thickness of film and the number specific site through electropolymerization method.

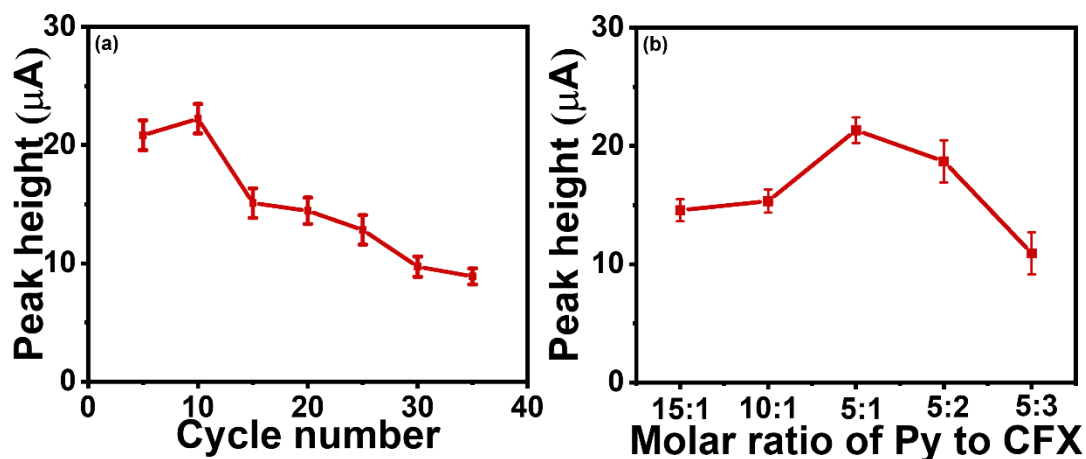


**Figure 4.12** Effects of (a) scan number and (b) the ratio of the monomer to template during the electropolymerization.

Concretely, the thickness of MIP(FQs) film can be adjusted by changing the scan number of CV during electropolymerization. As presented in Figure 4.12a, in the range of 5 to 35, the highest peak height shows when the scan number is 10, thus that was deduced as the optimal. Besides, the number of specific sites can be adjusted by changing the added amount of template. The lower amount of the added template in the electrolyte of electropolymerization leads to the limited number of specific sites, while too high amount may decrease the stability of the formed MIP(FQs). From the plot in Figure 4.12b, the optimal molar ratio of pyrrole to template is 5 to 1.

## 4.2.1 MIP(FQs)@Au-fMWCNTs based sensors

### 4.2.1.1 Morphological characterization

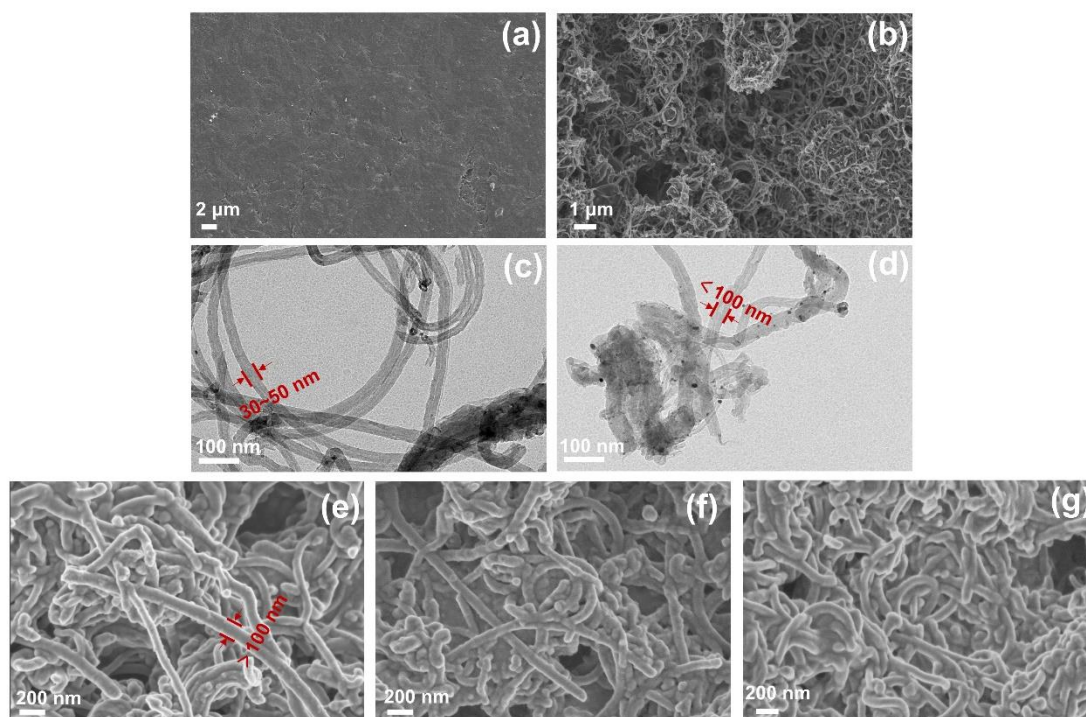


**Figure 4.13** SEM images of (a) bare GEC, (b) Au-fMWCNTs, (e) MIP(CFX)@Au-fMWCNTs before template extraction, (f) MIP(CFX)@Au-fMWCNTs after template extraction and (g) NIP@Au-fMWCNTs. TEM images of (c) pristine MWCNTs and (d) Au-fMWCNTs.

The morphology of different electrode materials was observed by SEM and TEM. By the clear contrast of Figure 4.13a and Figure 4.13b, it can be seen that the attachment of Au-fMWCNTs on GEC produces a 3D structure, increasing the porosity and specific surface area. Compared with Figure 4.13c showing TEM image of pristine MWCNTs, Figure 4.13d presents that there are some particles onto the MWCNTs, which is attributed to the decoration of AuNPs. In addition, the increases of the diameter of Au-fMWCNTs can be seen from Figure 4.13e to 4.13f that is ascribed to the growth of the MIP or NIP films on the surface.

### 4.2.1.2 Electrochemical characterization

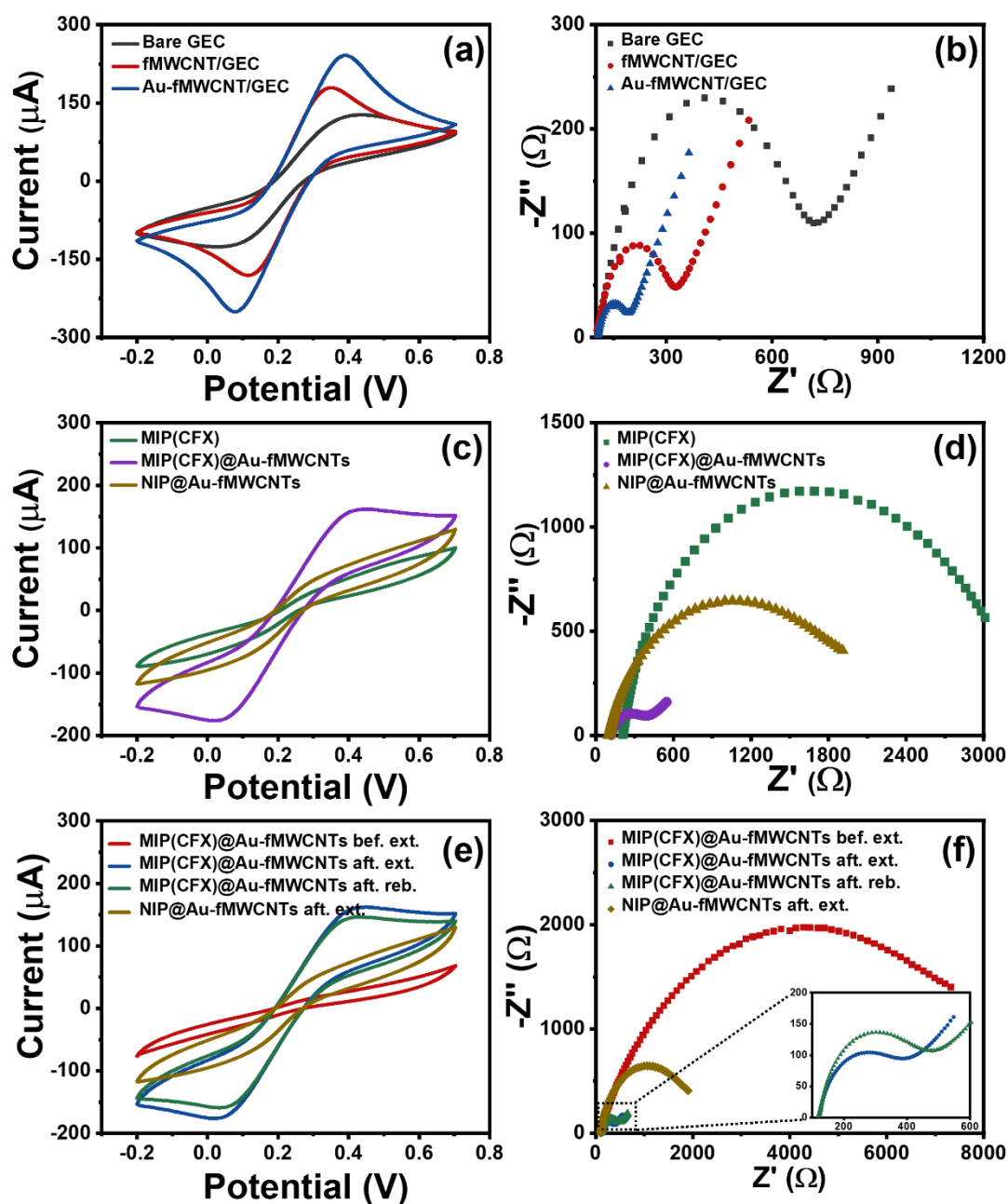


**Figure 4.14** Stepwise electrochemical characterization of sensors in the solution of 5 mM  $[\text{Fe}(\text{CN})_6]^{3-/4-}$  through CV and EIS.

The modification process of the sensors was investigated by CV and EIS using  $[\text{Fe}(\text{CN})_6]^{3-/4-}$  as probe. Firstly, Figure 4.14a and 4.14b present the improvement of the sensor's electrochemical behavior result from MWCNTs and AuNPs, based on the larger CV curves' profile and the smaller charge transfer impedance. Secondly, as

shown in Figure 4.14e and 4.14f, compared before and after the template extraction, there are obvious improvements of the electrochemical behavior both in the CV and EIS because the sites created during the extraction process facilitate the electron and mass transport. Thirdly, the rebinding of specific sites in the MIP film with the template contributes to the sluggish diffusion due to the "gate-controlled effect" that is clearly also reflected.

### 4.2.1.3 Optimization of measuring condition

In order to better investigate the response of MIP(FQs)@Au-fMWCNTs based sensors to FQs, various measuring conditions were optimized in the aspects of the pH of measured solution, incubation time before measuring and regeneration time after measuring.

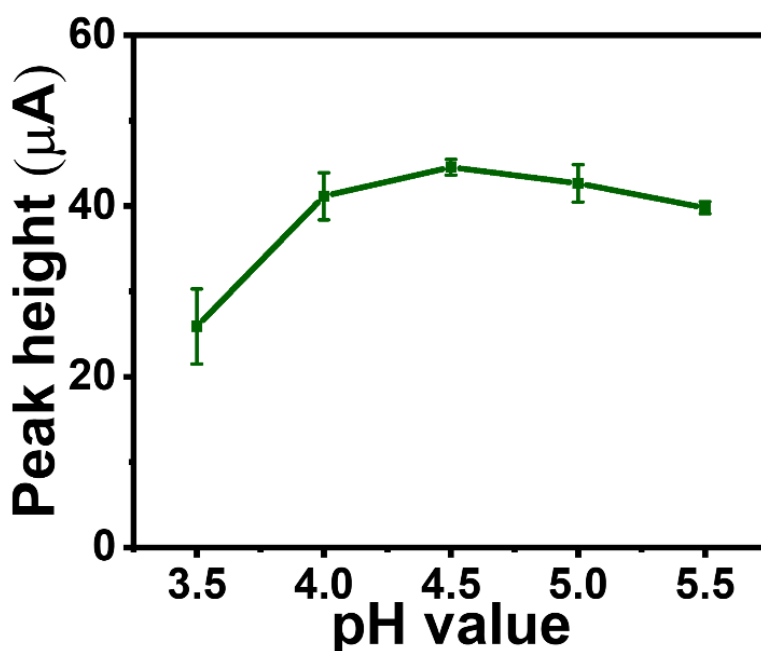


Figure 4.15 Effect of the pH during measurements.

Given the good solubility of FQs in acetate buffer, thus acetate buffer was chosen as the measuring media and the effect of its pH was studied in the range from 3.5 to 5.5. According to the recorded response peak height of MIP(CFX)@Au-fMWCNTs sensor

to 10  $\mu\text{M}$  CFX, pH 4.5 is taken as the optimal for measuring (Figure 4.15).

In order to make sure the sufficient absorption of MIP site to template, an adequate incubation time is essential. To this end, it was also tested by measuring the response of MIP(CFX)@Au-fMWCNTs sensor to 10  $\mu\text{M}$  CFX after immersing sensor into the solution under continuously stirring. From Figure 4.16a, 300s is considered as the proper. Besides, the sensor's regeneration was done by an electrochemical treatment in 0.1 M PBS (pH 10) and the effect of regeneration time was also studied. Although for the measurement of a 10  $\mu\text{M}$  CFX solution, 30 s is enough to recover the baseline (Figure 4.16b), but 90 s is chosen as the regeneration time for further experiments to ensure that proper regeneration is achieved even when higher target concentrations are measured.

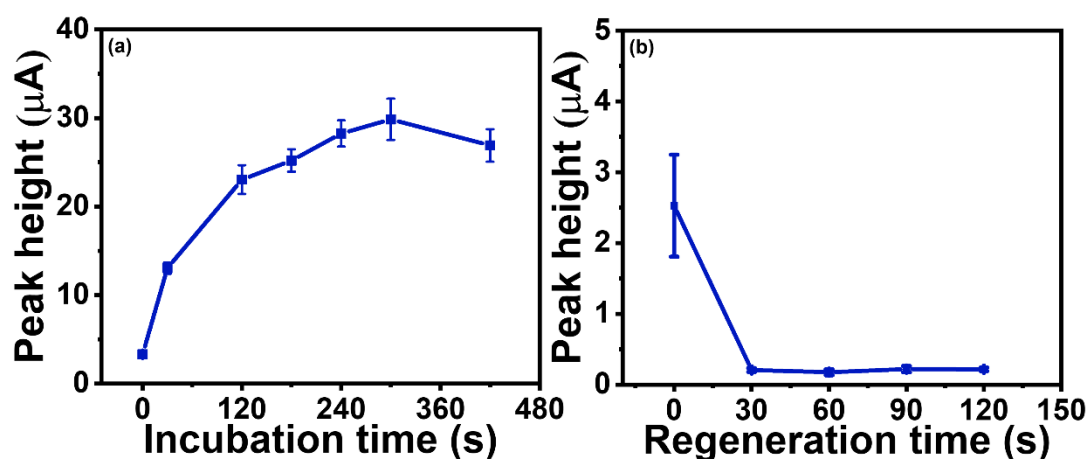
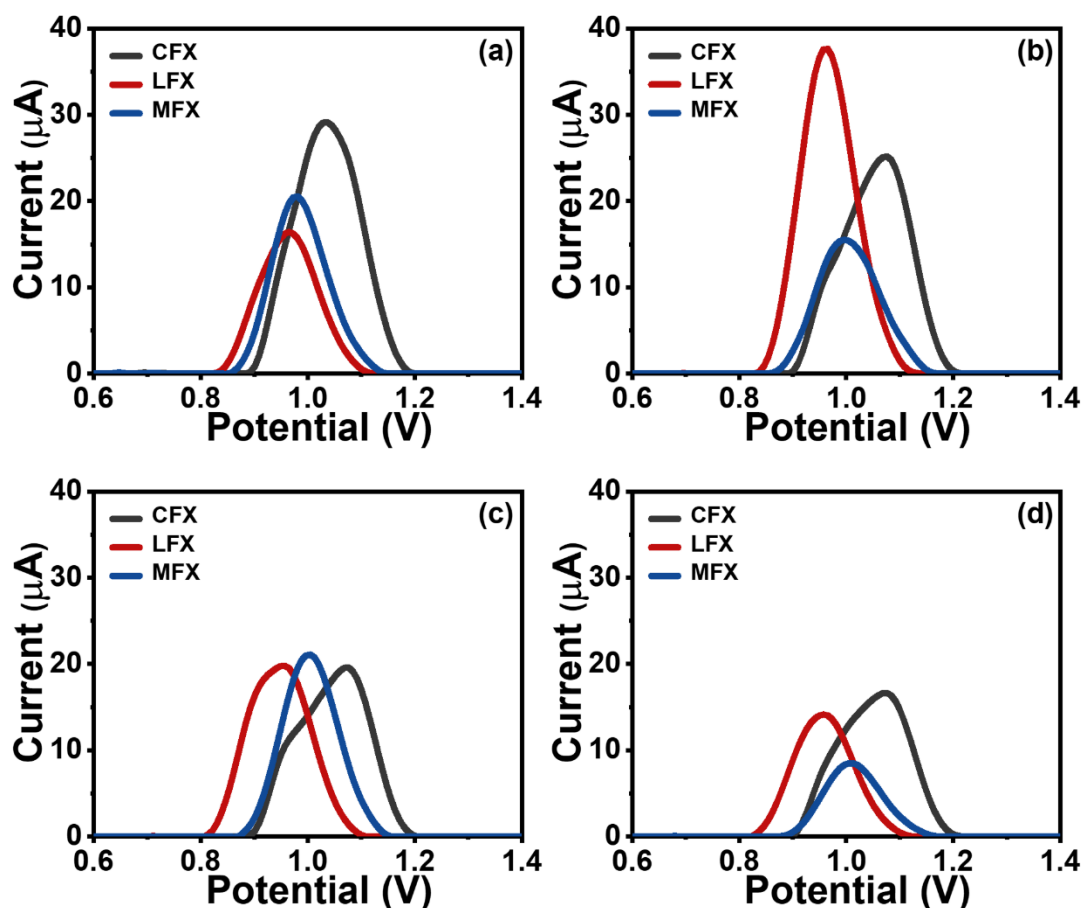


Figure 4.16 Effects of (a) incubation time before measuring and (b) regeneration time after measuring.

#### 4.2.1.4 Voltammetric response

Voltammetric responses of the three MIP(FQs)@Au-fMWCNTs and NIP@Au-fMWCNTs sensors towards various FQs were studied by DPV measurements under the optimized conditions. The DPV curves in Figure 4.17 depict that different sensors show different responses towards various FQs. As expected, among all four sensors, NIP@Au-fMWCNTs has the lowest response to CFX, LFX, and MFX, due to the lack of the specific sites. Moreover, the fact should be pointed out that all of three

MIP(FQs)@Au-fMWCNTs show the highest response to their respective template compounds, especially in the cases of MIP(CFX)@Au-fMWCNTs and MIP(LFX)@Au-fMWCNTs, which demonstrates the certain specificity of MIPs. However, in the case of MIP(MFX)@Au-fMWCNTs, its response to MFX is not as significantly higher, owing to the intrinsically higher electrochemical response of the other FQs, as is shown in the case of NIP@Au-fMWCNTs (Figure 4.17d).



**Figure 4.17** Baseline corrected DPV curves of different sensors towards 10  $\mu$ M FQs solutions. (a) MIP(CFX)@Au-fMWCNTs, (b) MIP(LFX)@Au-fMWCNTs, (c) MIP(MFX)@Au-fMWCNTs and (d) NIP@Au-fMWCNTs.

What's more, to evaluate the linear relationship between different sensor and different FQs, a set of DPV measurements were conducted as the increase of the FQs' concentration. From Figure 4.18, it can be seen that the peak currents increase steadily with increasing FQs' concentration. Based on Figure 4.19, the Langmuir model can be built, from which dissociation constant ( $k_D$ ) and the maximum binding response at



saturation ( $B_{\max}$ ) were calculated (Table 4.4).

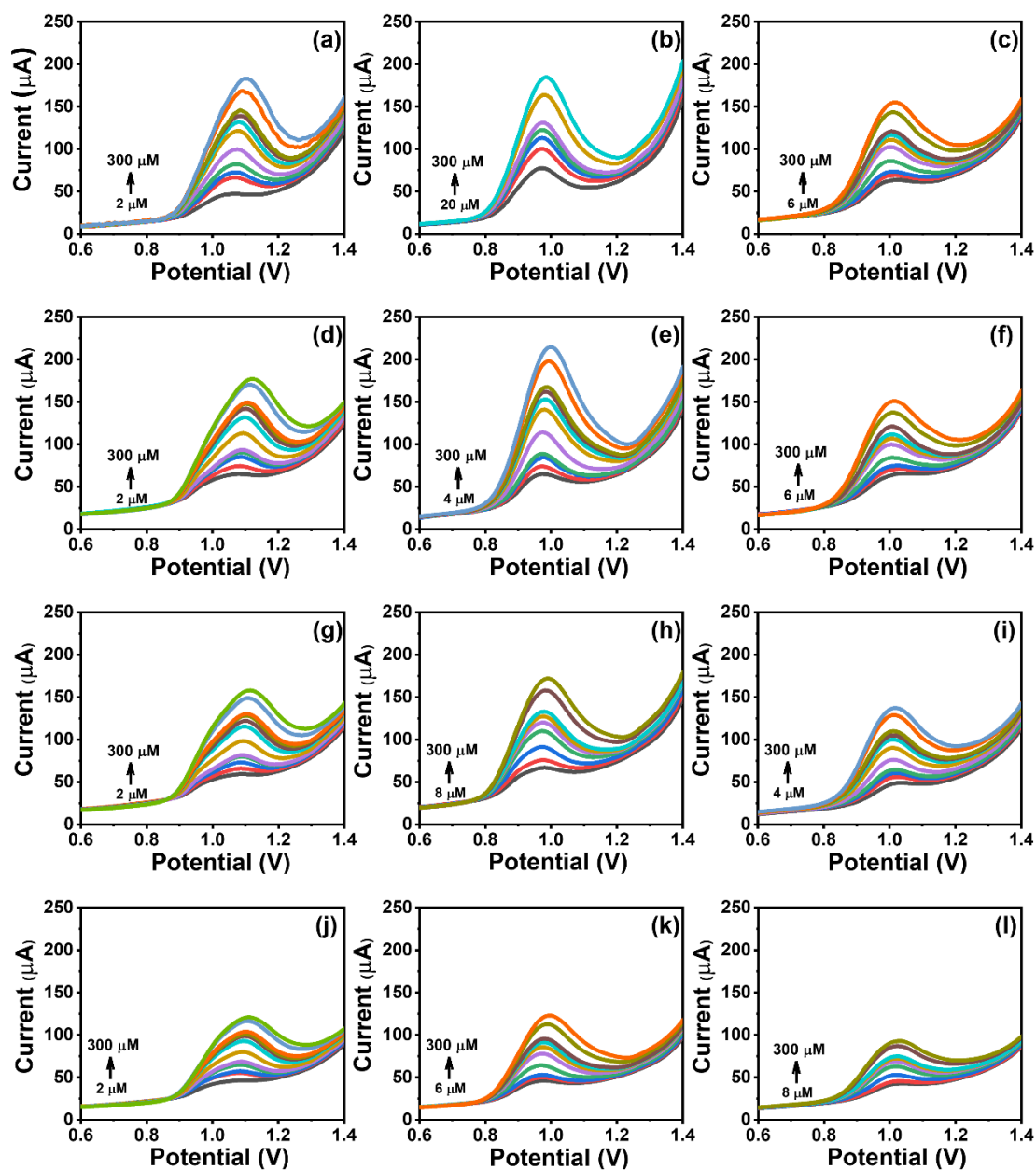


**Figure 4.18** DPV curves in the corresponding linear concentration range of (a-c) MIP(CFX)@Au-fMWCNTs towards CFX, LFX and MFX (d-f) MIP(LFX)@Au-fMWCNTs towards CFX, LFX and MFX (g-i) MIP(MFX)@Au-fMWCNTs towards CFX, LFX and MFX and (j-l) NIP@Au-fMWCNTs towards CFX, LFX and MFX.

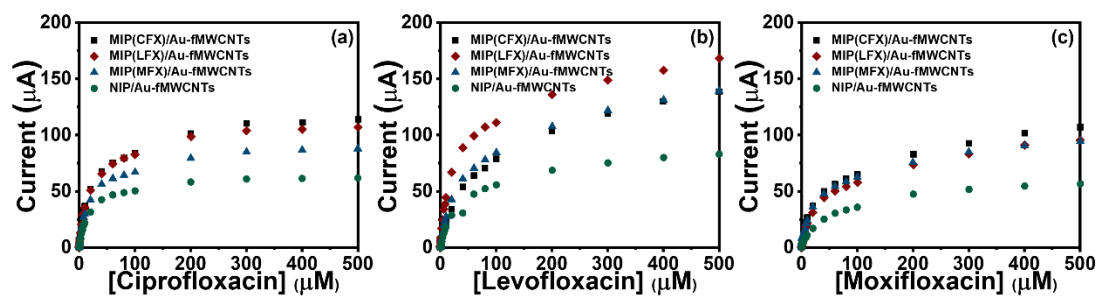


Figure 4.19 Calibration plots of sensors towards the three FQs.

Table 4.4 Analytical parameters of MIP(FQs)@Au-fMWCNTs sensors towards the three FQs calculated from DPV measurements.

Analyte	Sensor	$B_{\max}$ ( $\mu\text{A}$ )	$K_D$ ( $\mu\text{M}$ )
CFX	MIP(CFX)@Au-fMWCNTs	114	23.4
	MIP(LFX)@Au-fMWCNTs	108	22.3
	MIP(MFX)@Au-fMWCNTs	88.1	21.7
	NIP@Au-fMWCNTs	63.2	19.5
LFX	MIP(CFX)@Au-fMWCNTs	155	3.76
	MIP(LFX)@Au-fMWCNTs	165	33.2
	MIP(MFX)@Au-fMWCNTs	148	60.9
	NIP@Au-fMWCNTs	89.0	53.6
MFX	MIP(CFX)@Au-fMWCNTs	109	49.0
	MIP(LFX)@Au-fMWCNTs	99.4	54.2
	MIP(MFX)@Au-fMWCNTs	94.5	37.3
	NIP@Au-fMWCNTs	61.8	59.9

## 4.2.2 MIP(FQs)@Au-fMWCNTs based ET

Considering the limited specificity of MIP(FQs)@Au-fMWCNTs based sensor that rather can provide a class-selectivity to FQs than the high selectivity to each FQ, a novel ET was fabricated by incorporating modelling tools, such as PCA and ANN, with a sensor array composed by the produced three different MIP(FQs)@Au-fMWCNTs and one NIP@Au-fMWCNTs sensors.

### 4.2.2.1 Qualitative analysis

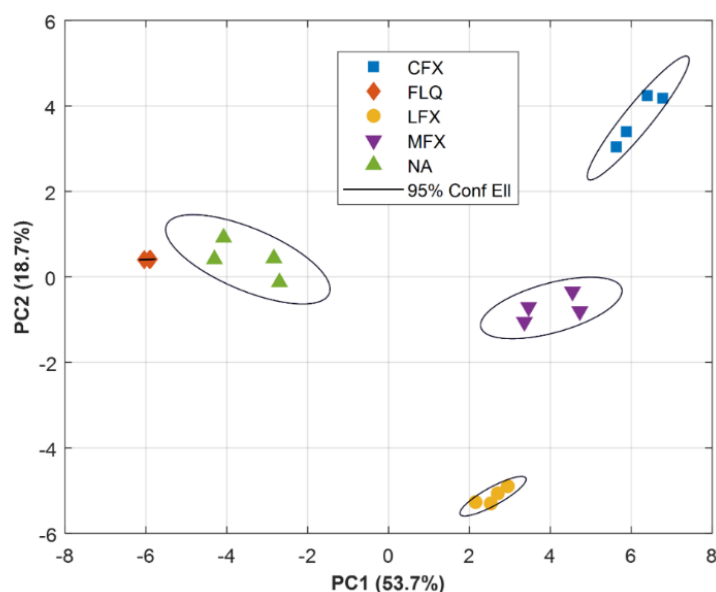


**Figure 4.20** Score plot of the first two principal components of five different FQs.

As shown in Figure 4.17, common MIPs sensor cannot effectively differentiate various FQs sharing similar nature and structure, because of severe overlapping of signals. To tackle this issue, the strategy combining chemometrics with MIPs was proposed. Specifically, the stock solutions of five different FQs were measured employing the assembled sensor array under the optimized conditions. The obtained voltammetric responses were compressed by means of DCT, and then submitted to PCA. From Figure 4.20, we can firstly see that ca. 72.4% of the original data variance is now condensed into only two first principal components (PCs), allowing to assess the samples' (dis)similarities easily. In addition, it can be noticed how different the clusters corresponding to each of the FQs are, and how these clusters separate from each other. Hence, the superb ability of MIP(FQs)@Au-fMWCNTs based ET to discriminate FQs is demonstrated, thanks to the complex and high dimensional multichannel information used.

### 4.2.2.2 Quantitative analysis

With the aim of quantification of CFX, LFX, MFX in the mixtures, a set of samples described in *Section 3.3* were measured using the sensor array under the same conditions as previous. After data compression by DCT, ANN model was built through the training subset, and assessed through testing subset. Figure 4.21 presents the comparison graphs of predicted vs. expected concentrations of the three FQs, both for the training and testing subsets. It can be deduced from the good results and data in Figure 4.21 that the built ET is able to quantify the three FQs individually in the mixtures.

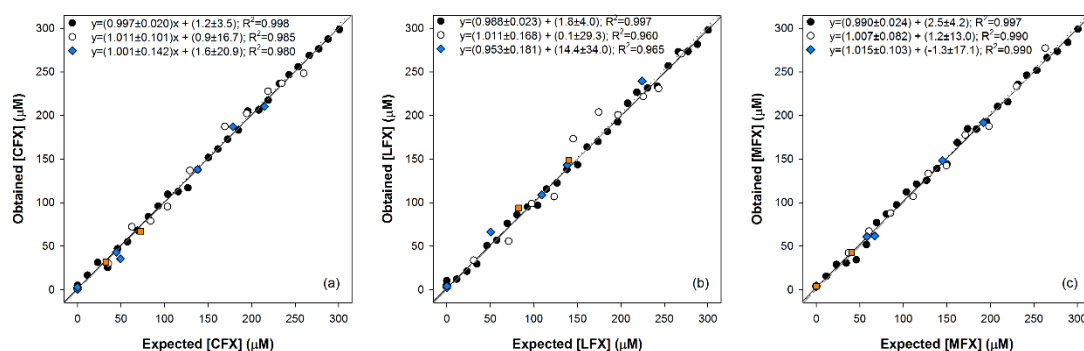


**Figure 4.21** Modeling ability of the DWT-ANN. (a) CFX, (b) LFX and (c) MFX. (●, solid line) training subsets, (○, dotted line) testing subsets, (◆) pharmaceutical samples, (■) spiked human urine samples and (dashed line) theoretical line:  $y = x$ .

Finally, as plotted in Figure 4.21, despite the complexity of matrices and no pretreatment procedures, a good agreement between the expected and predicted values is also observed when analyzing FQs in pharmaceutical and human urine samples, which proves the applicability of the built MIP(FQs)@Au-fMWCNTs based ET.



## ***CHAPTER 5 CONCLUSIONS AND PROSPECTS***



## **5 Conclusions and prospects**

### **5.1 Conclusions**

In this thesis, a novel technology in the laboratory has been developed, able to readily and easily prepare MIP-modified voltammetric sensors. Through the facile and generic electropolymerization by CV technique that using Py as monomer, MIPs-based sensors were fabricated concurrently and directly on the substrate when sets of MIPs were synthesized. The structure and performance of MIPs film were adjusted taking two distinctly different strategies, that is, doping functional anion into MIPs backbone and incorporating MIPs with other nanomaterials. Some of inevitable issues of MIPs-based sensors, such as deficient specificity when analyzing structurally similar families of compounds and inability to simultaneous determination in real applications, can be properly compensated by ET approach using chemometric tools. In this way, two ETs were constructed based on MIPs materials for analyzing varieties of pharmaceutical ingredients. The superb sensing performance of the built MIPs-based ETs firmly demonstrates the feasibility of the combination of MIPs and ET approaches. Moreover,



the applicability and adaptability of MIPs-based ETs represents their great potential promise for sensing more kinds of analytes not only in pharmaceutical fields, but also in other frontiers.

Based on the framework of *Chapter 4*, some more specifically conclusive points are summarized as following, in terms of the two different built MIPs-based ETs, respectively.

### **1. $pTS^-/PPy$ MIPs-based ET**

- I. Three different  $pTS^-/PPy$  MIPs were successfully synthesized through electropolymerization, using PA, AA, and UA as templates, respectively. As the doping anion,  $pTS^-$  endows the MIPs with superior structural and functional advantages.
- II. A generic synthesis routine can be raised, paving the way for the synthesis of more  $pTS^-/PPy$  MIPs.
- III.  $pTS^-/PPy$  MIPs were investigated in aspects of morphology, modification process and repeatability, proving its favorability as a sensing material.
- IV. The analytical characterization of  $pTS^-/PPy$  MIPs-based sensors was conducted, obtaining the corresponding voltametric response and good calibration data of different sensors to the three compounds, denoting its potential to be integrated into a sensor array coupling with chemometric tools for the determination of PA, AA, and UA in the mixtures.
- V. A  $pTS^-/PPy$  MIPs-based ET was constructed as proposed. The ET shows excellent performance both in the qualification and simultaneously quantification of PA, AA, and UA.
- VI. The satisfactory results of real sample analysis shed light on the applicability of the ET and the feasibility and merits of the combination of MIPs and ET.

## **2. MIP(FQs)@Au-fMWCNTs-based ET**

- I. Three MIP(FQs)@Au-fMWCNTs were successfully synthesized, using three different fluoroquinolones as templates respectively, that is, CFX, LFX, and MFX.
- II. MIP(FQs)@Au-fMWCNTs was electrochemically characterized in detailed. Taking the advantages of MWCNTs and AuNPs, the conductivity and sensitivity of MIPs got improved.
- III. In the response to the three fluoroquinolones, MIP(FQs)@Au-fMWCNTs sensors did not show a high specificity to individual analyte, but a class-selectivity.
- IV. The ET based on MIP(FQs)@Au-fMWCNTs represents an appealing and promising tool for both the qualitative and quantitative analysis of FQ antibiotics.
- V. This work proved the feasibility and practicality of combining MIPs with other advanced materials in constructing ETs, providing a new strategy of designing novel and high-performance ETs in the multi-analysis for more families of structurally similar compounds.

## **5.2 Prospects of MIPs-based ET**

Although the combination of MIPs with ETs brings many profitable merits, there are still some ongoing challenges and potentially developmental prospects along this research line. The development of MIPs-based ET is involved with many areas, such as imprinting technology, nanotechnology, and electronics. Herein, the possibly achievable ongoing work and future perspectives are put forward as follows.

As the recognition elements, MIPs' nature can be further improved. On the one hand, apart from pyrrole, other monomers could be attempted according to the imprinted template. Theoretical calculations can be introduced, that is favorable for the selection and design of the optimal monomer. On the other hands, some imprinting

strategies facilitate the formation of MIPs. such as dummy imprinting.

It is known that nanotechnology is in favor of fabricating sensing platforms with high performance. Nevertheless, except for enhancing the sensitivity and conductivity, MIPs' integration into nanomaterials with low-cost and high biocompatibility can be explored, to strengthen the capabilities of MIPs-based ETs for the analysis of a broad spectrum of compounds, such as biomarkers in vivo.

The new generation sensors are expected to be portable, flexible, disposable, and even wearable. Thus, the substrate for the modification of MIPs is required to be extended to scree printed electrodes, carbon fibers, and paper-based materials. Besides, the miniaturization in electronics and the introduction of microfluidics technology are essentially demanded.

## ***ANNEX: PUBLICATIONS***



---

# Article 1

---

**A novel electronic tongue using electropolymerized molecularly imprinted polymers for the simultaneous determination of active pharmaceutical ingredients**

Mingyue Wang, Xavier Cetó, Manel del Valle

Biosensors and Bioelectronics 198 (2022) 113807





# A novel electronic tongue using electropolymerized molecularly imprinted polymers for the simultaneous determination of active pharmaceutical ingredients

Mingyue Wang, Xavier Cetó, Manel del Valle<sup>\*</sup>

Sensors and Biosensors Group, Department of Chemistry, Universitat Autònoma de Barcelona, Edifici Cn, 08193, Bellaterra, Barcelona, Spain

## ARTICLE INFO

### Keywords:

Molecularly imprinted polymers  
Electronic tongues  
Electrochemical sensors  
Artificial neural networks  
Pharmaceutical analysis

## ABSTRACT

The combination of chemometrics and electrochemical sensors modified with molecularly imprinted polymers (MIPs) towards the development of MIP-based electronic tongues (ETs) was explored herein. To demonstrate the potential of such an approach, the simultaneous determination of paracetamol, ascorbic acid and uric acid mixtures in pharmaceutical samples was evaluated. To this aim, MIP-based sensors for the different compounds were prepared by in situ electropolymerization of pyrrole in the presence of *p*-toluenesulfonate anion ( $pTS^-$ ), which acted as functional doping ion of the polypyrrole (PPy) MIP backbone. Morphological characterization of the MIPs was done by scanning electron microscopy (SEM), while functionalization of the electrodes was monitored electrochemically. Under the optimized measuring conditions, the developed sensors showed a good performance, with good linearity at the  $\mu M$  level ( $R^2 > 0.992$ , limits of detection between 1 and 24  $\mu M$ ) as well as good repeatability (intra- and inter-day RSD values between 3 and 6% over 30 consecutive measurements). Finally, the quantification of the individual substances in different pharmaceutical samples was achieved by an artificial neural networks (ANNs) model, showing satisfactory agreement between expected and obtained values ( $R^2 > 0.987$ ).

## 1. Introduction

The greatly improved life quality and the extended life expectancy of human being witnessed over the past decades can be partly attributed to the ever-increasing use of pharmaceutical drugs against diseases and the more sophisticated methods for detecting key metabolite biomarkers that allow the diagnosis of pathologies.

Traditionally, drugs are administered on the basis of factors such as patients' weight or age, which works for most of the cases. However, certain drugs have a narrower therapeutic window, which can result in a patient easily being under- or over-dosed. The same happens with people who suffer altered metabolism or certain diseases. From this perspective, in comparison to mono-component drugs, multidrug formulations are less harmful because of the smaller incorporated amounts of each active component. Nevertheless, certain combinations of drugs are also likely to lead to unpredictable systemic levels (Hilberg et al., 2005; Meneghello et al., 2018). Thus, despite the great advantages that may offer, those still have some negative effects, especially in cases of overdosing (Bergh et al., 2021; Root-Bernstein et al., 2020). To

overcome such scenarios, therapeutic drug monitoring (TDM) is required, so as to ensure individually-directed proper dosing. Therefore, the accurate and rapid analysis of biomolecules and active pharmaceutical ingredients (APIs) aroused keen interest of researchers, pharmaceutical industry and clinicians.

Despite various analytical methods have already been applied for TDM, including high performance liquid chromatography (HPLC), spectrophotometry and titrimetry, drawbacks like being time-consuming, laborious, or expensive are inevitable. Compared with these conventional methods, the combination of electrochemical methods with molecularly imprinted polymers (MIPs) can be a competitive alternative for the detection of biomolecules owing to their numerous advantages such as rapid response, low-cost and high sensitivity and selectivity (BelBruno, 2019; Gui et al., 2018). MIPs are tailor-made biomimetic materials, sometimes referred to as plastic antibodies, not only possessing the "key and lock" specific recognition mechanism owing to the specific sites produced by template molecules, but also with advantages over natural antibodies in terms of reusability, and higher mechanical and chemical stability in harsh conditions (Chen

<sup>\*</sup> Corresponding author. Sensors and Biosensors Group, Universitat Autònoma de Barcelona, Campus UAB, Edifici Cn, 08193, Bellaterra, Spain.

E-mail addresses: [manel.delvalle@uab.cat](mailto:manel.delvalle@uab.cat), [manel.delvalle@gmail.com](mailto:manel.delvalle@gmail.com) (M. del Valle).

<https://doi.org/10.1016/j.bios.2021.113807>

Received 5 October 2021; Received in revised form 12 November 2021; Accepted 13 November 2021

Available online 17 November 2021

0956-5663/© 2021 The Authors.

Published by Elsevier B.V. This is an open access article under the CC BY-NC-ND license

(<http://creativecommons.org/licenses/by-nc-nd/4.0/>).



et al., 2011; Rebelo et al., 2021). Hence, MIP-based electrochemical sensors have been research hotspots for their broad-spectrum applications in environmental monitoring (Rebelo et al., 2021), disease diagnosis (Zaidi, 2018), food or medical safety evaluation (Cao et al., 2019) and so on (Herrera-Chacon et al., 2021; Wackerlig and Lieberzeit, 2015).

Among the different approaches for the synthesis of MIPs, electropolymerization is simple, facile, highly reproducible and facilitates the direct integration of MIPs with voltammetric sensors (Arabi et al., 2021; Herrera-Chacon et al., 2021). In this regard, pyrrole (Py) is a well-known functional monomer used to obtain imprinted structures without the necessity of cross-linkers or initiators (Kumar et al., 2021; Zhang et al., 2018). However, anions must be introduced into the polypyrrole (PPy) backbones to ensure its structural stability. Although perchlorate ( $\text{ClO}_4^-$ ) is the most commonly used, different anions can greatly influence the properties of the resulting polymer and its morphology (Bolat et al., 2019; Carquigny et al., 2008; Raudsepp et al., 2008). It has been reported that *p*-toluenesulfonate ( $\text{pTS}^-$ ) doped PPy film holds high electrical conductivity, good mechanical properties, higher flexibility and durability, and a micro-porous structure (Rajesh et al., 2004; Raudsepp et al., 2008; Solanki et al., 2007).

Despite the improved sensitivity and selectivity of MIP-based electrochemical sensors, those can still show some cross-response towards other molecules, especially with chemically analogous structures. Moreover, when attempting the multi-determination of several compounds, the use of multivariate regression methods might demonstrate advantageous. In this direction, electronic tongues (ETs) approach may help to overcome such issues (Cetó et al., 2016; del Valle, 2010; Herrera-Chacon et al., 2021). ETs are based on the combination of an array of (bio)sensors able to provide a wide and complete response of the analyzed species, plus a modelling tool able to interpret and extract meaningful data from the complex readings. However, even with the large number of publications reporting the development of MIP-based electrochemical sensors and the great benefits that could be derived from the combination of MIPs with ET approach, few publications exploiting this approach can be found (Herrera-Chacon et al., 2018; Huynh and Kutner, 2015).

In order to demonstrate the potential of MIP-based ETs for TDM, the quantitative analysis of paracetamol (PA), ascorbic acid (AA) and uric acid (UA) mixtures is investigated herein as a proof-of-concept of what can be achieved. Moreover, having as ultimate goal, to provide a generic protocol for the development of MIP-based ETs towards almost any other analyte.

In this context, overdose of PA, which is widely used as an analgesic and antipyretic drug, could lead to fatal hepato- and nephro-toxic effects (Vale and Proudfoot, 1995). Precisely, its wide availability in conjunction with its relatively high toxicity lead to PA being one of the most common causes of poisoning worldwide (Prince et al., 2000). Similarly, AA is a valuable vitamin that is extensively employed in combination with other medicines (such as PA) in the treatment of the common cold (Naidu, 2003). It has been proven that the deficiency of AA is closely related to terrible scurvy, the disturbance in the collagen metabolism and the reduction of women's fertility (Brambilla et al., 2018; Dosedel et al., 2021; Grewal et al., 2019). On the contrary, AA abuse can cause deep vein thrombosis (Bergh et al., 2021). Moreover, some studies have suggested that AA intake is related to UA concentration in body fluids (Huang et al., 2005; Juraschek et al., 2011); the latter being associated with various diseases, such as gout, hyperuricemia or Lesch-Nyhan syndrome, arthritis, diabetes, high cholesterol, renal, neurological, cardiovascular and kidney diseases (Sieminska et al., 2020).

Based on the aforementioned, herein we report on the preparation of three PPy MIP-based sensors for PA, AA and UA in the presence of  $\text{pTS}^-$  anion through a generic, facile and simple electropolymerization method, and their subsequent integration into a sensor array to construct a voltammetric ET for the simultaneous determination of those three analytes in pharmaceutical samples. The voltammetric responses of the developed MIP-based sensors were firstly characterized to assess

the performance of the built sensors. Next, the registered voltammograms were analyzed by chemometric tools to achieve the simultaneous quantification of the ternary mixtures. Benefiting from the complementary advantages of MIPs structure and ETs approach, the MIP-based sensor array exhibited superb sensitivity, selectivity and a wide detection range in the simultaneous determination of PA, AA and UA. Furthermore, the novel ET sensor was successfully applied in the analysis of real pharmaceutical samples.

## 2. Experimental section

### 2.1. Reagents and instruments

All the reagents were analytical reagent grade and used in the experiments without any further purification process. Solutions were prepared using deionized water from a Milli-Q System (Millipore, Billerica, MA, USA). Pyrrole (Py), *p*-toluenesulfonic acid ( $\text{pTS}^-$ ) sodium salt, potassium chloride, potassium hydrogenphosphate, potassium dihydrogenphosphate, paracetamol (PA), ascorbic acid (AA) and uric acid (UA) were purchased from Sigma-Aldrich (St. Louis, MO, USA). Phosphate buffered saline (PBS 50 mM, pH 7.0) used in this work contained 100 mM potassium chloride. Graphite powder (particle size  $<50\ \mu\text{m}$ ) was bought from BDH Laboratory Supplies (Poole, UK) and epoxy resin kit was supplied by Resinco green composites (Barcelona, Spain).

Scanning electron microscopy (SEM) was observed by EVO MA10 (Zeiss, Oberkochen, Germany) operated at 30 kV.

### 2.2. Preparation of the $\text{pTS}^-$ /PPy MIPs and NIP sensors

Hand-made graphite-epoxy composite electrodes (GEC, geometric area of  $28.3\ \text{mm}^2$ ) acted as platforms for the electropolymerization of  $\text{pTS}^-$ /PPy MIPs and non-imprinted polymer (NIP). The construction procedures for GEC are based on previous reports from the group (Alegret et al., 1996). Firstly, the epoxy resin was mixed with its corresponding weight of hardener and graphite powder until completely homogenized. Then, the mixture was loaded into the cavity of a PVC tube, in which a copper disk soldered to a connector had been previously introduced, and dried in the oven at  $40\ ^\circ\text{C}$  for 48h. Finally, the dried GECs are polished with sandpapers of decreasing grain size until a smooth surface was obtained.

For the electropolymerization of  $\text{pTS}^-$ /PPy MIPs onto the GEC electrodes, 20 mL of an aqueous solution containing 0.05 M pyrrole monomer, 0.1 M  $\text{pTS}^-$  and 0.02M of the template molecule (either PA, AA or UA) were purged with nitrogen for 10 min before cycling the potential from  $-0.6\ \text{V}$  to  $+0.8\ \text{V}$  vs. Ag/AgCl at a scan rate of  $100\ \text{mV s}^{-1}$ . In this manner, replacing the template solution, the different  $\text{pTS}^-$ /PPy MIPs could be obtained. For PA and AA, those were dissolved in Milli-Q water directly. But in the case of UA, due to its lower solubility, UA was firstly dissolved in a NaOH solution (20 mL, pH 10.0) by stirring and sonicating, and then pyrrole and  $\text{pTS}^-$  were added into the filtered UA solution. Next, in order to extract the template molecules from the PPy film, the electrodes were dipped into PBS and cycled 35 times at a scan rate of  $50\ \text{mV s}^{-1}$  in the range of  $-0.6\ \text{V}$  to  $+1.0\ \text{V}$  vs. Ag/AgCl. Finally, the electrodes were rinsed and kept dry at  $4\ ^\circ\text{C}$  in the fridge when not in use.

For control purposes, the  $\text{pTS}^-$ /PPy NIP modified GEC was prepared following the same procedure as above-mentioned, but without the addition of the template molecules into the polymerization solution. The lack of the template molecule during the polymerization leads to the formation of a polymer with non-specific and non-homogeneous sites, what should clearly demote its selectivity towards the target analyte. Thus, by benchmarking the performance of the MIP against the NIP, it is possible to demonstrate and evaluate the imprinting effect, as it provides a measurement of the specific interactions in the generated MIP sites to the unspecific interactions between the analyte and polymeric material.

### 2.3. Electrochemical measurements

Electrochemical measurements were all carried out at room temperature, in a multichannel configuration using an Autolab PGSTAT30 (Ecochemie, Netherlands) controlled by GPES Multichannel and FRA software packages. A standard three-electrode cell composed of an Ag/AgCl (3 M KCl) reference electrode, a Pt wire as counter electrode and the modified GECs with  $pTS^-/PPy$  MIPs and NIP as working electrodes. Electrochemical characterizations of bare and modified GECs were performed by cyclic voltammetry (CV) and electrochemical impedance spectroscopy (EIS) in a 5 mM  $K_3[Fe(CN)_6]/K_4[Fe(CN)_6]$  solution in PBS. CV measurements were conducted in the potential range from  $-0.2$  V to  $+0.7$  V at a scan rate of  $50\text{ mV s}^{-1}$ . Impedance spectra were recorded in the frequency range between 50 kHz and 50 mHz with a fixed AC amplitude of 10 mV and an applied potential of  $+0.23$  V. For the analysis of the impedance spectra, data was fitted to the Randles equivalent circuit (inset of Fig. 1f), composed of the solution resistance ( $R_s$ ), the charge transfer resistance between the solution and the electrode surface ( $R_{ct}$ ), the Warburg impedance ( $Z_w$ , related to the diffusion of the electroactive species from the solution towards the electrode surface), and the double-layer capacitance ( $C_{dl}$ ).

For the analysis of APIs, differential pulse voltammetry (DPV) was

the chosen technique. The potential was scanned from  $-0.4$  V to  $+0.8$  V with a step potential of 5 mV and a pulse amplitude of 50 mV without stirring. Before each measurement, the electrodes were immersed for 180 s in the solution to be analyzed under stirring to allow for the enrichment of the analytes in the MIP sites. After each measurement, the electrodes were electrochemically cleaned in PBS by applying a fix potential of  $+0.8$  V for 180 s.

### 2.4. Samples under study

On the one hand, stock solutions of each of the different APIs were prepared in PBS. From those, intermediate working solutions at different concentrations were prepared by appropriate dilution in PBS, and used to characterize the analytical response of each of the developed MIP-based sensors in terms of linearity, sensitivity, limit of detection (LOD), etc.

On the other hand, for the simultaneous determination of APIs, a set of 38 samples divided into two subsets were prepared by appropriate dilution and mixing of the stock solutions. The first subset used to establish the response model (training subset), was based on a  $3^3$  tilted factorial design, as shown in Fig. S1. The concentrations for each of the compounds were in the range  $0\text{--}50\text{ }\mu\text{M}$  for PA,  $0\text{--}1000\text{ }\mu\text{M}$  for AA and

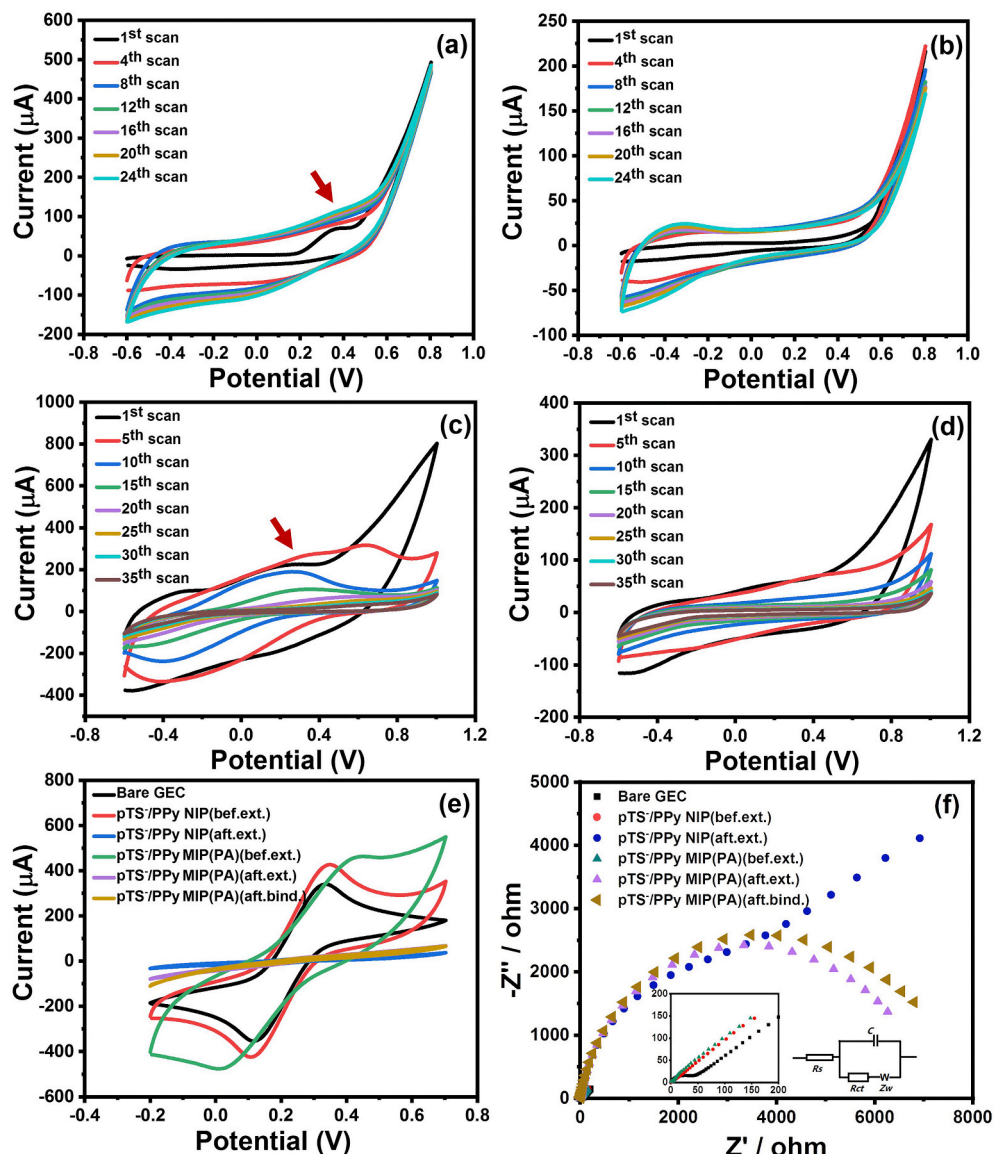


**Fig. 1.** Cyclic voltammograms taken during the electropolymerization of  $pTS^-/PPy$  onto a GEC (a) with paracetamol (MIP(PA)) and (b) without template molecule (NIP). Cyclic voltammograms taken during the template extraction of (c)  $pTS^-/PPy$  MIP(PA) and (d)  $pTS^-/PPy$  NIP. (e) Voltammetric and (f) impedimetric responses towards a 5 mM  $[Fe(CN)_6]^{3-/4-}$  solution in PBS after each modification step and rebinding experiments: (black) bare electrode, (red and green) after Py electropolymerization, (blue and purple) after extraction of the template, (green and brown) after rebinding of the template. (For interpretation of the references to colour in this figure legend, the reader is referred to the Web version of this article.)

50–500  $\mu\text{M}$  for UA. Next, in order to assess the performance of the built model, a set of 11 samples (testing subset) randomly distributed along the experimental domain defined by the factorial design was also prepared and measured under the same conditions.

Lastly, in order to demonstrate the applicability of the developed ET in real-world scenario, the analysis of commercial tablets bought from local drugstores was attempted. To this aim, tablets were dissolved in PBS so that the expected concentrations fall within the experimental domain of the built model, without requiring further pre-treatment. Furthermore, some of them were also spiked with UA to evaluate its recovery values as well. Concretely, the three following pharmaceutical preparations were evaluated: *Efferaldol* (330 mg paracetamol and 200 mg ascorbic acid (vitamin C); Bristol Myers Squibb, S.A., Madrid), *Multicentrum* (800  $\mu\text{g}$  vitamin A, 15 mg vitamin E, 100 mg vitamin C, 30  $\mu\text{g}$  vitamin K, 1.4 mg thiamine (vitamin B1), 1.75 mg riboflavin (vitamin B2), 2 mg vitamin B6, 2.5  $\mu\text{g}$  vitamin B12, 5  $\mu\text{g}$  vitamin D, 62.5  $\mu\text{g}$  biotin (vitamin B7), folic acid (vitamin B9), 20 mg niacin (vitamin B3), 7.5 mg pantothenic acid (vitamin B5), 162 mg calcium, 125 mg phosphorous, 100 mg magnesium, 5 mg iron, 100  $\mu\text{g}$  iodine, 500  $\mu\text{g}$  copper, 2 mg manganese, 40  $\mu\text{g}$  chromium, 50  $\mu\text{g}$  molybdenum, 30  $\mu\text{g}$  selenium and 5 mg zinc; GlaxoSmithKline España, Madrid) and *Redoxon* (1000 mg vitamin C, 10 mg zinc, 10  $\mu\text{g}$  vitamin D; Bayer Hispania, S.L., Sant Joan Despí).

## 2.5. Data analysis

Processing of the data was done in Matlab 7.1 (MathWorks, Natick, MA, USA) with the aid of its Neural Network toolbox, while final representation and analysis were done in Origin 2019 (OriginLab Corporation, Northampton, MA, USA). The potential of the ET to discriminate between the different APIs was assessed by means of principal component analysis (PCA), whereas artificial neural networks (ANNs) were chosen as the modelling tool for the quantification of their mixtures. To this end, recorded voltammograms were first compressed by means of discrete cosine transform (DCT) (Cetó and Pérez, 2020), and the obtained coefficients were then submitted to PCA or ANNs.

Briefly, the use of DCT was motivated to reduce the dimensionality and complexity of the voltammetric signals, which allows to gain advantages in the modelling stage such as a reduction in training time, to avoid redundancy in input data and to obtain a model with better generalization ability (Cetó et al., 2013a,b). PCA allows to evaluate samples (dis)similarities and assess initial patterns in the data, whilst ANNs represent a high-performance modelling tool able to achieve the

simultaneous multi-determination of the different compounds in mixtures.

## 3. Results and discussion

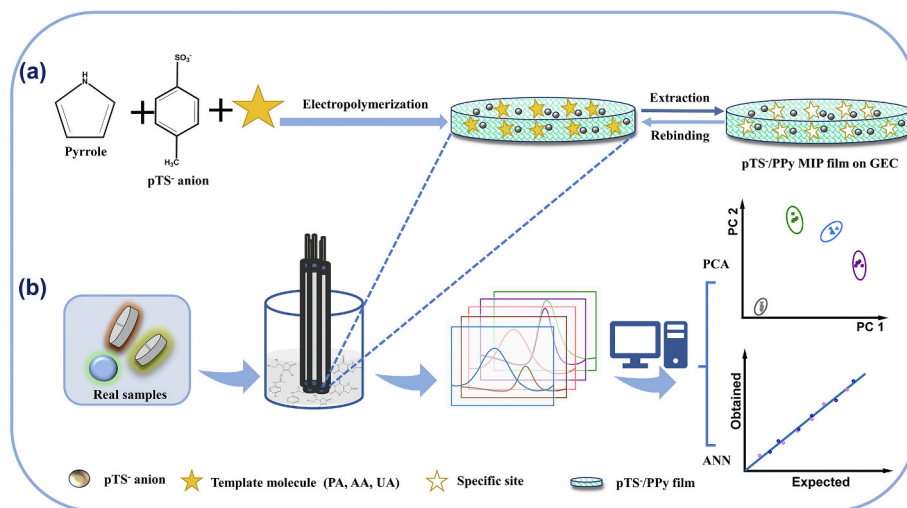
As already introduced, the aim of this work is to develop a voltammetric ET consisting of an array of MIP-based sensors targeting a mixture of oxidizable APIs. In this direction, herein we propose a facile and generic strategy for the synthesis of MIPs based on the electropolymerization of Py, an approach that can be easily adapted to different target analytes (the templates). Moreover, another main asset of this approach is that it's a one-step electrochemical-synthesis, which makes the integration of the MIP onto the electrode straightforward, while allowing to control the thickness of the MIP by changing the total charge flown at the electrode, the polymerization media or the electrolyte nature.

Next, the developed sensors are combined into an array, and the registered responses are analyzed by means of different chemometric methods that allow the discrimination or quantification of the substances in the samples. The general procedure for the synthesis and usage of  $p\text{TSS}^-/\text{PPy}$  MIPs with different template molecules is illustrated in Scheme 1.

Such an approach seeks to combine the advantages of MIPs to address the lack of selectivity of sensors used in ETs, with the modelling capabilities of ETs to address possible interferences or matrix effects from MIPs (Herrera-Chacón et al., 2021). The idea is similar to bioETs, but with the advantage of MIPs being cheaper, more stable, more resistant to harsh conditions and tailor-made, offering a suitable receptor to almost any analyte of interest.

### 3.1. Synthesis and morphological characterization

CV was used for the electropolymerization of Py monomer in the presence of the template molecules (PA, AA or UA) and  $p\text{TSS}^-$  as supporting electrolyte and doping counter ion to maintain the electro-neutrality of the synthesized polymer. Such procedure includes both the synthesis and immobilization of the MIP onto the electrode in a single step (Özcan and Şahin, 2007). Production of specific MIP sites is favored by hydrogen bonding interactions between the N–H groups of PPy and electron lone pairs of the template molecules. Moreover, compared with small-sized inorganic anions such as  $\text{ClO}_4^-$ , medium-sized organic ones such as  $p\text{TSS}^-$ , play an important role in improving the performance of PPy MIPs films. Firstly, with the benzene



**Scheme 1.** (a) Preparation of the different  $p\text{TSS}^-/\text{PPy}$  MIPs by electropolymerization of Py in the presence of the template molecules and (b) incorporation of the fabricated MIP-based sensors into the ET sensor array and its application to the analysis of APIs in pharmaceutical samples.



ring, it helps enhancing its binding ability because of the  $\pi$ - $\pi$  interactions between  $pTS^-$  and the analytes. Secondly, PPy films deposited in the presence of such aromatic anions exhibit an anisotropic molecular organization, resulting in higher conductivity and crystallinity (Raudsepp et al., 2008). What's more, as a sulfonate surfactant,  $pTS^-$  provides additional benefits by generating higher degree of electrostatic cross-linking and PPy films with a much more microporous structure, which favors a larger sensing surface and higher mass transfer coefficient (Solanki et al., 2007; Suematsu et al., 2000).

The use of amperometric methods allows the control of the polymeric films' thickness by tuning the charge (Coulombs), but even more, CV allows to monitor the entrapment of the template molecules during its growth. As shown in Fig. 1a and b, the capacitive currents increase during the process of electropolymerization with the increase of the number of cycles as a result of the growing thickness of  $pTS^-$ /PPy film. There are remarkable differences between Fig. 1a and b, where the oxidation peak potential shifts to higher potentials in the presence of PA, suggesting that it is being entrapped into the polymeric chains (Özcan and Şahin, 2007).

Upon synthesis of the MIP, the next step was the removal of the template molecules, which was also done by CV, triggering the recognition at the MIP specific sites. Correspondingly, it can be seen from Fig. 1c that as the number of cycle increases, the oxidation peak of PA disappears gradually, demonstrating that PA molecules are being released. Similarly, electropolymerization and extraction of  $pTS^-$ /PPy MIP(AA) and  $pTS^-$ /PPy MIP(UA) are shown in Fig. S2. Due to the different nature and electrochemical behavior of the different template molecules, different voltammetric profiles are obtained during the electropolymerization, but following the same trend overall.

Undoubtedly, the thickness of the modified film plays a crucial role in the performance of the MIP-based sensor, which can be controlled by changing the number of cycles during the electropolymerization. Therefore, the thickness of the film was optimized by changing the number of scans from 8 to 40 cycles (Fig. S3). As can be seen, a low number of cycles leads to higher responses both for the MIP and the NIP as the films are too thin. Oppositely, when this is too high, the MIP behaves similarly as the NIP a fact that can be attributed to the difficulty of the molecules to diffuse through the thicker film, and the difficulty of being oxidized when being too far from the electrode surface due to the

low conductivity of the film. Thus, for the selection of the optimal number of cycles, the ratio between the MIP and NIP responses was taken as the selection criteria, selecting 24 cycles as the optimum.

Next, the morphology of the modified electrodes was observed by SEM (Fig. 2). Low magnification images show a homogenous and uniform distribution of  $pTS^-$ /PPy MIPs and NIP films over the surface of the GEC. From their comparison, it is conspicuous that  $pTS^-$ /PPy MIPs are rougher than  $pTS^-$ /PPy NIP, which provides a larger active area for charge and mass transportation. Moreover, to further characterize the synthesized material and confirm the adhesion of the film, elemental composition analysis of the cross-section area for  $pTS^-$ /PPy MIP(PA) and NIP were measured by energy-dispersive X-ray spectrometry (EDX). Concretely, the analysis of nitrogen, oxygen and sulfur were targeted to confirm the expected composition of the material. A clear change can be observed for nitrogen and oxygen, which confirms the extent of the surface modification of both MIP and NIP as N can be attributed to PPy while sulfur to the doping  $pTS^-$  anions.

### 3.2. Electrochemical characterization

Apart from the morphological characterization, each of the different modification stages was confirmed electrochemically by CV and EIS measurements using  $[Fe(CN)_6]^{3-/4-}$  as the redox probe (Fig. 1e and f). Initially, we can see how the bare GEC displays the typical reversible peaks of  $[Fe(CN)_6]^{3-/4-}$ , while the overall current increases slightly due to the higher capacitive component after the electropolymerization, confirming the attachment of PPy onto the electrode surface. The worse electrochemical behavior of the  $pTS^-$ /PPy MIP was attributed to the presence of the template affecting the conductivity of PPy. Similarly, analyzing the EIS spectra, it can be seen how initially the charge transfer resistance ( $R_{ct}$ ) is rather small, but still observing the typical semicircle shape, while after the electropolymerization, the  $R_{ct}$  decreased significantly as could be expected from the voltammetric measurement. The next step was the extraction of the template, which should release the sites so that the redox probe obtains easier access to the electrode surface. However, the PPy film was over-oxidized during this step, which resulted in a decrease of its conductivity. This is why there is such a large increase in the  $R_{ct}$  and, accordingly, a drastic decrease in the voltamogram current if comparing to the one before the removal of the

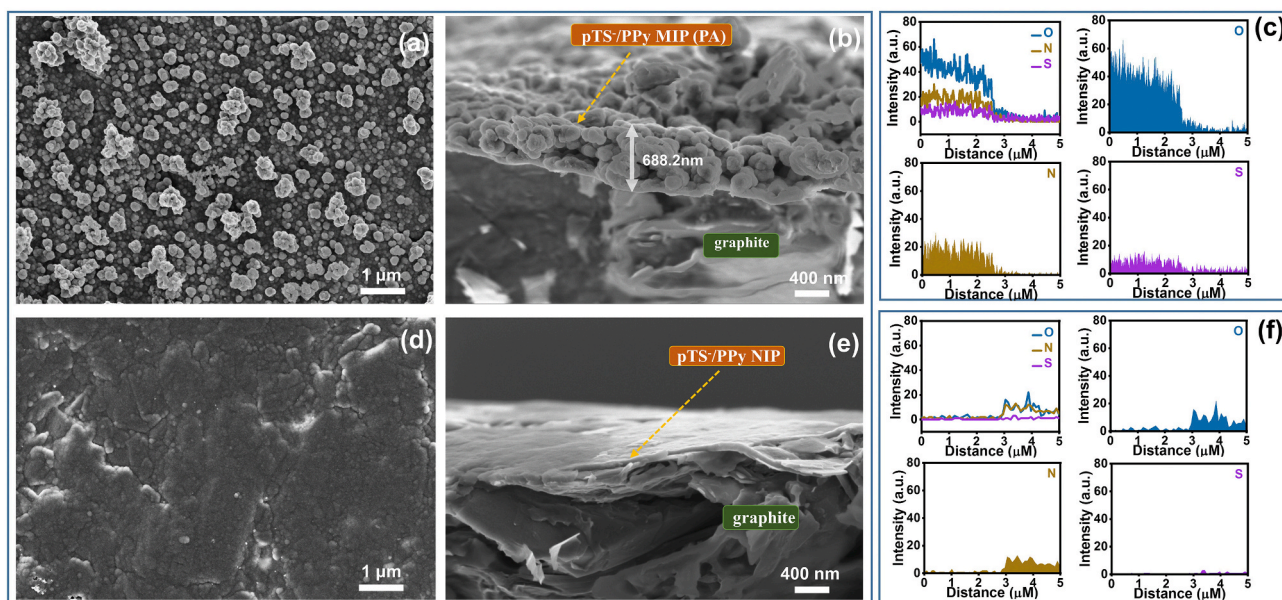


**Fig. 2.** (a) Top and (b) cross-section SEM images of  $pTS^-$ /PPy MIP(PA). (d) Top and (e) cross-section SEM images of  $pTS^-$ /PPy NIP. EDX pattern of (c)  $pTS^-$ /PPy MIP (PA) and (f)  $pTS^-$ /PPy NIP; (blue) oxygen, (brown) nitrogen and (purple) sulfur. (For interpretation of the references to colour in this figure legend, the reader is referred to the Web version of this article.)

template. Finally, after the incubation with the template, which is expected to block the diffusion of  $[\text{Fe}(\text{CN})_6]^{3-/4-}$ , a decrease of the voltammetric current and an increase of the  $R_{\text{ct}}$  upon rebinding of the template molecules with the specific MIP sites was observed. From the voltammetric data, it may hardly be seen how the diffusion of the redox probe was blocked to some extent, but it is much clearer from the Nyquist plot due to the higher sensitivity of the impedimetric measurements. Overall, CV and EIS measurements are in agreement with each other, both confirming the functionalization of the electrode.

### 3.3. Voltammetric characterization

#### 3.3.1. Calibration curves

The next step before proceeding with the ET approach was the characterization of the electrochemical responses of each sensor towards each considered compound to assess their linear range and sensitivity, as well as confirming that the sensors show certain cross-response and that their responses are stable over time, as otherwise those are not suitable to be used in ETs.

To this aim, calibration curves were built for each of the APIs by DPV due to its higher sensitivity in comparison to CV. However, before proceeding with the electrochemical characterization, the incubation time had to be optimized, taking a compromise between the maximum signal and shorter analysis time (Fig. S4). As could be expected, there is a logarithmic increase of the signal with the incubation time, reaching almost saturation after incubating in the analytes' solution for 180s. Consequently, 180s was taken as the suitable incubation time for further experiments.

The voltammetric responses of the three  $p\text{TS}^-/\text{PPy}$  MIPs towards increasing concentrations of their respective template molecules are shown in Fig. 3a–c, with current peaks increasing as the concentration increases. From those, the peak heights were calculated and the calibration curves were built (Fig. 3d–f), evidencing a linear trend with high correlation coefficients. Furthermore, not only the response of each MIP was evaluated towards its template, but also the cross-responses towards the other analytes were evaluated (Figs. S5, S6 and S7 as well as Table 1). From the comparison of the calibration curves of the three different  $p\text{TS}^-/\text{PPy}$  MIPs and the NIP against PA and AA, it can be clearly seen that both MIP-based sensors show higher sensitivity towards their own template molecule than the other sensors (other MIPs and NIP), which demonstrates the specificity of the developed MIPs, but also

**Table 1**

Analytical parameters of the different  $p\text{TS}^-/\text{PPy}$  MIPs and NIP towards the three target analytes in PBS extracted from the DPV measurements (results averaged from three different electrodes; the limit of detection (LOD) was calculated on the basis of typical error of the regression line ( $S/N = 3$ )).

Analyte	LOD ( $\mu\text{M}$ )	Sensitivity ( $\text{nA}\cdot\mu\text{M}^{-1}$ )	Linear range ( $\mu\text{M}$ )	$R^2$
<b><math>p\text{TS}^-/\text{PPy}</math> MIP(PA)/GEC</b>				
Paracetamol	1.8	139	0.5–50	0.992
Ascorbic acid	177	0.8	500–2000	0.988
Uric acid	1.9	91	2–50	0.994
<b><math>p\text{TS}^-/\text{PPy}</math> MIP(AA)/GEC</b>				
Paracetamol	177	57	1–1000	0.999
Ascorbic acid	19	18	5–1000	0.997
Uric acid	17	53	0.5–1000	0.997
<b><math>p\text{TS}^-/\text{PPy}</math> MIP(UA)/GEC</b>				
Paracetamol	1.3	82	0–50	0.997
Ascorbic acid	320	0.2	100–2500	0.983
Uric acid	24	26	50–500	0.996
<b><math>p\text{TS}^-/\text{PPy}</math> NIP/GEC</b>				
Paracetamol	1.1	78	0.5–50	0.997
Ascorbic acid	157	0.1	500–2500	0.999
Uric acid	3.1	39	5–100	0.996

that there is still some degree of cross-response. However, the fact that  $p\text{TS}^-/\text{PPy}$  MIP(UA) doesn't show the highest sensitivity to UA may be attributed to the lower solubility of UA in the electrolyte solution, which ultimately affects the number of specific sites generated in  $p\text{TS}^-/\text{PPy}$  MIP(UA).

#### 3.3.2. Repeatability study

Another important feature when developing a sensor, and especially significant from the perspective of ETs, is the repeatability of the developed devices. In order to assess the repeatability, 30 consecutive measurements for each  $p\text{TS}^-/\text{PPy}$  MIP-based sensor were conducted in their respective template solutions (PA solution was used for NIP-based sensors). After each measurement, electrodes were cleaned in PBS as described in Section 2.3. Furthermore, a blank was also measured in fresh PBS after cleaning as control to evaluate any possible fouling effect. The day-to-day repeatability was evaluated in the same way, using the same MIPs and NIP electrodes during three consecutive days. From those, the relative standard deviation (expressed as percentage, RSD%) were calculated, with values below 6.5% for all the sensors under the two different scenarios (Table S1), asserting that all MIPs and NIP

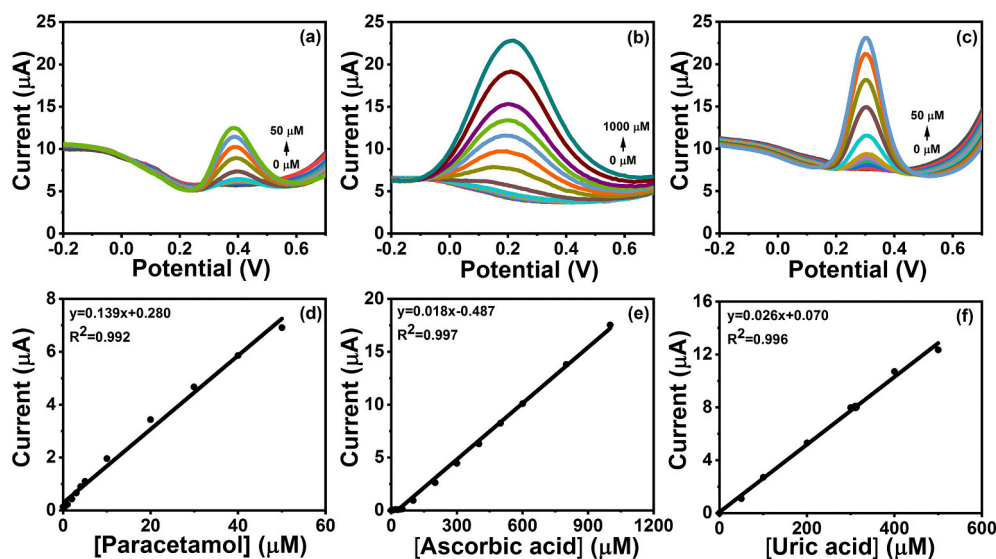


**Fig. 3.** (Top) DPV responses of the MIP-based sensors towards their respective templates: (a)  $p\text{TS}^-/\text{PPy}$  MIP(PA) to paracetamol, (b)  $p\text{TS}^-/\text{PPy}$  MIP(AA) to ascorbic acid and (c)  $p\text{TS}^-/\text{PPy}$  MIP(PA) to uric acid. (Bottom) Calibration graphs derived from the measured peak heights of  $p\text{TS}^-/\text{PPy}$  MIP(PA),  $p\text{TS}^-/\text{PPy}$  MIP(AA),  $p\text{TS}^-/\text{PPy}$  MIP(UA) and  $p\text{TS}^-/\text{PPy}$  NIP based sensors for the three analytes: (d) paracetamol, (e) ascorbic acid and (f) uric acid.

sensors render great repeatability.

### 3.4. MIP-based ET

As already mentioned, the use of chemometric methods could assist in improving the selectivity of MIP-based sensors by shifting the complexity from the chemical to the modelling side (Cetó et al., 2016; del Valle, 2010). To demonstrate such a statement, discrimination of the three considered APIs was first attempted by means of PCA from different stock solutions. This represents a preliminary step to confirm that the MIP-based ET is able to discriminate the different compounds, and therefore has the potential to achieve its simultaneous quantification by developing a proper quantitative model (in this case, by means of ANNs) using an appropriate set of samples.

In both cases, the set of samples were measured by the MIP-based sensor array and the recorded voltammograms were then compressed by means of DCT down to 16 coefficients prior to the qualitative analysis by PCA or quantitative modelling by ANNs. This step, apart from denoising the voltammetric data, assists in reducing the complexity of the input signal, which in turn allows to obtain simpler and more robust

models (Cetó et al., 2013a,b).

#### 3.4.1. Qualitative analysis

Under the described conditions in Section 2.3, five replicate samples of 50  $\mu\text{M}$  solutions of each of the APIs were measured employing the developed sensor array (3 MIPs plus the NIP) and then submitted to DCT-PCA.

The main advantage of PCA is allowing to summarize the information contained in large data sets (e.g., the four voltammograms registered with the different sensors for each sample) down to a two- or three-coordinates point in a scores plot, where all the considered samples are also represented. Thus, it provides a better representation of samples (dis)similarities and allows to rapidly detect and assess initial patterns in the data.

The obtained 2D score plot is shown in Fig. 4a, with a cumulative variance of ca. 91.2%, a large value denoting that almost all the variance present in the original data is now summarized with only the first two principal components (PCs). More significantly, we can see how clear clusters are obtained for each of the APIs as well as for the buffer solution, all of them clearly separated with very small confidence intervals

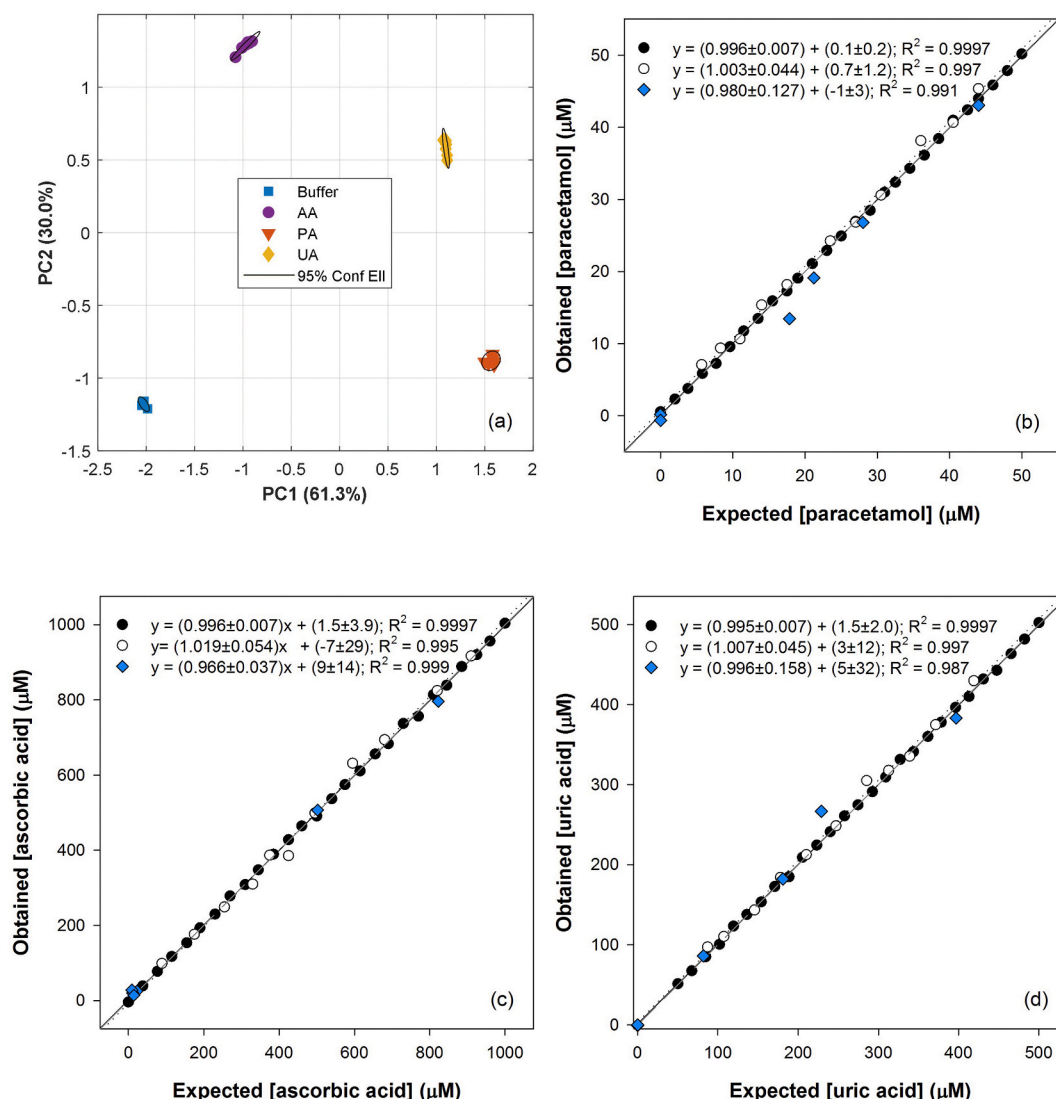


**Fig. 4.** (a) Score plot of the first two principal components obtained from the DCT-PCA of the voltammetric responses of the  $p\text{TS}^-/\text{PPy}$  MIPs and NIP modified sensors towards: (■) PBS, (▼) paracetamol, (●) ascorbic acid and (◆) uric acid. Ellipses plotted correspond to 95% confidence limits for each of the clusters. (b,c,d) Modeling ability of the optimized DCT-ANNs. Comparison graphs of obtained vs. expected concentrations for (b) paracetamol, (c) ascorbic acid and (d) uric acid, for both the training (●, solid line) and testing subsets (○, dotted line). Dashed line corresponds to the ideal comparison line ( $y = x$ ). Additionally, the results of the analysis of the pharmaceutical samples are also plotted (◆).



for each of the groups. The clustering is so clear that either PC1 or PC2 would be enough to distinguish the different compounds, with the buffer being in one of the extremes of the plot, further from any other cluster.

Moreover, from the comparison of the current PCA plot with the ones reported in previous publications based on arrays of graphite epoxy composites (GECs) (Sarma et al., 2020) or screen-printed electrodes (SPEs) (Ortiz-Aguayo et al., 2019) modified with different electrocatalysts such as Prussian blue or metallic nanoparticles (representing a “conventional” voltammetric ET), we can see how the combination of MIPs and ETs significantly improves the former.

To numerically quantify this improvement, Silhouette clustering metric was considered (Kaufman and Rousseeuw, 1990). Silhouette index provides a measure of how good the clustering is by comparing the intra-cluster distances (cohesion) with respect to the intra-cluster distances (separation). Its value is normalized between  $-1$  and  $+1$ , where high values are indicative of good clustering (highly cohesioned groups with good separation between them), and oppositely, low values indicate very poor separation between clusters. The cohesion can be interpreted as a measure of sensors' reproducibility, while separation as a measure of the sensor capability to discriminate the considered compounds.

In our case, the Silhouette index calculated from the PCA score plot was 0.998 (a high value very close to the index maximum), while this was 0.947 and 0.838 for the above-mentioned GEC- and SPE-based ETs. The highest value of the current approach is related to the highest selectivity and specificity of MIPs, while in the case of the GECs, the improved performance arises from a preliminary optimization on the sensors that constituted the ET. Thus, these values confirm the higher performance of the MIP-based ET approach and its potential to succeed in the simultaneous quantification of APIs mixtures.

#### 3.4.2. Quantitative analysis

The set of samples described in section 2.4 were prepared and analyzed under the same conditions as earlier, recording a voltammogram for each of the sensors. As can be seen from Fig. S8, despite each MIP-based sensor responds mainly to its target analyte, there is still some cross-response and peak overlapping for certain samples, hampering the quantification of each API from the univariate regression curves. Nevertheless, as demonstrated with PCA, the use of chemometric methods can greatly assist in improving MIPs' selectivity. Thus, an ANN model was used to achieve the simultaneous determination of the three APIs. The whole set of voltammograms were compressed with DCT and the ANN model was built employing the data of the train subset, using the data of the test subset to assess its performance. This data splitting was done to ensure that the system was not over-fitted, providing a more realistic evaluation of the model performance as test data was not used at all during the modelling stage.

The topology of the neural network was optimized by systematically varying the number of neurons in the hidden layer as well as the transfer functions between the different layers. After the optimization, the selected ANN model had 64 neurons in the input layer (corresponding to the DCT coefficients for each of the sensors), 4 neurons and *purelin* transfer function in the hidden layer, and 3 neurons (one for each of the APIs) and *purelin* transfer function in the output layer.

To visualize the performance of the model, the comparison graphs of obtained vs. expected concentrations were built for each of the analytes (Fig. 4b–d), and the equations of the linear regressions as well as their confidence intervals calculated (Table S2). As shown, an excellent agreement is attained with regression lines almost indistinguishable from the theoretical ones, demonstrating the superb specificity derived from the combination of MIPs and chemometrics. This good behavior is also confirmed numerically from the slope, intercept and correlation coefficient values, which are all close to the ideal values (1, 0 and 1, respectively). Additionally, the root mean square error (RMSE) and its normalization (NRMSE) were also calculated to obtain a unique metric of the overall model performance.

To evaluate the improvement derived from the usage of the proposed MIP-based sensor array, the same set of samples were also measured employing a bare GEC electrode, and the data was processed in the same way. After optimization of the ANN topology, a total NRMSE of 0.084 was obtained; a value that is significantly larger than the one of the MIP-based ET, which was 0.020.

Lastly, to benchmark the performance of the MIP-based developed ET, the obtained results were compared to the ones reported in previous works in which the same mixtures were analyzed (Table S2) (Cetó et al., 2013a,b; Gútes et al., 2007; Ortiz-Aguayo et al., 2019; Sarma et al., 2020). Despite it has to be reckoned that some of the differences attained in the final performance originate from the modelling stage itself, that is, depending on the choice of the machine learning algorithms, it can be neglected that the richer and more relevant the raw data is, the better performance will be attained. From the comparison, we can see how the current approach clearly outperforms all the previous reported ETs, therefore, further confirming the benefits derived from the combination of MIPs and ETs.

#### 3.4.3. Real sample analysis

Finally, after generating and validating the performance with the samples of the training and testing subsets, respectively, the developed ET was applied to the analysis of some pharmaceutical preparations. The pharmaceutical samples were prepared as described in Section 2.4 and measured as previous, without performing any sample pre-treatment step. Obtained voltammograms were compressed with DCT and fed to the ANN model which provided the actual amount of API present in the pharmaceutical formulation after multiplying by the proper dilution factor.

In this manner, the analysis of seven different samples prepared from raw and spiked dilutions of the three different pharmaceutical formulations was carried out, and the results are summarized in Fig. 4 and Table S3. As can be observed, a good agreement between obtained and expected values is obtained, again being the values for the slope and intercept close to the ideal ones and within the confidence interval. This is highly relevant as pharmaceutical formulations have a relatively complex matrix with many compounds (excipients, fillers, disintegrants, binders, etc.) or other APIs not considered when building the chemometric model. However, it is evident that those do not affect the performance of the model, as no significant differences are found between the results derived from the stock solutions and the pharmaceutical tablets. This can be attributed not only to the use of ETs, which are known to allow minimizing possible matrix effects, but especially favored by the higher selectivity of the used MIP-based sensors.

## 4. Conclusions

The potential and advantages derived from the incorporation of MIPs into the ET sensor array have been demonstrated herein through the analysis of APIs mixtures. For the development of the MIP-based ET, a generic facile electropolymerization method of Py in the presence of  $pTS^-$  and the target analytes (the templates) has been proposed, which lead to the synthesis of a new kind of  $pTS^-/PPy$  MIPs. Doping of  $pTS^-$  anions into the MIPs structures was confirmed from the SEM-EDX analysis. Apart from the SEM morphological characterization, the modification of the electrode was also confirmed electrochemically after the different steps involved in the synthesis of the MIP as well as its application for sensing.

Upon completing the analytical characterization of the  $pTS^-/PPy$  MIPs, those were combined into a sensor array, and the developed ET was applied towards the simultaneous accurate determination of PA, AA and UA mixtures. Recorded voltammograms were compressed by means of DCT and an ANN model was built, which showed excellent performance in comparison to previously reported ETs attempting the quantification of the same mixtures.

On the one hand, the obtained results prove the high specificity,

great stability and superb resolution of the developed MIP-based sensors. On the other hand, it also demonstrates that the combination of chemometric methods with MIPs represents a very promising approach as evidenced from both the PCA and ANN models. More importantly, the main advantage of the proposed approach is that MIPs towards other molecules might be generated following the same procedure providing a generic protocol for the development of MIP-based ETs towards other analytes. Overall, the development of MIP-based ETs stands for an extremely promising route for a broad-spectrum of sensing applications in TDM, but also in many other fields.

### CRedit authorship contribution statement

**Mingyue Wang:** Investigation, Methodology, Writing – original draft. **Xavier Cetó:** Conceptualization, Methodology, Software, Writing – original draft. **Manel del Valle:** Conceptualization, Methodology, Writing – review & editing, Funding acquisition. All authors have read and agreed to the published version of the manuscript.

### Declaration of competing interest

The authors declare that they have no known competing financial interests or personal relationships that could have appeared to influence the work reported in this paper.

### Acknowledgments

The authors acknowledge the support of the Spanish Ministry of Science and Innovation (MCINN) through project PID2019-107102RB-C21. M.d.V. thanks the program ICREA Academia.

### Appendix A. Supplementary data

Supplementary data to this article can be found online at <https://doi.org/10.1016/j.bios.2021.113807>.

### References

- Alegret, S., Alonso, J., Bartolí, J., Céspedes, F., Martínez-Fàbregas, E., del Valle, M., 1996. Amperometric biosensors based on bulk-modified epoxy graphite biocomposites. *Sens. Mater.* 8 (3), 147–154. <https://myukk.org/SM2017/article.php?ss=10231>.
- Arabi, M., Ostovan, A., Li, J., Wang, X., Zhang, Z., Choo, J., Chen, L., 2021. *Adv. Mater.* 33, 2100543–2100575.
- BelBruno, J.J., 2019. *Chem. Rev.* 119 (1), 94–119.
- Bergh, M.S., Oiestad, A.M.L., Baumann, M.H., Bogen, I.L., 2021. *Int. J. Drug Policy* 90, 103065–103069.
- Bolat, G., Yaman, Y.T., Abaci, S., 2019. *Sens. Actuators B-Chem.* 299, 127000–1270008.
- Brambilla, A., Pizzi, C., Lasagni, D., Lachina, L., Resti, M., Trapani, S., 2018. *Front. Pediatr.* 6, 126–129.
- Cao, Y., Feng, T., Xu, J., Xue, C., 2019. *Biosens. Bioelectron.* 141, 111447–111464.
- Carquigny, S., Segut, O., Lakard, B., Lallemand, F., Fievet, P., 2008. *Synthetic Met.* 158 (11), 453–461.
- Cetó, X., Céspedes, F., del Valle, M., 2013a. *Microchim. Acta* 180, 319–330.
- Cetó, X., Gutiérrez, A., del Valle, M., 2013b. *Acta Manilana* 61, 39–49.
- Cetó, X., Pérez, S., 2020. *Talanta* 219, 121253–121260.
- Cetó, X., Voelcker, N.H., Prieto-Simón, B., 2016. *Biosens. Bioelectron.* 79, 608–626.
- Chen, L., Xu, S., Li, J., 2011. *Chem. Soc. Rev.* 40 (5), 2922–2942.
- del Valle, M., 2010. *Electroanalysis* 22, 1539–1555.
- Dosedel, M., Jirkovsky, E., Macakova, K., Krcmova, L.K., Javorska, L., Pourouva, J., Mercolini, L., Remiao, F., Novakova, L., Mladenka, P., 2021. *Nutrients* 13 (2), 615–648.
- Grewal, A.S., Singh, S., Sharma, N., Rani, L., 2019. *Int. J. Pharm. Qual. Assur.* 10, 605–612, 04.
- Gui, R., Jin, H., Guo, H., Wang, Z., 2018. *Biosens. Bioelectron.* 100, 56–70.
- Gutés, A., Calvo, D., Céspedes, F., del Valle, M., 2007. *Microchim. Acta* 157, 1–6.
- Herrera-Chacon, A., Cetó, X., del Valle, M., 2021. *Anal. Bioanal. Chem.* 413, 6117–6140.
- Herrera-Chacon, A., González-Calabuig, A., Campos, I., del Valle, M., 2018. *Sens. Actuators B-Chem.* 258, 665–671.
- Hillberg, A.L., Brain, K.R., Allender, C.J., 2005. *Adv. Drug Deliver. Rev.* 57 (12), 1875–1889.
- Huang, H.Y., Appel, L.J., Choi, M.J., Gelber, A.C., Charleston, J., Norkus, E.P., Miller 3rd, E.R., 2005. *Arthritis Rheum.* 52 (6), 1843–18477.
- Huynh, T.P., Kutner, W., 2015. *Biosens. Bioelectron.* 74, 856–864.
- Juraschek, S.P., Miller 3rd, E.R., Gelber, A.C., 2011. *Arthritis Care Res.* 63 (9), 1295–1306.
- Kaufman, L., Rousseeuw, P.J., 1990. *Finding Groups in Data: an Introduction to Cluster Analysis*. John Wiley & Sons, Inc, NJ.
- Kumar, D.R., Dhakal, G., Nguyen, V.Q., Shim, J.J., 2021. *Anal. Chim. Acta* 1141, 71–82.
- Meneghello, A., Tartaggia, S., Alvau, D.M., Polo, F., Toffoli, G., 2018. *Curr. Med. Chem.* 25 (34), 4354–4377.
- Naidu, A.K., 2003. *Nutr. J.* 2, 1–10.
- Ortiz-Aguayo, D., Bonet-San-Emeterio, M., del Valle, M., 2019. *Sensors* 19 (15), 3286–3298.
- Özcan, L., Şahin, Y., 2007. *Sens. Actuators B-Chem.* 127 (2), 362–369.
- Prince, M.I., Thomas, S.H.L., James, O.F.W., Hudson, M., 2000. *The Lancet* 355 (9220), 2047–2048.
- Rajesh, Takashima, W., Kaneto, K., 2004. *React. Funct. Polym.* 59 (2), 163–169.
- Raudsepp, T., Marandi, M., Tamm, T., Sammelselg, V., Tamm, J., 2008. *Electrochim. Acta* 53 (11), 3828–3835.
- Rebello, P., Costa-Rama, E., Seguro, I., Pacheco, J.G., Nows, H.P.A., Cordeiro, M., Delerue-Matos, C., 2021. *Biosens. Bioelectron.* 172, 112719–112736.
- Root-Bernstein, R., Churchill, B., Turke, M., 2020. *Int. J. Mol. Sci.* 21 (17), 6230–6250.
- Sarma, M., Romero, N., Cetó, X., del Valle, M., 2020. *Sensors* 20 (17), 4798–4712.
- Sieminska, E., Sobczak, P., Skibinska, N., Sikora, J., 2020. *Med. Hypotheses* 142, 109791–109801.
- Solanki, P.R., Arya, S.K., Singh, S.P., Pandey, M.K., Malhotra, B.D., 2007. *Sens. Actuators B-Chem.* 123 (2), 829–839.
- Suematsu, S., Oura, Y., Tsujimoto, H., Kanno, H., Naoi, K., 2000. *Electrochim. Acta* 45, 3813–3821.
- Vale, J.A., Proudfoot, A.T., 1995. *The Lancet* 346, 547–552.
- Wackerlig, J., Lieberzeit, P.A., 2015. *Sens. Actuators B-Chem.* 207, 144–157.
- Zaidi, S.A., 2018. *Sens. Actuators B-Chem.* 265, 488–497.
- Zhang, W., Duan, D., Liu, S., Zhang, Y., Leng, L., Li, X., Chen, N., Zhang, Y., 2018. *Biosens. Bioelectron.* 118, 129–136.



# Supporting Information

**A novel electronic tongue using electropolymerized molecularly imprinted polymers for the simultaneous determination of active pharmaceutical ingredients**

Mingyue Wang, Xavier Cetó and Manel del Valle<sup>1</sup>

*Sensors and Biosensors Group, Department of Chemistry, Universitat Autònoma de Barcelona, Faculty of Sciences, 08193 Bellaterra, Barcelona, Spain*

---

<sup>1</sup>e-mail: [manel.delvalle@uab.cat](mailto:manel.delvalle@uab.cat)

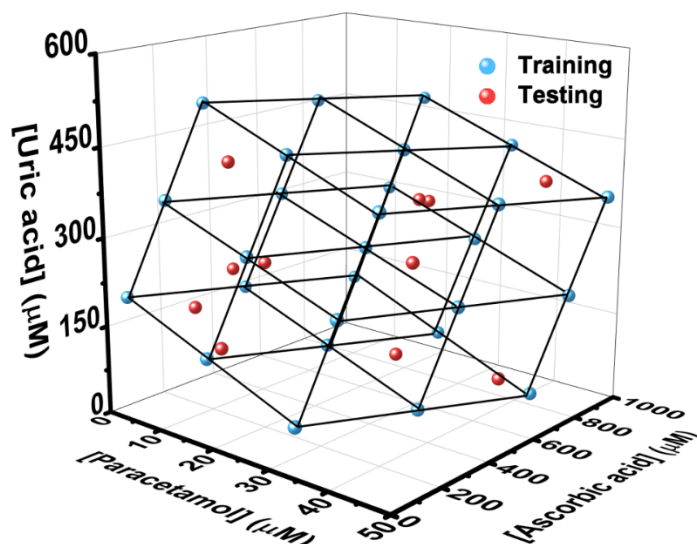


**Fig. S1.** Composition of the samples prepared for the analysis of paracetamol, ascorbic acid and uric acid mixtures: (blue) training subset based on a tilted  $3^3$  factorial design and (red) test subset based on random distribution along the experimental domain.

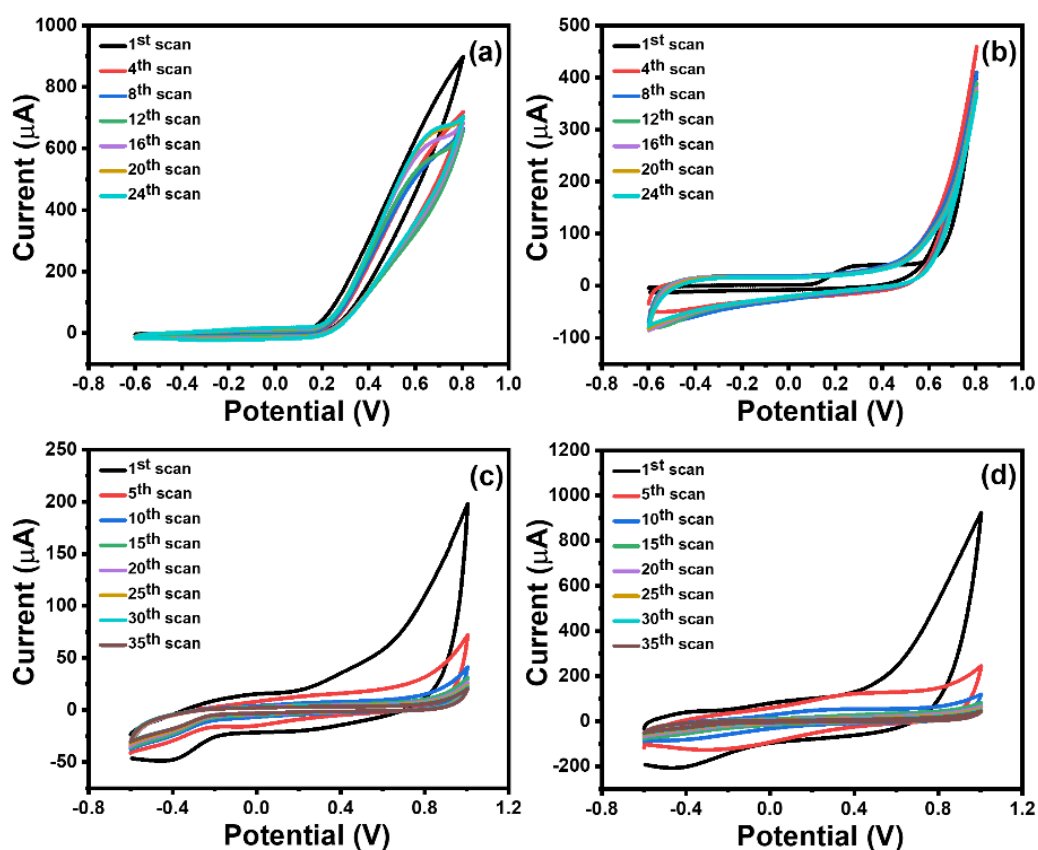


**Fig. S2.** Cyclic voltammograms recorded during the electropolymerization of pTS-/PPy onto a GEC in the presence of (a) ascorbic acid and (b) uric acid. Cyclic voltammograms recorded during the template extraction of (c) pTS-/PPy MIP(AA) and (d) pTS-/PPy MIP(UA).

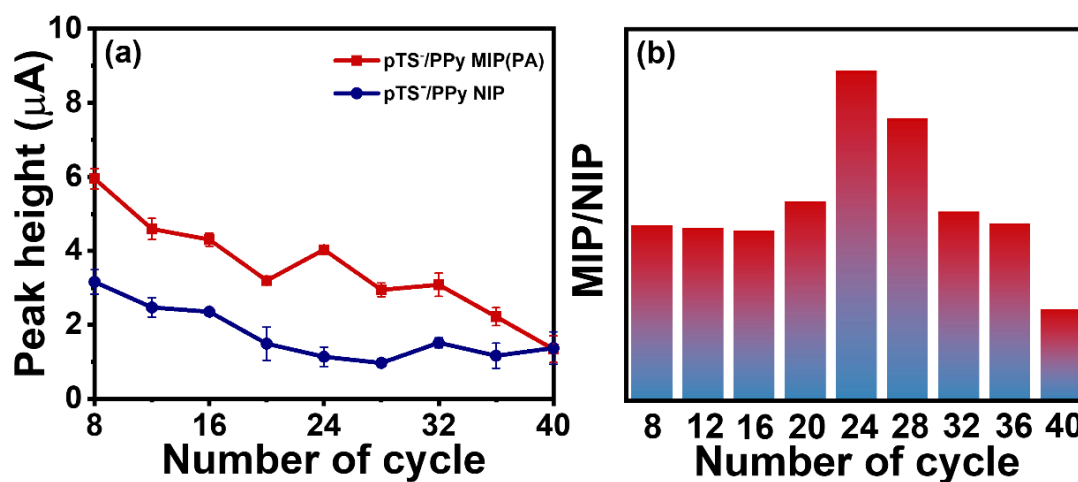


**Fig. S3.** Optimization of the number of scans during the electropolymerization. (a) Peak height derived from the DPV measurements towards a 30 μM PA solution in PBS for *p*TS-/PPy MIP(PA) and *p*TS-/PPy NIP. (b) Peak height ratio for *p*TS-/PPy MIP(PA) to *p*TS-/PPy NIP.

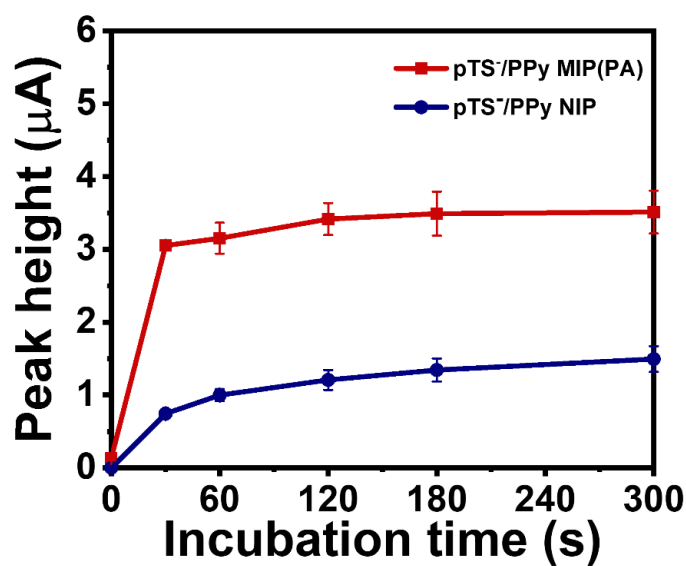


**Fig. S4.** Optimization of the incubation time of the MIP with the analytes before taking the measurement. Peak height derived from DPV measurements towards a 30 μM PA solution in PBS for *p*TS-/PPy MIP(PA) and *p*TS-/PPy NIP.

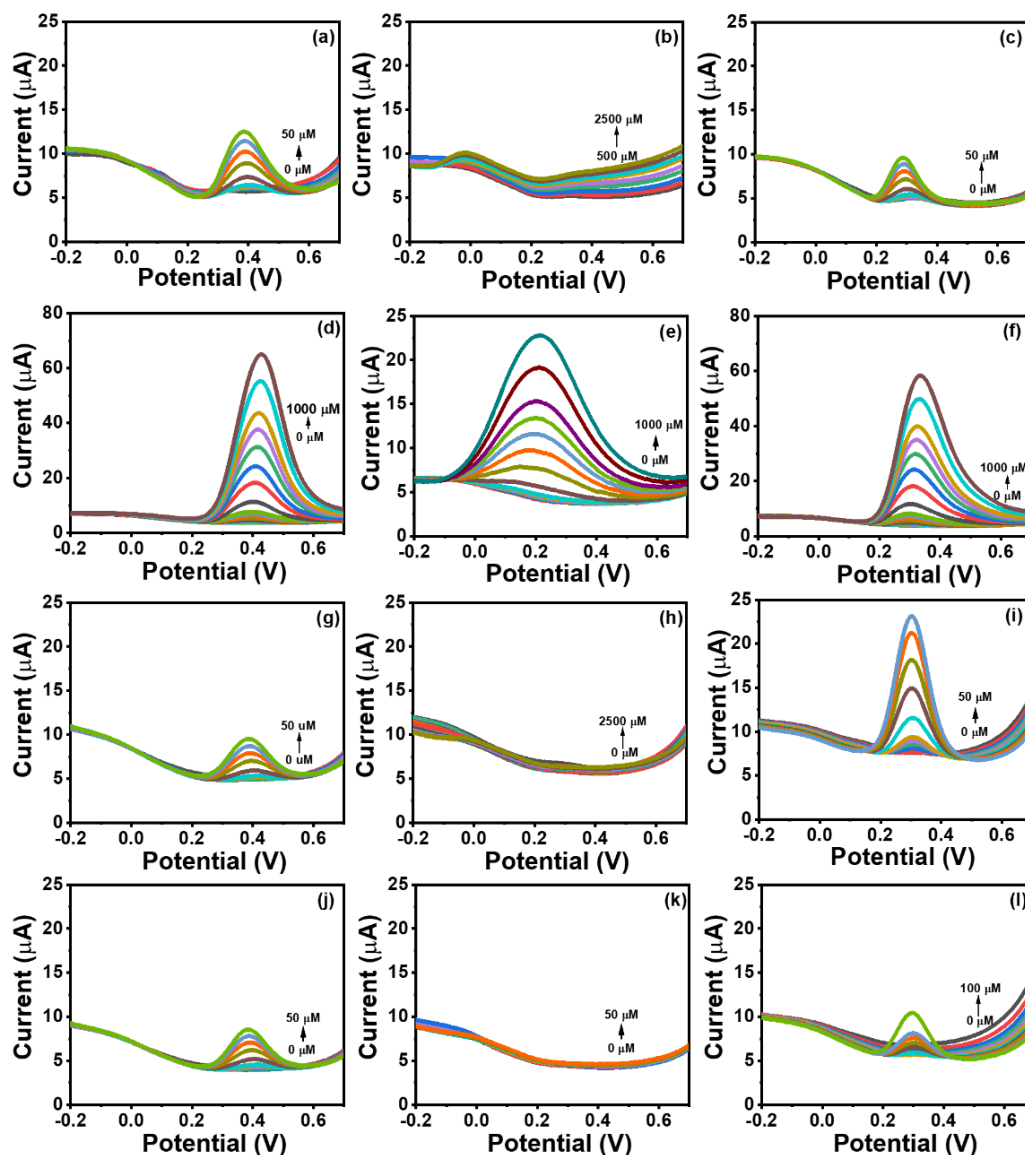


**Fig. S5.** DPV responses of *p*TS/PPy MIP(PA) to (a) PA, (b) AA and (c) UA. DPV responses of *p*TS<sup>-</sup>/PPy MIP(AA) to (d) PA, (e) AA and (f) UA. DPV responses of *p*TS<sup>-</sup>/PPy MIP(UA) to (g) PA, (h) AA and (i) UA. DPV responses of *p*TS/PPy NIP to (j) PA, (k) AA and (l) UA.

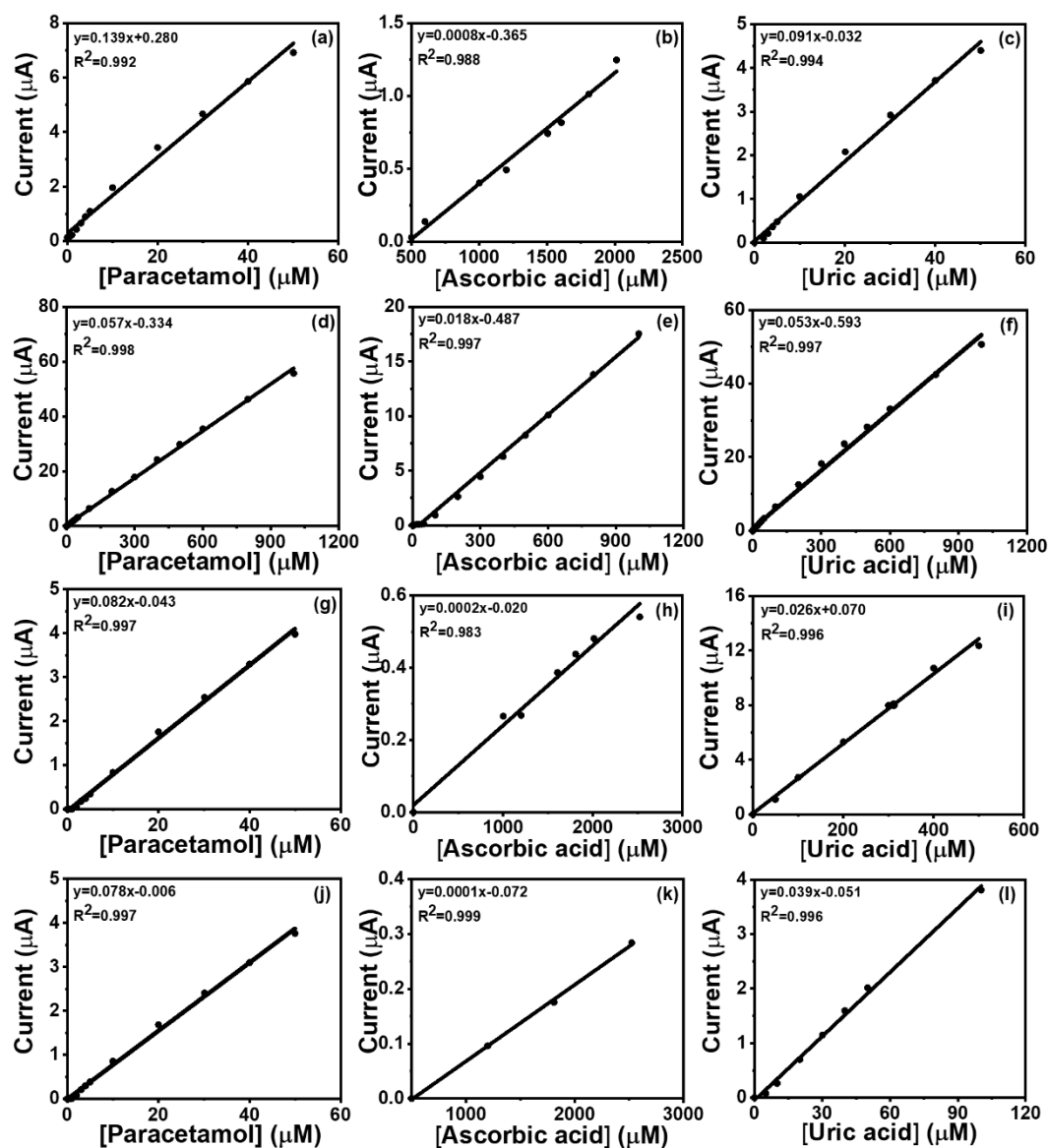


**Fig. S6.** Calibration graphs derived from the DPV peak heights of *p*TS/PPy MIP(PA) to (a) PA, (b) AA and (c) UA; *p*TS/PPy MIP(AA) to (d) PA, (e) AA and (f) UA; *p*TS/PPy MIP(UA) to (g) PA, (h) AA and (i) UA; and *p*TS/PPy NIP to (j) PA, (k) AA and (l) UA.

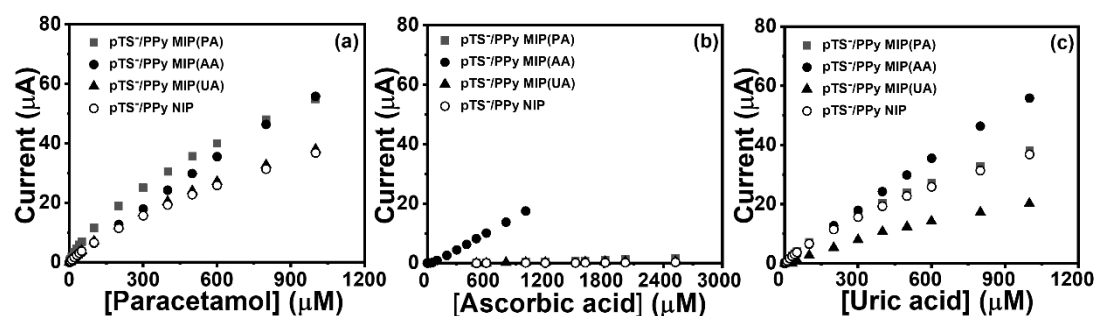


**Fig. S7.** Calibration graphs of the obtained  $pTS^-/PPy$  MIP(PA),  $pTS^-/PPy$  MIP(AA),  $pTS^-/PPy$  MIP(UA) and  $pTS^-/PPy$  NIP based biosensors for the three analytes (a) paracetamol, (b) ascorbic acid and (c) uric acid determined by DPV.

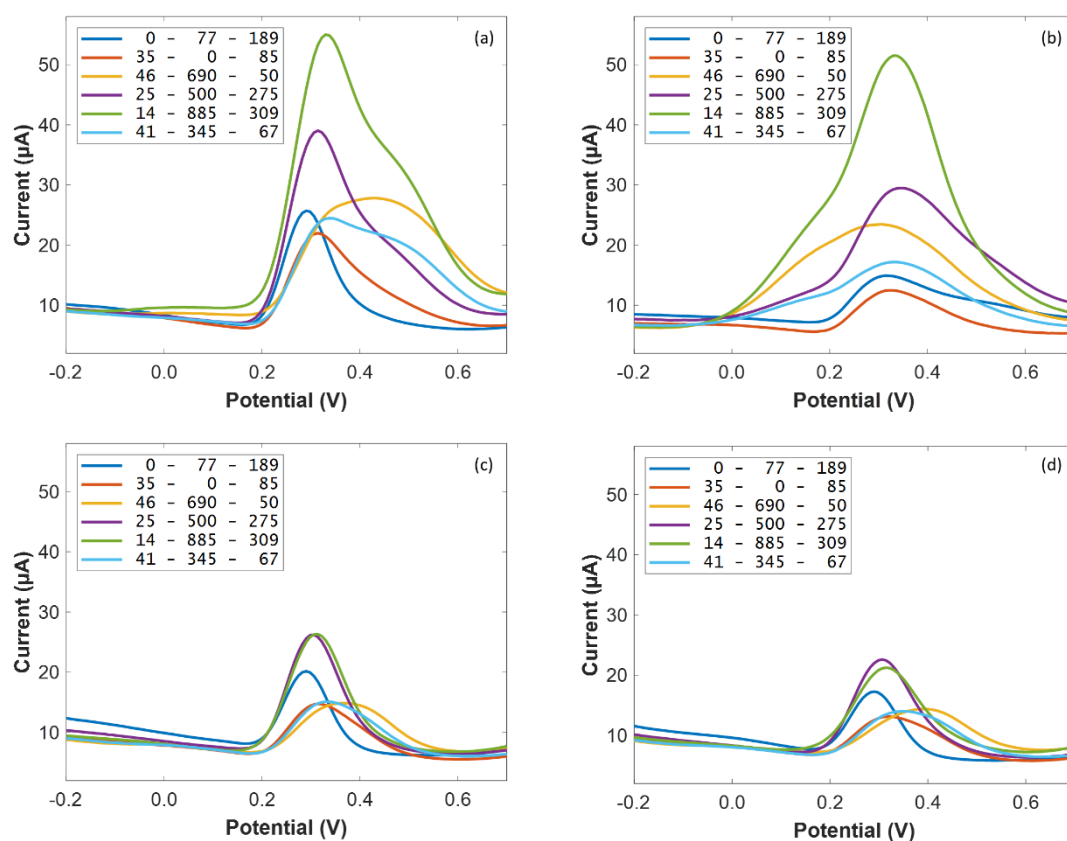


**Figure S8.** DPV responses of (a)  $pTS^-/PPy$  MIP(PA), (b)  $pTS^-/PPy$  MIP(AA), (c)  $pTS^-/PPy$  MIP(UA) and (d)  $pTS^-/PPy$  NIP to certain arbitrary mixtures of PA, AA and UA (the concentration for each compound is indicated in the legend).

**Table S1.** Intra-day repeatability expressed as the percentage of the relative standard deviation (RSD%) over 30 consecutive measurement cycles of blank/standard for each sensor and inter-day (day-to-day) repeatability over three consecutive days.

<b>Sensor</b>	<b>intra-day (RSD%)</b>	<b>inter-day (RSD%)</b>
pTS <sup>-</sup> /PPy NIP	6.1	6.5
pTS <sup>-</sup> /PPy MIP(PA)	3.5	4.1
pTS <sup>-</sup> /PPy MIP(AA)	3.3	4.6
pTS <sup>-</sup> /PPy MIP(UA)	5.9	6.2

**Table S2.** Reported and current values of the fitted regression lines of the obtained *vs.* expected comparison plots for the different sets of samples and the three considered APIs. Intervals are calculated at the 95% confidence level.

	Compound	Slope	Intercept ( $\mu\text{M}$ )	$R^2$	RMSE ( $\mu\text{M}$ )	Total NRMSE	Sensor array	Ref.		
train (n=33)	PA	$0.942 \pm 0.031$	$32 \pm 21$	0.968	$^{-1}$	$^{-1}$	Bare GEC plus metallic Pt and Au electrodes	(Gutés et al., 2007)		
	AA	$0.933 \pm 0.040$	$36 \pm 25$	0.947	$^{-1}$					
	UA	$0.873 \pm 0.046$	$58 \pm 25$	0.923	$^{-1}$					
test (n=15)	PA	$0.895 \pm 0.105$	$82 \pm 71$	0.848	$^{-1}$	$^{-1}$				
	AA	$0.919 \pm 0.081$	$65 \pm 41$	0.908	$^{-1}$					
	UA	$0.871 \pm 0.138$	$-8 \pm 86$	0.753	$^{-1}$					
train (n = 33)	PA	$0.981 \pm 0.032$	$13 \pm 24$	0.992	29	0.0257	Bare GEC plus metallic Pt and Au electrodes	(Cetó et al., 2013)		
	AA	$0.990 \pm 0.031$	$6 \pm 17$	0.993	25					
	UA	$0.981 \pm 0.027$	$9 \pm 16$	0.994	23					
test (n=15)	PA	$0.990 \pm 0.143$	$-2 \pm 80$	0.945	97	0.101				
	AA	$1.009 \pm 0.136$	$-28 \pm 78$	0.952	66					
	UA	$0.992 \pm 0.208$	$36 \pm 125$	0.891	73					
train (n=27)	PA	$1.000 \pm 0.082$	$0 \pm 25$	0.962	29	1	SPCEs modified with CoPc, PB, graphite and CuO	(Ortiz Aguayo et al., 2019)		
	AA	$1.000 \pm 0.089$	$0 \pm 25$	0.955	31					
	UA	$1.000 \pm 0.104$	$0 \pm 31$	0.94	36					
test (n=12)	PA	$1.021 \pm 0.219$	$-13 \pm 28$	0.915	32	1.03				
	AA	$1.073 \pm 0.422$	$-3 \pm 54$	0.762	71					
	UA	$1.044 \pm 0.334$	$-32 \pm 36$	0.829	44					
train (n=27)	PA	$0.996 \pm 0.006$	$0.9 \pm 1.9$	0.9998	2.43	0.00378	GECs modified with ZnO, PB, and PPy plus Pt metallic electrode	(Sarma et al., 2020)		
	AA	$0.999 \pm 0.004$	$1.1 \pm 4.6$	0.9999	5.86					
	UA	$0.996 \pm 0.004$	$1.1 \pm 1.2$	0.9999	1.64					
test (n=11)	PA	$1.021 \pm 0.134$	$9 \pm 36$	0.971	26.4	0.0368				
	AA	$1.017 \pm 0.049$	$-20 \pm 57$	0.996	31.2					
	UA	$0.999 \pm 0.096$	$1 \pm 27$	0.984	16.2					
train (n=27)	PA	$0.996 \pm 0.007$	$0.1 \pm 0.2$	0.9997	0.25	0.00511	GECs modified with pTS-/PPy MIP and NIP	This work		
	AA	$0.996 \pm 0.007$	$1.5 \pm 3.9$	0.9997	5.06					
	UA	$0.995 \pm 0.007$	$1.5 \pm 2.0$	0.9997	2.33					
test (n=11)	PA	$1.003 \pm 0.044$	$0.7 \pm 1.2$	0.997	1.12	0.0204				
	AA	$1.019 \pm 0.054$	$-7 \pm 29$	0.995	19.6					
	UA	$1.007 \pm 0.045$	$3 \pm 12$	0.997	8.44					

<sup>1</sup> data not available; RMSE: root mean square error; NRMSE: normalized root mean square error; GEC: graphite epoxy composite; SPCE: screen printed carbon electrode.



**Table S3.** Fitted regression lines for the comparison between obtained *vs.* expected values for the pharmaceutical samples and the three considered APIs. Intervals are calculated at the 95% confidence level.

Compound	Slope	Intercept ( $\mu\text{M}$ )	R <sup>2</sup>	RMSE ( $\mu\text{M}$ )	Total NRMSE
PA	0.980 $\pm$ 0.127	-1 $\pm$ 3	0.991	2.28	0.0363
AA	0.966 $\pm$ 0.037	9 $\pm$ 14	0.999	15.2	
UA	0.996 $\pm$ 0.158	5 $\pm$ 32	0.987	18.2	

## References

- Cetó, X., Gutés, A., del Valle, M., 2013. *Acta Manilana* 61, 39-49.
- Gutés, A., Calvo, D., Céspedes, F., del Valle, M., 2007. *Microchim. Acta* 157, 1-6.
- Ortiz-Aguayo, D., Bonet-San-Emeterio, M., del Valle, M., 2019. *Sensors* 19(15), 3286-3299.
- Sarma, M., Romero, N., Cetó, X., del Valle, M., 2020. *Sensors* 20(17), 4798-4813.

---

# Article 2

---

**A sensor array based on molecularly imprinted polymers and machine learning for the analysis of fluoroquinolone antibiotics**

Mingyue Wang, Xavier Cetó, Manel del Valle

ACS Sensors, submitted



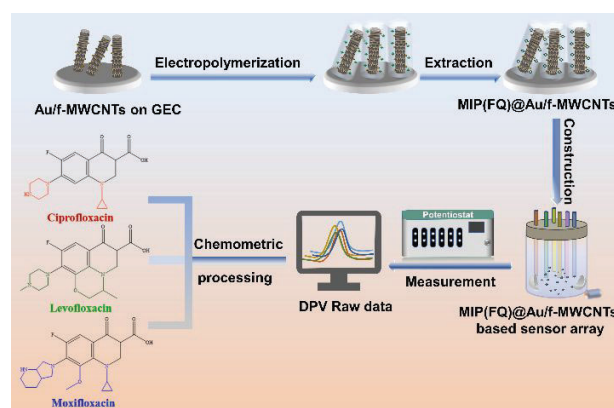
# A sensor array based on molecularly imprinted polymers and machine learning for the analysis of fluoroquinolone antibiotics

Mingyue Wang, Xavier Cetó and Manel del Valle\*

Sensors and Biosensors Group, Department of Chemistry, Universitat Autònoma de Barcelona, Faculty of Sciences, 08193 Bellaterra, Barcelona, Spain

**KEYWORDS:** *Molecularly imprinted polymers, electronic tongues, artificial neural networks, fluoroquinolones, antibiotics, pharmaceutical analysis*

**ABSTRACT:** Fluoroquinolones (FQs) are one of the most important types of antibiotics in the clinical, poultry and aquaculture industries, and their monitoring is required as the abuse has led to severe issues, such as antibiotic residues and antimicrobial resistance. In this work, we report a voltammetric electronic tongue (ET) for the simultaneous determination of ciprofloxacin, levofloxacin and moxifloxacin in both pharmaceutical and biological samples. The ET comprises four sensors modified with three different customized molecularly imprinted polymers (MIPs) and a non-imprinted polymer (NIP) incorporated with Au nanoparticles decorated multi-wall carbon nanotubes (Au-fMWCNTs). MWCNTs were first functionalized to serve as supporting substrate, while anchored Au nanoparticles acted as catalyst. Subsequently, MIP films were obtained by electropolymerization of polypyrrole in the presence of the different target FQs. The sensors' morphology was characterized by scanning electron microscopy (SEM) and transmission electron microscopy (TEM), while the modification process was followed electrochemically step by step employing  $[\text{Fe}(\text{CN})_6]^{3-/4-}$  as the redox probe. Under the optimal conditions, the MIP(FQs)@Au-fMWCNTs sensors exhibited differentiated responses, limits of detection (LOD) of *ca.* 0.1  $\mu\text{M}$  and a wide detection range up to 300  $\mu\text{M}$  for the three FQs. Lastly, the developed ET presents satisfactory agreement between expected and obtained values when used for the simultaneous determination of the three FQs in the mixtures ( $R^2 \geq 0.960$ , testing subset), that was successfully applied to the analysis of FQs in commercial pharmaceuticals and spiked human urine samples.



Fluoroquinolones (FQs), one of the most important family of antibiotics, are used individually or in combination against a broad spectrum of Gram-positive and Gram-negative bacteria in clinical and animal husbandry<sup>1,2</sup>. Among them, ciprofloxacin (CFX), levofloxacin (LFX) and moxifloxacin (MFX) are the most common in current clinical practice. LFX and MFX are considered as respiratory drugs that have good bactericidal activity against most of respiratory pathogens, while CFX is used to treat the infections of the urinary tract and intestine. Structurally, FQs are similar as they are all derived from nalidixic acid (NA), sharing the same quinoline ring, but with different substitutions. Although FQs usage is approved worldwide and their significant curative effects have been demonstrated, consequences resulting from their misuse such as antibiotic residues (mainly related to food safety and environmental contamination) or antimicrobial resistance (essentially requiring therapeutic drug monitoring) cannot be neglected<sup>3-5</sup>. Thus, FQs monitoring is required in different

stages, such as in pharmaceutical factories when produced, in hospitals during its administration to the patients or in the environment for the treatment of wastewater.

To date, the detection of FQs using electrochemical sensors has been proposed as a cheaper, time- and labor-saving alternative to complex detection methods such as high-performance liquid chromatography (HPLC) or gas chromatography-mass spectrometry (GC-MS)<sup>6</sup>. Nevertheless, most reported electrochemical sensors target only one specific FQ, and cannot achieve the simultaneous multi-determination in practical applications, or deal with the interferences that may arise from certain complicated matrices<sup>7,8</sup>. This can be rather thorny in the case of FQs family given the common-shared structure and similar natures.

Compared with the conventional approach, by coupling a sensor array providing responses to various analytes with appropriate data processing, electronic tongues (ETs) allow the discrimination and simultaneous quantification

of multiple analytes<sup>9,10</sup>, while they might also be able to solve other problems related to sensors such as drifts, interferences, cross-sensitivity and/or matrix effects.

To further improve the performance of ETs, one of trending strategies is using a proper set of biorecognition elements such as enzymes, peptides, etc.<sup>11</sup>. Recently, the feasibility of incorporating molecularly imprinted polymers (MIPs) into ETs has been investigated for the simultaneous determination of structurally similar analytes in various fields<sup>12,13</sup>. As artificial customized receptors, MIPs not only can afford equivalent specificity to a bioreceptor, but offer higher physical and chemical stability than biological recognition elements<sup>14,15</sup>. More importantly, the key-lock recognition mechanism between MIPs and the target compounds defined by the size and structure of the template molecules offers a simple and straightforward procedure for developing a series of MIP-based sensors to be combined into a sensor array for the development of ETs. However, despite MIPs' many merits, there is still space for the improvement of their integration into sensors, especially in regards to sensitivity<sup>16</sup>. Compared with other polymerization methods, electropolymerization can generate controllable MIPs thin films directly onto the sensors, representing a simpler, and highly reproducible approach for the integration of MIPs with electrochemical sensors<sup>17,18</sup>. Besides, the lower sensitivity derived from MIPs' intrinsically inferior conductivity and electrocatalytic activity could be improved by introducing nanomaterials<sup>19</sup>, *e.g.*, carbon nanotubes (CNTs)<sup>20</sup> or metallic nanoparticles (NPs)<sup>21</sup>.

To this end, herein we explore the electropolymerization of pyrrole onto multi-wall CNTs (MWCNTs) as supporting substrate that can lead to MIPs with a larger surface area, higher conductivity and amplified signal. In addition, the incorporation of metallic gold NPs (Au-NPs) can also act as a catalyst for the electrochemical reactions and further enhancing sensitivity. In this manner, MIPs integrated with these nanomaterials were synthesized towards ciprofloxacin, levofloxacin, and moxifloxacin. Next, the obtained sensors were characterized both morphologically and electrochemically, and finally combined into a sensor array, which was successfully employed to develop a MIP-based ET for the analysis of FQ antibiotics in commercial drugs and spiked human urine samples.

## Experimental section

**Materials and reagents.** Graphite powder (particle size <50  $\mu\text{m}$ ) and epoxy resin kit for fabricating graphite-epoxy composite (GEC) electrodes were supplied by Resinco (Barcelona, Spain). Pristine MWCNTs (outer diameter ~10-30nm) were obtained from SES Research Inc. (Houston, TX, USA). Pyrrole (Py) and anhydrous trisodium citrate were purchased from Alfa-Aesar (Ward Hill, MA, USA). Gold (III) chloride solution in hydrochloric acid (30 wt.%  $\text{HAuCl}_4$ ), perfluorinated resin solution containing Nafion, ciprofloxacin (CFX), levofloxacin (LFX), moxifloxacin (MFX), flumequine (FLQ) and nalidixic acid (NA) were purchased from Aldrich (St. Louis, MO, USA),

while sodium borohydride, potassium hexacyanoferrate (II) trihydrate and potassium hexacyanoferrate (III) from Panreac (Barcelona, Spain). Ethanol (EtOH, 96 vol. %) and NaOH were bought from Scharlau (Barcelona, Spain).

All solutions employed in the experiments were prepared using deionized water from a Milli-Q System (Millipore, Billerica, MA, USA). Various buffer solutions were used in this work for different purposes. Concretely, 50 mM phosphate buffer (PBS) at pH 7.0 containing 100 mM potassium chloride was used for the electrochemical characterization, while 100 mM PBS at pH 10.0 was used for the electrochemical extraction and cleaning. 100 mM acetate buffer at pH 3.5 was used for the electropolymerization and the preparation of the stock solutions', while 100 mM acetate buffer at pH 4.5 was employed for the analysis of FQs.

**Apparatus.** A EVO MA10 (Zeiss, Oberkochen, Germany) and a JEOL 1210 (Peabody, MA, USA) were used for scanning and transmission electron microscopy (SEM/TEM), respectively. An Autolab PGSTAT30 (Ecochemie, Utrecht, Netherlands) with multichannel configuration controlled by GPES and FRA software packages was used for the electrochemical measurements.

**Fabrication of MIP(FQs)@Au-fMWCNTs sensor.** Hand-crafted GEC electrodes, that served as sensor platforms for the construction of the MIP-based sensor array, were prepared according to the previous reports from our group<sup>22</sup>. Briefly, the paste was prepared by mixing 58 % of graphite powder and 42 % of the epoxy resin. Next, this paste was placed into a PVC tube, in which a copper disc soldered to a connector had previously been inserted, and cured at 40  $^{\circ}\text{C}$  for 2 days. Finally, the electrodes were polished and ready to use.

Pristine MWCNTs were pre-treated with strong acids to obtain carboxylic functionalized MWCNTs (fMWCNTs). First of all, MWCNTs were dispersed in an acid mixture of concentrated  $\text{H}_2\text{SO}_4/\text{HNO}_3$  (v/v 3:1) by ultrasonication for 6h at 40  $^{\circ}\text{C}$ . Then, washed with Milli-Q water until neutralized, and dried in the oven for further using.

The decoration of fMWCNTs with AuNPs was performed according to the previously reported procedures<sup>23</sup>. Specifically, 500  $\mu\text{L}$  of 10 mM  $\text{HAuCl}_4$ , 500  $\mu\text{L}$  of 10 mM tri-sodium citrate and 18.4 mL Milli-Q water were mixed in a round-bottom flask, to which 20 mg of fMWCNTs and 10 mL of anhydrous ethanol were added. After sonicating for 10 min, 600  $\mu\text{L}$  of a 100 mM freshly prepared cold  $\text{NaBH}_4$  solution were also added into the mixture. The reaction lasted for 10 hours under continuous stirring. The obtained product (denoted as Au-fMWCNTs) was thoroughly washed with Milli-Q water and dried in the oven at 40  $^{\circ}\text{C}$  overnight.

For the modification of the sensors, 2.0 mg of the dried Au-fMWCNTs powder was dispersed in 1 mL of N, N-dimethylformamide (DMF), into which 100  $\mu\text{L}$  of Nafion were added to improve the stability of Au-fMWCNTs on the surface of the electrodes upon drop casting. Finally, 4  $\mu\text{L}$  of Au-fMWCNTs dispersion in DMF was evenly dropped onto

the surface of the GEC and dried in the oven.

The synthesis of the MIP(FQs) film on the surface of Au-fMWCNTs was performed by the electropolymerization method. The solution containing 0.05 M pyrrole as the functional monomer, 0.01M FQ (either CFX, LFX, or MFX) as the template molecule and 20 mL of acetate buffer (pH 3.5) as the supporting electrolyte was purged with nitrogen for 10 min before using for the synthesis of the MIP(FQ) film. The electropolymerization was conducted by cycling the potential from 0.0 V to +1.3 V vs. Ag/AgCl at a scan rate of 50 mV·s<sup>-1</sup> (Figure S1). Subsequently, extraction of the template molecules from the polymer film was done in a two steps procedure. First, cycling the potential from 0.0 V to +1.5 V vs. Ag/AgCl at a scan rate of 100 mV·s<sup>-1</sup> in PBS (pH 10.0) (Figure S1), followed by the immersion of the electrodes into a mixture of EtOH/0.1 M NaOH (1:1 v/v) for 30 min.

Similarly, the same procedures as above-mentioned were used for the synthesis of the non-imprinted polymer on Au-fMWCNTs (NIP@Au-fMWCNTs), except that no FQ was added during the electropolymerization. The purpose of the NIP is to be used as control.

**Electrochemical measurements.** All electrochemical measurements were performed at room temperature in a standard three electrode cell made up of an Ag/AgCl (3 M KCl) reference electrode, a Pt wire as auxiliary electrode and the MIP(FQs)@Au-fMWCNTs or NIP@Au-fMWCNTs modified GECs as the working electrodes. Both cyclic voltammetry (CV) and electrochemical impedance spectroscopy (EIS) for the electrochemical characterization were conducted in a 5 mM K<sub>3</sub>[Fe(CN)<sub>6</sub>]/K<sub>4</sub>[Fe(CN)<sub>6</sub>] solution in PBS (pH 7.0). For CV measurements, the potential was scanned in the range from -0.2 V to +0.7 V at a scan rate of 50 mV·s<sup>-1</sup>, while for EIS, a frequency range between 100 kHz to 100 mHz with a fixed AC amplitude of 10 mV and an applied potential of +0.24 V was considered.

For the analysis of FQs, differential pulse voltammetry (DPV) measurements were performed by scanning the potential from +0.6 V to +1.5 V with a step potential of 5 mV and a pulse amplitude of 50 mV without stirring. Prior to each measurement, the electrodes were incubated in the solution to be analyzed for 300s under stirring to enhance the enrichment of the analytes into the material. To regenerate the electrodes, a fix potential of +1.2 V for 90 s was applied in PBS (pH 10.0) after each measurement.

**Samples preparation.** Given the different solubility of the different FQs, the stock solutions of CFX, LFX, MFX and NA were prepared in acetate buffer (pH 3.5), whilst the stock of FLQ was prepared in 0.1M NaOH solution. In order to characterize the analytical response of the developed sensors towards each of the analytes, the individual calibration curves were constructed by measuring solutions of increasing concentrations prepared by proper dilution of the FQs' stock solutions in buffer (pH 4.5).

For the simultaneous quantification of CFX, LFX and MFX, two subsets of samples were prepared and measured

under identical conditions in randomized order. On the one side, the training subset was composed by 27 samples based on a 3<sup>3</sup> tilted factorial design<sup>24</sup>, in which the concentrations of FQs were specified in the range from 2 to 300 μM for CFX, LFX and MFX. On the other side, to evaluate the performance of the proposed model, the testing subset was composed by 10 samples that were randomly distributed in the concentration domain defined by the factorial design.

To demonstrate its applicability, the MIP-based ET was applied to the determination of the FQs under study both in commercial pharmaceuticals and biological fluids. On the one hand, commercial antibiotic drugs were bought from the local drug stores with the doctor's prescription. Specifically, four different FQ antibiotic drugs were evaluated: *Cetraxal plus* (3 mg·ml<sup>-1</sup> ciprofloxacin and 0.25 mg·ml<sup>-1</sup> fluocinolone acetonide; Laboratorios SALVAT, S.A., Barcelona, Spain), *Ciprofloxacin Normon* (250 mg ciprofloxacin; Normon Laboratories, S.A., Madrid, Spain), *Levofloxacin Aurovitas* (500 mg levofloxacin; APL Swift Services Limited, Birzebbugia, Malta) and *Moxifloxacin Qualigen* (400 mg moxifloxacin; Pharmathen, S.A., Attiki, Greece). For the analysis, drugs were dissolved or diluted in acetate buffer (pH 4.5) directly to make the expected concentrations fit in the experimental domain of the built model. Moreover, as there might be the cases in the clinical use where multiple antibiotics are used in combination, or for quality control purposed during drugs production, the above antibiotic drugs were analyzed both individually or in mixtures. On the other hand, considering the urine excretion rate of FQ antibiotics<sup>25</sup>, the analysis of FQs in human urine was also attempted. Urine samples were collected in sterile bottles from volunteers, diluted 40 times with acetate buffer (pH 4.5), and then spiked with the FQ stocks. Again, the dilution of urine samples was required so as to ensure the concentration falls within the experimental domain of the model. All real samples were measured under the same conditions as already described, without any further pre-treatment.

**Data Processing.** Multivariate analysis was carried out in Matlab 7.1 (MathWorks, Natick, MA, USA) by means of specific routines developed by the authors employing its Statistics and Neural Network toolboxes. The voltammetric responses of the sensor array were combined and compressed employing discrete cosine transform (DCT), which allowed to reduce the dimensionality of the input signals, while preserving the relevant information<sup>26</sup>. Next, the obtained coefficients were either submitted to principal component analysis (PCA) or artificial neural networks (ANNs).

## Results and discussion

**Design of MIP(FQs)@Au-fMWCNTs based ET.** The main goal of this work is the development of a sensitive ET for the simultaneous identification and quantification of FQs (Figure S2). In this regard, the fabrication of MIP-based electrochemical sensors towards FQs (MIP(FQs)) is based on the electropolymerization approach. To further



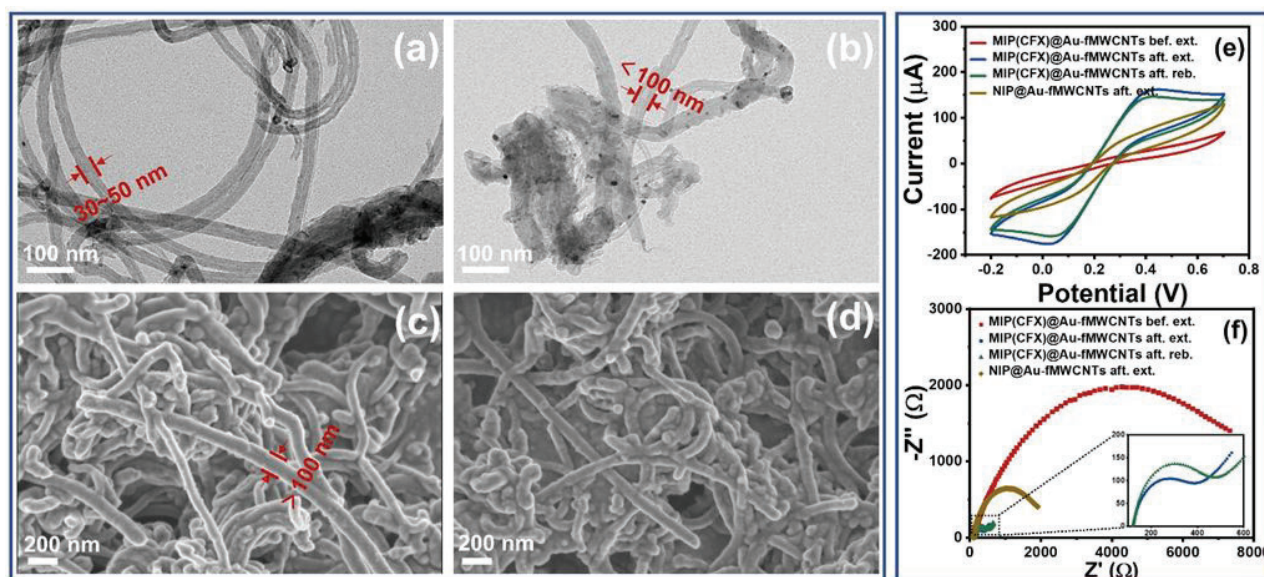


**Figure 1.** TEM images of (a) fMWCNTs and (b) Au-fMWCNTs. SEM images of MIP(CFX)@Au-fMWCNTs on GEC (c) before and (d) after the extraction of the template. Electrochemical characterization of the different steps involved from the preparation of the sensors to the actual sensing by means of (e) CV and (f) EIS employing a 5 mM  $[\text{Fe}(\text{CN})_6]^{3-/4-}$  solution in PBS: (from top to bottom) synthesis of the MIP towards CFX, before and after extraction of the template; MIP towards CFX upon rebinding; and NIP after extraction process.

improve the performance of the MIP-based sensors, fMWCNTs that have high conductivity and AuNPs that have electrocatalytic properties were incorporated before the electropolymerization of MIP(FQs) films, as depicted in Scheme S1a. Upon synthesis of the different MIPs, those sensors were combined into a sensor array to achieve the simultaneous determination of the three FQs in the mixtures. (Scheme S1b).

One of the key parameters for MIP-based sensors is the thickness of the MIP films, which is critical for the mass and electron transport. This was optimized by adjusting the number of cycles during the electropolymerization in the range from 5 to 35 cycles. As shown in Figure S3a, the current peak of MIP(CFX)@Au-fMWCNTs is higher when 10 cycles were selected, thick film cannot ensure an efficient electron and mass transport. Moreover, a sufficient number of specific sites also plays an important role in the specific recognition of the template by the MIP. While a low concentration of the template might lead to a poor imprinting, a too large amount of the template is not good for the formation of the polymers. To this end, the molar ratio of Py to CFX in the electropolymerization solution was optimized (Figure S3b), from which a ratio of 5:1 was selected as the optimal.

**Morphological characterization of MIP(FQs)@Au-fMWCNTs sensors.** Both SEM and TEM were used to characterize the morphology of the fabricated nanomaterials. Figure S4a corresponds to the SEM top view of the bare GEC electrode, showing a smooth and uniform surface, which is in contrast to the images after Au-fMWCNTs casting (Figure S4b) and electropolymerization (Figure S4c), undoubtedly

confirming the modification of the electrode. As mentioned earlier, the combination of MWCNTs and AuNPs with MIP films allows to obtain a synergistic effect that results in an improvement of the sensor's performance. Figure 1a-b show the TEM images of fMWCNTs before and after its decoration with AuNPs, from which it can be seen that the diameter of the CNTs in both cases is certainly smaller than 100 nm. Furthermore, the surface of the CNTs seen in Figure 1a is smooth and without particles on them, while the ones in Figure 1b are clearly decorated with small particles on the surface, corresponding to the AuNPs.

Since different MIPs were obtained by introducing different FQs molecules during the electropolymerization process, the MIP(CFX) film grown onto Au-fMWCNTs will be presented as an example. The morphology of the MIP(CFX)@Au-fMWCNTs before and after the extraction of the template molecule was characterized by SEM, as shown in Figure 1c-d, respectively. From Figure 1c, it can be seen how the diameter of Au-fMWCNTs increased significantly due to the growth of the MIP film on the surface, as this is now larger than 100 nm. It is noteworthy that a thin and uniform MIP film grew along the surface of the Au-fMWCNTs instead of integrally aggregating as a top layer that covers the whole. A peculiar morphology is attributed to the electropolymerization method employed, which not only allows a better control over the distribution and thickness of the MIP film, but also facilitates the surface imprinting and the formation of a core-shell structure<sup>27</sup>. Finally, from the comparison of Figure 1c-d, it can be seen how there are no significant morphological changes in the MIP(CFX)@Au-fMWCNTs structure after the extraction of the template and immersion in the EtOH-NaOH mixture, confirming the stability of the developed

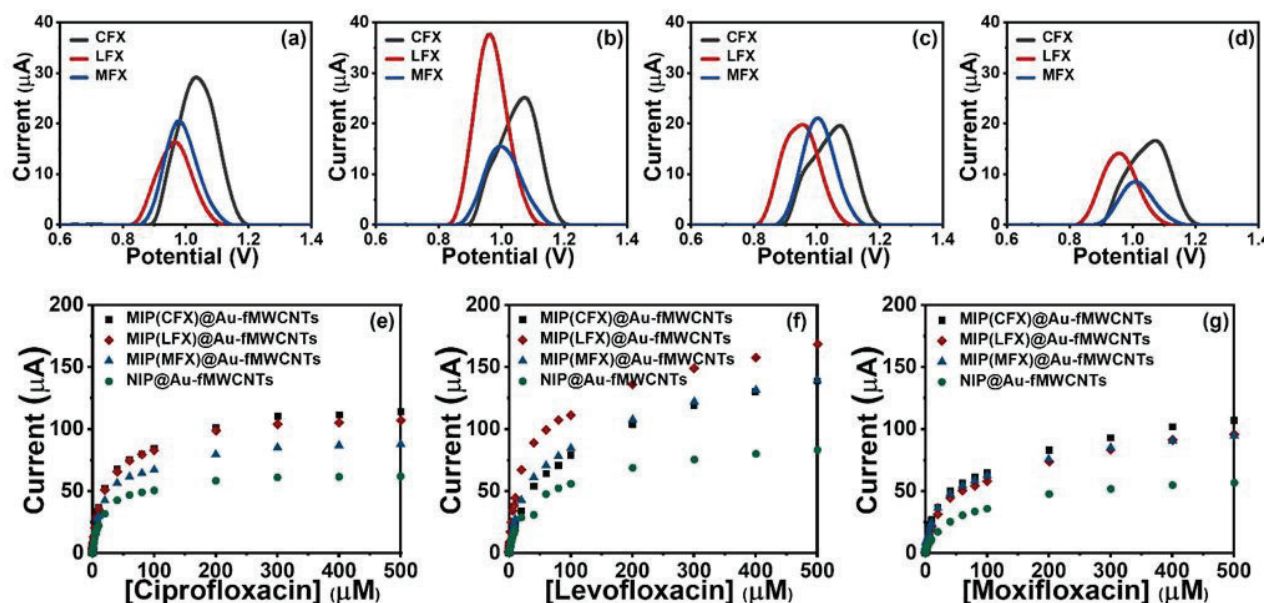


**Figure 2.** (a-d) Baseline corrected DPV curves of (a) MIP(CFX)@Au-fMWCNTs, (b) MIP(LFX)@Au-fMWCNTs, (c) MIP(MFX)@Au-fMWCNTs and (d) NIP@Au-fMWCNTs towards  $10\text{ }\mu\text{M}$  solutions of: (black) CFX, (red) LFX and (blue) MFX. (e-g) Calibration plots of the three target FQs (e) CFX, (f) LFX and (g) MFX with the MIPs- and NIP-based sensors.

nanocomposite material. Moreover, the SEM image of the NIP@Au-fMWCNTs (Figure S4c) also shows a similar morphology, confirming the expected similarities between the different synthesized MIP and NIP films.

**Electrochemical characterization of MIP(FQs)@Au-fMWCNTs sensors.** The electrochemical behavior of the sensors was investigated by CV and EIS in a  $5\text{ mM K}_3[\text{Fe}(\text{CN})_6]/\text{K}_4[\text{Fe}(\text{CN})_6]$  solution. Firstly, the response of the bare GEC was evaluated (Figure S5a), from which the reversible redox peaks of  $[\text{Fe}(\text{CN})_6]^{3-/4-}$  were observed. Next, this was compared to fMWCNTs and Au-fMWCNTs modified GEC, demonstrating that loading of fMWCNTs with AuNPs enhanced the electron transfer, which is reflected in more intense peaks in CV and a much lower charge transfer resistance in EIS. Subsequently, analogous comparison was conducted between the bare MIP and that incorporating Au-fMWCNTs (Figure S5c-d). As it can be seen, the MIP(CFX)@Au-fMWCNTs provides a better electrochemical performance than the MIP(CFX), but worse than Au-fMWCNTs (Figure S5c-d). As it can be seen, the MIP(CFX)@Au-fMWCNTs provides a better electrochemical performance than the MIP(CFX), but worse than Au-fMWCNTs (Figure 2 and S5) due to the poor electrical conductivity and blocked electron transport contributed by polymeric matrix. After the extraction of the template, we can observe a significant improvement of the electrochemical behavior both in the CV and EIS for the MIP because the sites created during the extraction process facilitate the electron and mass transport, while the NIP still showed a quite resistive behavior. Lastly, rebinding of these sites in the MIP film with the template was evaluated, and the sluggish diffusion of  $[\text{Fe}(\text{CN})_6]^{3-/4-}$  due to the "gate-controlled effect" is clearly reflected in the

graph. Consequently, taking the above results from CV and EIS, the suitability of the developed MIP-based electrochemical sensor has been confirmed.

**Optimization of the measuring conditions.** In order to enhance the voltammetric responses of the sensors, the measuring conditions of FQs were optimized. As previous, the response of the MIP(CFX)@Au-fMWCNTs sensor is shown as an example, taking the peak height from the DPV measurement towards a stock solution of CFX as the parameter to maximize. Firstly, the influence of the pH of the buffer was investigated in the range from 3.5 to 5.5 (Figure S6), obtaining that pH 4.5 is the most suitable.

Secondly, the incubation time was also optimized as an essential factor for the binding of the target analytes into the MIP film sites. Figure S7a shows how the response of the MIP-based sensor increases with the incubation time, until reaching a maximum at 300 s, indicating that the saturation has been reached. In addition, the time of the electrochemical treatment required for the sensor's regeneration after the sensing was also studied, observing that for the measurement of a  $10\text{ }\mu\text{M}$  CFX solution, 30 s is sufficient to recover the baseline (Figure S7b). However, to ensure that proper regeneration is achieved even when higher target concentrations are tested, 90 s is chosen as the regeneration time for further experiments.

**Calibration of MIP(FQs)@Au-fMWCNTs to FQs.** One of the fundamental steps when developing sensors is the characterization of their response in terms of linearity, sensitivity, limit of detection (LOD), reproducibility, etc. Furthermore, when developing an ET, it is also important to assess the cross-responses towards the different target analytes. To this aim, solutions with increasing concentrations of different FQs were analyzed using the



different sensors by DPV under the optimized conditions. An extract of the voltammetric responses is provided in Figure 2a-d (extracted from Figure S8a-d), where it can be seen how the three different MIP-based sensors show a voltammetric response to the three FQs (CFX, LFX and MFX respectively), and so does the NIP-based sensor. However, the differences in the peaks' position and height should be noted. As anticipated, the NIP@Au-fMWCNTs based sensor shows the lowest response to the three FQs compared with the other three MIP-based sensors due to the lack of recognition sites towards the FQs. Furthermore, when comparing the responses of specific MIP(FQ)@Au-fMWCNTs based sensor to the different FQs, it can be found that each MIP shows the highest response to its specific template (Figure 2). That is, MIP(CFX)@Au-fMWCNTs clearly shows the highest peak to CFX, while MIP(LFX)@Au-fMWCNTs does to LFX, confirming the specific recognition of the different MIP(FQ) films. The fact that MIP(MFX)@Au-fMWCNTs response to MFX is not as significantly higher, is attributed to the intrinsically higher electrochemical response of the other FQs, as is seen for the NIP. In this regard, it can be deduced that the similar structure and nature of FQs, all based on different substitutions made to the quinoline ring, hinders the obtaining of a highly specific MIP-based sensor, but leading to a class-selective material rather than a highly-specific one; a situation, which is well suited for ET approaches, as the chemometrics can assist in improving its specificity.

After preliminary assessing the responses of the different sensors to the different FQs, the proper calibration of each MIP(FQs)@Au-fMWCNTs and NIP@Au-fMWCNTs was carried out. From Figure S9, it can be seen how the peak currents increase steadily with increasing FQs' concentration. A hyperbolic response was observed as evidenced in Figure 2e-g, from which the dissociation constant ( $K_D$ ) and the maximum binding response at saturation ( $B_{max}$ ) were calculated, by fitting those to a one site saturation ligand binding model (Langmuir model, Table S1). Furthermore, a logarithmic relationship between the concentrations and the corresponding peak heights was found for low concentrations (from which the limit of detection could be calculated). In all the cases, a good linear relationship for the three FQs is obtained, with  $R^2$  values close to 1.

**Qualitative analysis of FQs.** Despite MIP-based sensors are meant to be highly specific, those might still show certain cross-response when analogous molecules are analyzed; for instance, when analyzing the various FQs. Generally speaking, one of optional solution to the issue of deficient selectivity may be seeking to synthesize more advanced MIP-based materials. For example, in this case, deficient selectivity for FQs may be partially attributed to the use of electropolymerized Py instead of a more sophisticated polymerization method employing carefully screened monomers and cross-linkers. However, the truth is that similar behavior has also been reported with other polymerization strategies<sup>28,29</sup>. In this direction, herein we

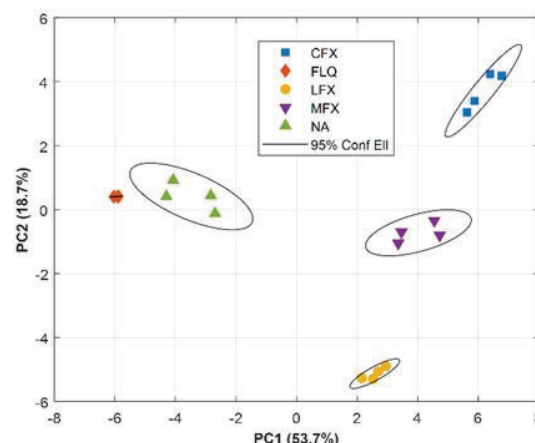


**Figure 3.** Scores plot obtained from the DCT-PCA of the voltammetric responses of the MIP-based ET towards five different FQs. Ellipses plotted correspond to 95% confidence limits for each of the clusters.

propose the combination of chemometrics with MIPs as a straightforward solution to further improve its selectivity. Such an approach allows to shift the complexity from the chemistry to the data processing side, while in turn, further advantages might also be obtained; e.g., being able to work with non-linear systems or to counterbalance possible matrix effects<sup>9,30</sup>.

In order to demonstrate such statement, the analysis of stock solutions of five different FQs was carried out employing the three developed MIP- and the NIP-based sensors under the optimized conditions. Next, the voltammetric responses were compressed by means of DCT, from 114 points down to 12 coefficients with high fidelity as evidenced from Figure S10, and submitted to PCA (Figure 3). Firstly, it should be noted that *ca.* 72.4% of the original data variance is now represented by only those two first principal components (PCs), providing a better representation of samples' measurements that allows an easier assessment of its (dis)similarities. Secondly, we can see how different clusters corresponding to each of the FQs are, and how these clusters separate from each other. Consequently, the superb ability of ET to discriminate FQs being well denoted.

**Quantification of FQs.** In view of the above results, the quantification of mixtures of different FQs was attempted; concretely, mixtures of CFX, LFX and MFX. To this aim, the set of samples described in experimental section were analyzed, and as before, the obtained responses were compressed by means of DCT. In this case, ANNs were chosen for the data modelling, making use of the samples of the training subset to optimize the topology of the neural network, while those of the test subset were used to assess the model performance. In this manner, ensuring a more realistic assessment of the model performance as different data subsets are used for each step.

After an iterative trial-and-error process, in which the

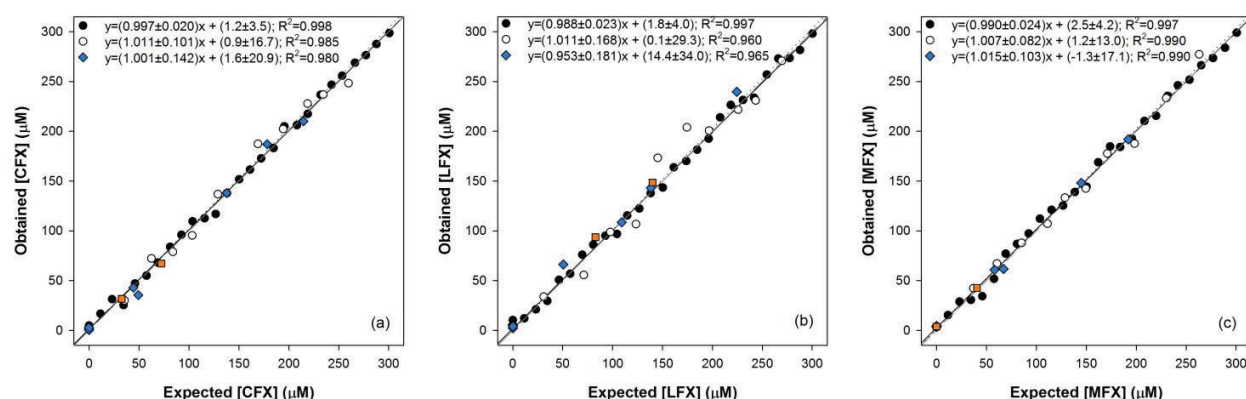


**Figure 4.** Modeling ability of the DCT-ANN. Comparison graphs of obtained vs. expected concentrations for (a) CF, (b) LF and (c) MF, for both the training (●, solid line) and testing subsets (○, dotted line). Dashed line corresponds to the ideal comparison line ( $y=x$ ). The results of the analysis of the pharmaceutical samples (◆) and spiked human urine samples (■) are also plotted.

different neural network parameters were tuned, the final architecture had 48 inputs neurons (12 coeffs. x 4 sensors) in the input layer, 7 neurons and *logsig* transfer function in the hidden layer and 3 neurons and *tansig* transfer function in the output layer (one for each of the FQs under study). Subsequently, comparison graphs of predicted vs. expected concentrations were built, both for the training and testing subsets, to easily assess its performance (Figure 4). Moreover, the regression parameters were also calculated to numerically assess the goodness of the modelling. As can be observed from Figure 4, for each FQ, a good trend was obtained with regression lines close to the ideal ones ( $y=x$ , slope, intercept and correlation coefficient values of 1, 0 and 1, respectively). Consequently, confirming the potential of the approach not only to discriminate between different FQs (as shown previously with the PCA), but also to quantify them individually even in the mixtures. Finally, to further demonstrate the applicability of the proposed MIP-based ET, some pharmaceutical and human urine samples were analyzed. For both of them, no other sample pretreatment than its proper dilution to fit within the evaluated range of concentrations was carried out. As before, the corresponding readings of the sensors were compressed with DCT and interpolated into the built ANN model. Those are also plotted in Figure 4, where a good agreement between the expected and predicted values is also observed despite the relatively complex matrixes of the pharmaceutical tablets (excipients, fillers, disintegrants, binders, etc.) and urine (urea, inorganic salts, creatinine, uric acid, proteins, vitamin, etc.). Again, confirming the suitability and advantages derived from the combination of MIPs and ETs, as not only the lack of selectivity of MIPs has been addressed, but those were successfully applied to the quantification of FQs mixtures in real samples.

## Conclusions

Herein, a sensitive ET based on different MIPs incorporating Au-NPs decorated MWCNTs has been developed for the analysis of FQs. In contrast to the

conventional methods for MIPs' synthesis, in this work, MIPs films were electropolymerized directly on the surface of Au-fMWCNTs. The use of electropolymerization facilitates the integration of MIPs with voltammetric sensors, while the combination of CNTs large surface/mass ratio and high conductivity and the catalytic effect of Au-NPs with the specific recognition of MIPs, leads to a synergistic effect that leads to an improved performance of the developed sensors.

The developed sensors were morphologically and electrochemically characterized to confirm the modification of the electrodes and assess their analytical responses. Despite the good performance obtained, the similar structure of the different FQs, hinders the obtaining of highly specific MIPs, leading to a class-selective material rather than a highly-specific one. In this direction, to improve its specificity, developed MIP-based sensors were combined into a sensor array to develop a MIP-based ET. Thanks to the use of chemometrics, it was possible not only to discriminate between different FQs, but also to achieve the simultaneous quantification of ciprofloxacin, levofloxacin and moxifloxacin. Finally, the developed ET was applied to the analysis of pharmaceutical and biological samples, with satisfactory recovery values obtained, confirming the lack of matrix effects.

Overall, the proposed approach represents an appealing and promising tool for the determination of FQs, but more importantly, paves the way for the development of similar applications. On the one side, electropolymerization represents a facile approach for the fabrication of MIP-based sensors, while the integration of nanomaterials leads to an improved electrochemical behavior. On the other side, chemometric methods provide a straightforward approach to tackle MIPs cross-response.

## ASSOCIATED CONTENT

**Supporting Information.** Molecular structure of analytes; SEM images of the sensors; voltammograms recorded during the electropolymerization; optimization of the experimental conditions; characterization of the voltammetric responses;

detailed results of the data treatment. This material is available free of charge via the Internet at <http://pubs.acs.org>.

## ACKNOWLEDGMENT

The authors acknowledge the support of the Spanish Ministry of Science and Innovation (project PID2019-107102RBC21).

## REFERENCES

- (1) Majdinasab, M.; Mitsubayashi, K.; Marty, J. L., Optical and Electrochemical Sensors and Biosensors for the Detection of Quinolones. *Trends Biotechnol.* **2019**, *37* (8), 898-915.
- (2) Kergaravat, S. V.; Gagnetten, A. M.; Hernandez, S. R., Development of an Electrochemical Method for the Detection of Quinolones: Application to Cladoceran Ecotoxicity Studies. *Microchem. J.* **2018**, *141*, 279-286.
- (3) Rusu, A.; Hancu, G.; Uivarosi, V., Fluoroquinolone Pollution of Food, Water and Soil, and Bacterial Resistance. *Environ. Chem. Lett.* **2014**, *13* (1), 21-36.
- (4) Marchant, J., When Antibiotics Turn Toxic. *Nature* **2018**, *555*, 431-433.
- (5) Leder, C.; Suk, M.; Lorenz, S.; Rastogi, T.; Peifer, C.; Kietzmann, M.; Jonas, D.; Buck, M.; Pahl, A.; Kümmerer, K., Reducing Environmental Pollution by Antibiotics through Design for Environmental Degradation. *ACS Sustain. Chem. Eng.* **2021**, *9* (28), 9358-9368.
- (6) Rudnicki, K.; Sipa, K.; Brycht, M.; Borgul, P.; Skrzypek, S.; Poltorak, L., Electrochemical Sensing of Fluoroquinolone Antibiotics. *TrAC, Trends Anal. Chem.* **2020**, *128*, 115907.
- (7) Gayen, P.; Chaplin, B. P., Selective Electrochemical Detection of Ciprofloxacin with a Porous Nafion/Multiwalled Carbon Nanotube Composite Film Electrode. *ACS Appl. Mater. Interfaces* **2016**, *8* (3), 1615-26.
- (8) Ye, C.; Chen, X.; Zhang, D.; Xu, J.; Xi, H.; Wu, T.; Deng, D.; Xiong, C.; Zhang, J.; Huang, G., Study on the Properties and Reaction Mechanism of Polypyrrole@Norfloxacin Molecularly Imprinted Electrochemical Sensor Based on Three-Dimensional CoFe-MOFs/AuNPs. *Electrochim. Acta* **2021**, *379*, 138174.
- (9) Cetó, X.; Voelcker, N. H.; Prieto-Simon, B., Bioelectronic Tongues: New Trends and Applications in Water and Food Analysis. *Biosens. Bioelectron.* **2016**, *79*, 608-626.
- (10) Cui, F.; Yue, Y.; Zhang, Y.; Zhang, Z.; Zhou, H. S., Advancing Biosensors with Machine Learning. *ACS Sens.* **2020**, *5* (11), 3346-3364.
- (11) Wasilewski, T.; Kamysz, W.; Gebicki, J., Bioelectronic Tongue: Current Status and Perspectives. *Biosens. Bioelectron.* **2020**, *150*, 111923.
- (12) Herrera-Chacon, A.; Cetó, X.; del Valle, M., Molecularly imprinted polymers - towards electrochemical sensors and electronic tongues. *Anal. Bioanal. Chem.* **2021**, *24*, 6117-6140.
- (13) Huynh, T.P.; Kutner, W., Molecularly imprinted polymers as recognition materials for electronic tongues. *Biosens. Bioelectron.* **2015**, *74*, 856-864.
- (14) Ahmad, O. S.; Bedwell, T. S.; Esen, C.; Garcia-Cruz, A.; Piletsky, S. A., Molecularly Imprinted Polymers in Electrochemical and Optical Sensors. *Trends Biotechnol.* **2019**, *37* (3), 294-309.
- (15) BelBruno, J. J., Molecularly Imprinted Polymers. *Chem. Rev.* **2019**, *119* (1), 94-119.
- (16) Gui, R.; Jin, H.; Guo, H.; Wang, Z., Recent Advances and Future Prospects in Molecularly Imprinted Polymers-Based Electrochemical Biosensors. *Biosens. Bioelectron.* **2018**, *100*, 56-70.
- (17) Rebelo, P.; Costa-Rama, E.; Seguro, I.; Pacheco, J. G.; Nouws, H. P. A.; Cordeiro, M.; Delerue-Matos, C., Molecularly Imprinted

Polymer-Based Electrochemical Sensors for Environmental Analysis. *Biosens. Bioelectron.* **2021**, *172*, 112719.

- (18) Karimian, N.; Stortini, A. M.; Moretto, L. M.; Costantino, C.; Bogialli, S.; Ugo, P., Electrochemosensor for Trace Analysis of Perfluorooctanesulfonate in Water Based on a Molecularly Imprinted Poly( O-Phenylenediamine) Polymer. *ACS Sens.* **2018**, *3* (7), 1291-1298.
- (19) Ozcelikay, G.; Kaya, S. I.; Ozkan, E.; Cetinkaya, A.; Nemutlu, E.; Kir, S.; Ozkan, S. A., Sensor-Based MIP Technologies for Targeted Metabolomics Analysis. *TrAC, Trends Anal. Chem.* **2022**, *146*, 116487.
- (20) Anirudhan, T. S.; Athira, V. S.; Nair, S. S., Detection of Chlorpyrifos Based on Molecular Imprinting with a Conducting Polythiophene Copolymer Loaded on Multi-Walled Carbon Nanotubes. *Food Chem.* **2022**, *381*, 132010.
- (21) Surya, S. G.; Khatoon, S.; Ait Lahcen, A.; Nguyen, A. T. H.; Dzantiev, B. B.; Tarannum, N.; Salama, K. N., A Chitosan Gold Nanoparticles Molecularly Imprinted Polymer Based Ciprofloxacin Sensor. *RSC Advances* **2020**, *10* (22), 12823-12832.
- (22) Alegret, S.; Alonso, J.; Bartroli, J.; Cespedes, F.; Martinez Fabregas, E.; del Valle, M., Amperometric Biosensors Based on Bulk-Modified Epoxy Graphite Biocomposites. *Sensor. Mater.* **1996**, *8* (3), 147-153.
- (23) Sá, A.; Cipri, A.; González-Calabuig, A.; Ramos Stradiotto, N.; del Valle, M., Resolution of Galactose, Glucose, Xylose and Mannose in Sugarcane Bagasse Employing a Voltammetric Electronic Tongue Formed by Metals Oxy-Hydroxide/MWCNT Modified Electrodes. *Sens. Actuators B Chem.* **2016**, *222*, 645-653.
- (24) Cetó, X.; Cespedes, F.; Pividori, M. I.; Gutierrez, J. M.; del Valle, M., Resolution of Phenolic Antioxidant Mixtures Employing a Voltammetric Bio-Electronic Tongue. *Analyst* **2012**, *137* (2), 349-356.
- (25) Rodvold, K. A.; Piscitelli, S. C., New Oral Macrolide and Fluoroquinolone Antibiotics: An Overview of Pharmacokinetics, Interactions, and Safety. *Clin. Infect. Dis.* **1993**, *17*, S192-S199.
- (26) Cetó, X.; Perez, S., Voltammetric Electronic Tongue for Vinegar Fingerprinting. *Talanta* **2020**, *219*, 121253.
- (27) Ansari, S., Combination of Molecularly Imprinted Polymers and Carbon Nanomaterials as a Versatile Biosensing Tool in Sample Analysis: Recent Applications and Challenges. *TrAC, Trends Anal. Chem.* **2017**, *93*, 134-151.
- (28) Benito-Pena, E.; Martins, S.; Orellana, G.; Moreno-Bondi, M. C., Water-Compatible Molecularly Imprinted Polymer for the Selective Recognition of Fluoroquinolone Antibiotics in Biological Samples. *Anal. Bioanal. Chem.* **2009**, *393* (1), 235-245.
- (29) Urraca, J. L.; Castellari, M.; Barrios, C. A.; Moreno-Bondi, M. C., Multiresidue Analysis of Fluoroquinolone Antimicrobials in Chicken Meat by Molecularly Imprinted Solid-Phase Extraction and High Performance Liquid Chromatography. *J. Chromatogr. A* **2014**, *1343*, 1-9.
- (30) del Valle, M., Electronic Tongues Employing Electrochemical Sensors. *Electroanalysis* **2010**, *14*, 1539-1555.

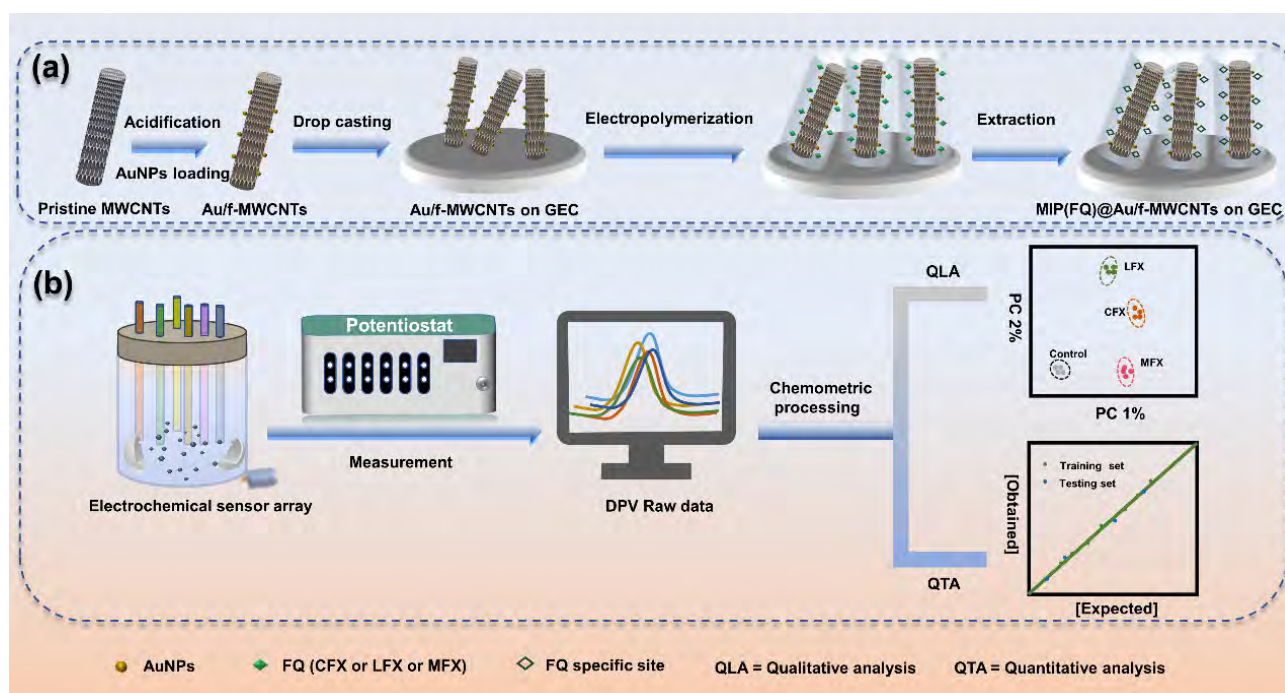


# A sensor array based on molecularly imprinted polymers and machine learning for the analysis of fluoroquinolone antibiotics

Mingyue Wang, Xavier Cetó and Manel del Valle\*

*Sensors and Biosensors Group, Department of Chemistry, Universitat Autònoma de Barcelona, Faculty of Sciences,  
08193 Bellaterra, Barcelona, Spain*

## Supporting Information



**Scheme S1.** Design of the ET based on MIP(FQ)@Au/f-MWCNTs: (a) Main steps related to the fabrication of the MIP(FQ)@Au/f-MWCNTs sensors, and (b) combination of the sensors into an array to develop the ET for the qualitative and quantitative analysis of FQs.

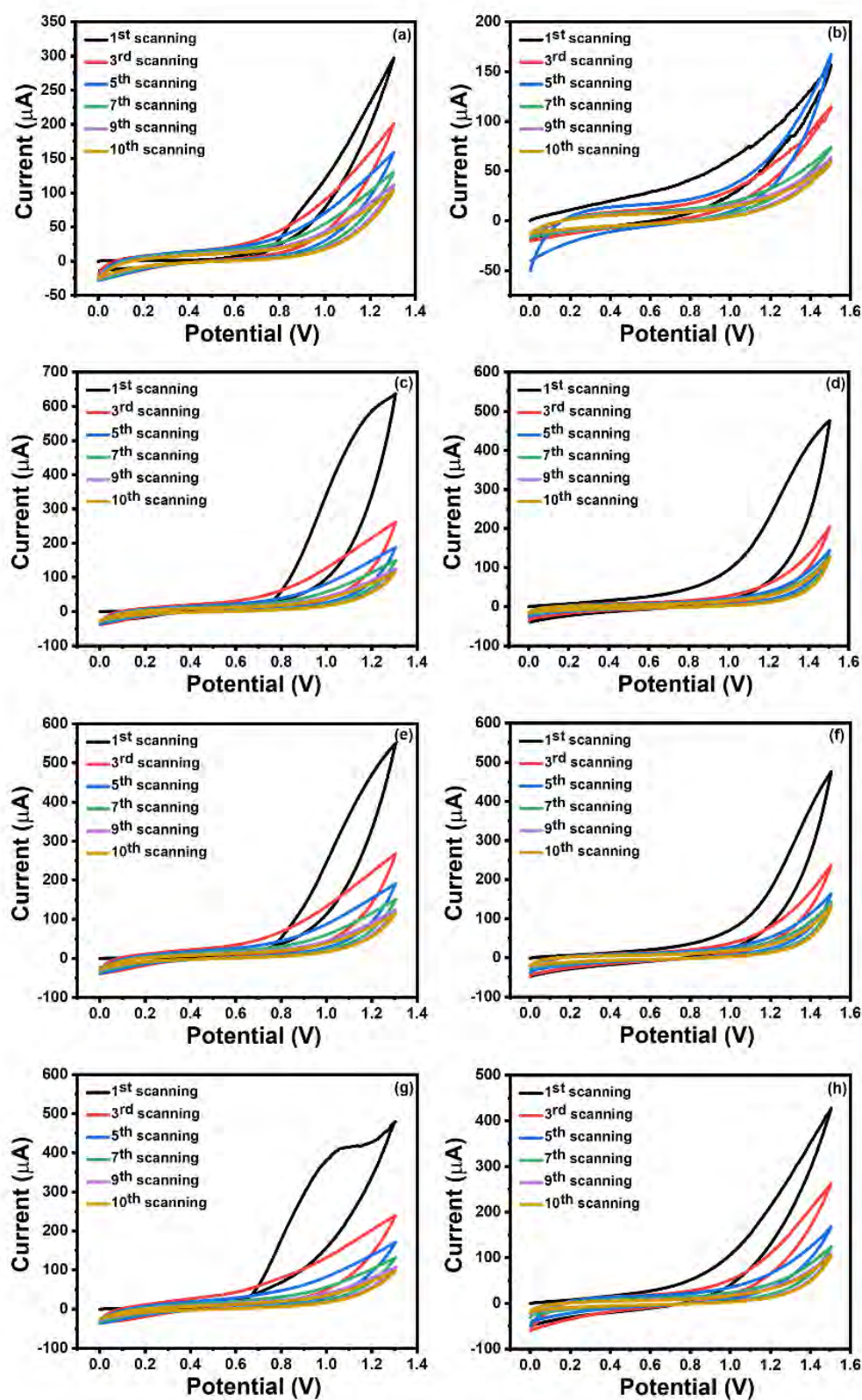


**Figure S1.** The CV curves on the left were recorded during the electropolymerization of MIP(FQ) films onto Au-fMWCNTs (a) with CFX, (c) with LFX, (e) with MFX and (g) without any FQ template molecules. The CV curves on the right were recorded during the extraction of FQ template molecules (b) CFX, (d) LFX, (f) MFX and (h) NIP as control for MIP(FQ<sub>s</sub>)@Au-fMWCNTs.

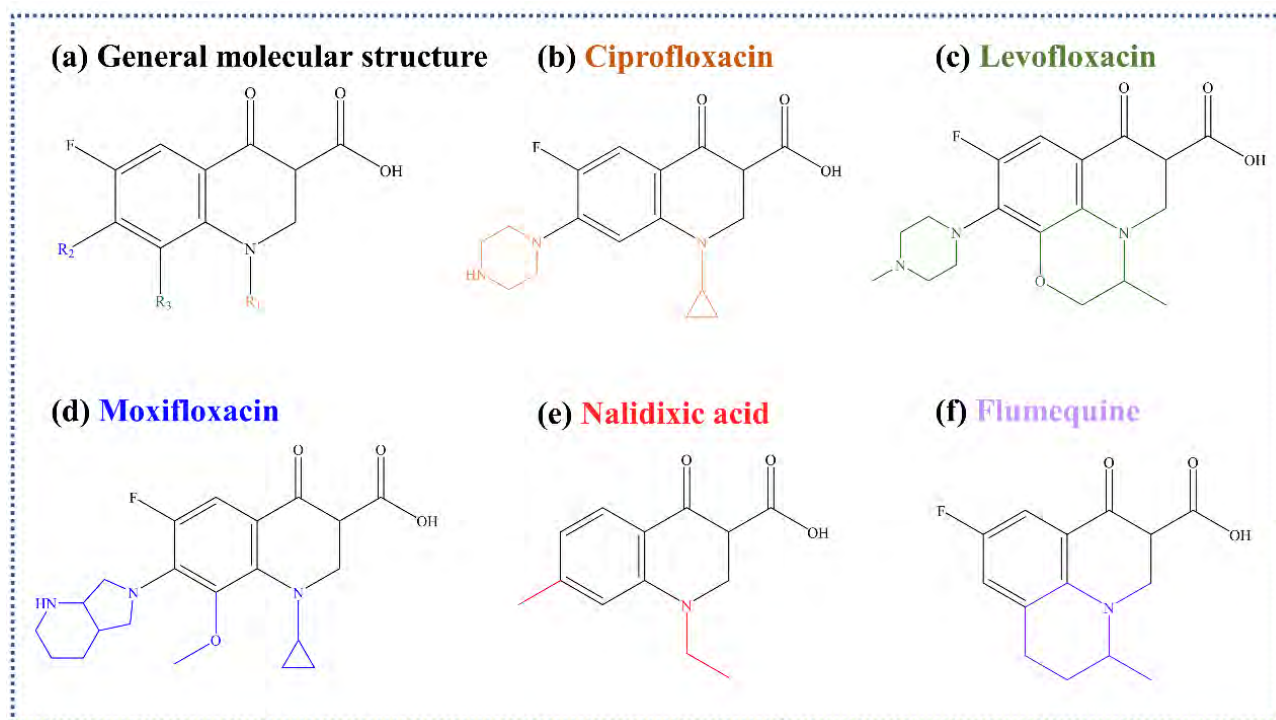


**Figure S2.** Molecular structure of FQ antibiotics: (a) general structure of FQs, (b) ciprofloxacin (CFX), (c) levofloxacin (LFX), (d) moxifloxacin (MFX), (e) flumequine (FLQ) and (f) nalidixic acid (NA).

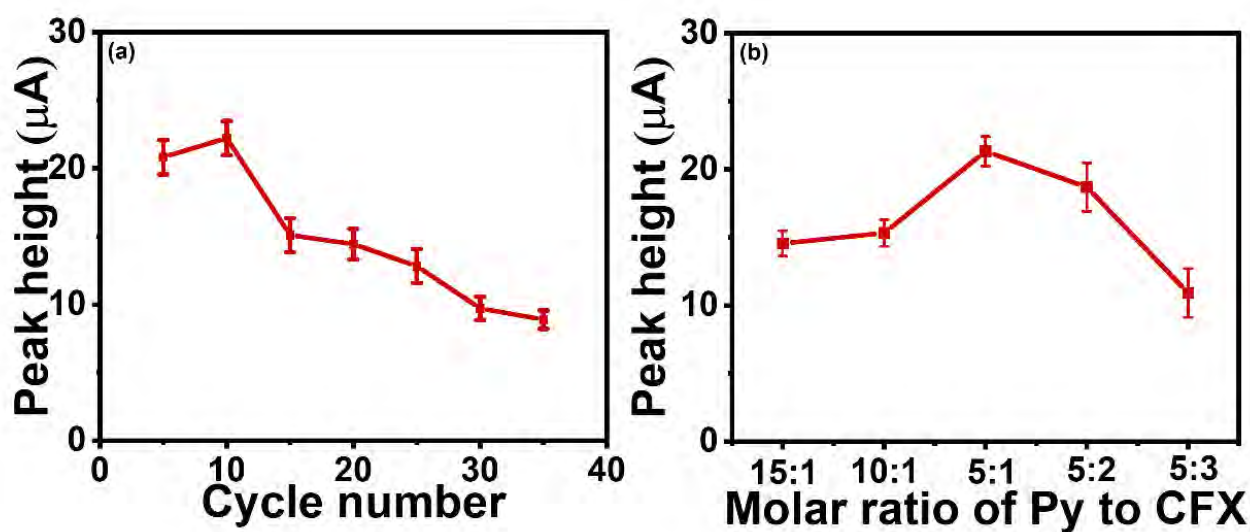


**Figure S3.** Effect on the sensor response of (a) the number of cycles and (b) the ratio of the monomer to template during the electropolymerization. The peak height was taken from DPV measurements with MIP(CFX)@Au-fMWCNTs sensor towards a 5  $\mu\text{M}$  CFX solution. The electrolyte used to study the effect of cycle number was composed by Py and CFX at ratio of 5:1, while the scanning cycle number was fixed at 10 when investigated the effect of molar ratio of monomer to template.



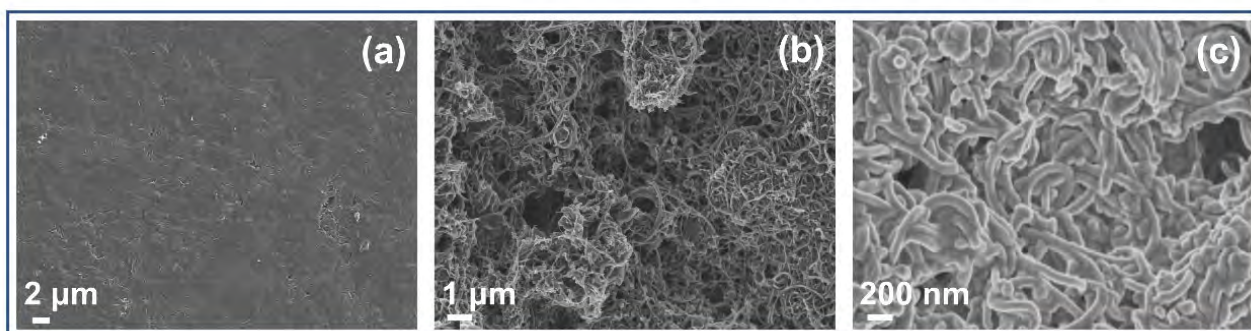


**Figure S4.** SEM images of (a) bare GEC, (b) Au-fMWCNTs and (c) NIP @Au-fMWCNTs.

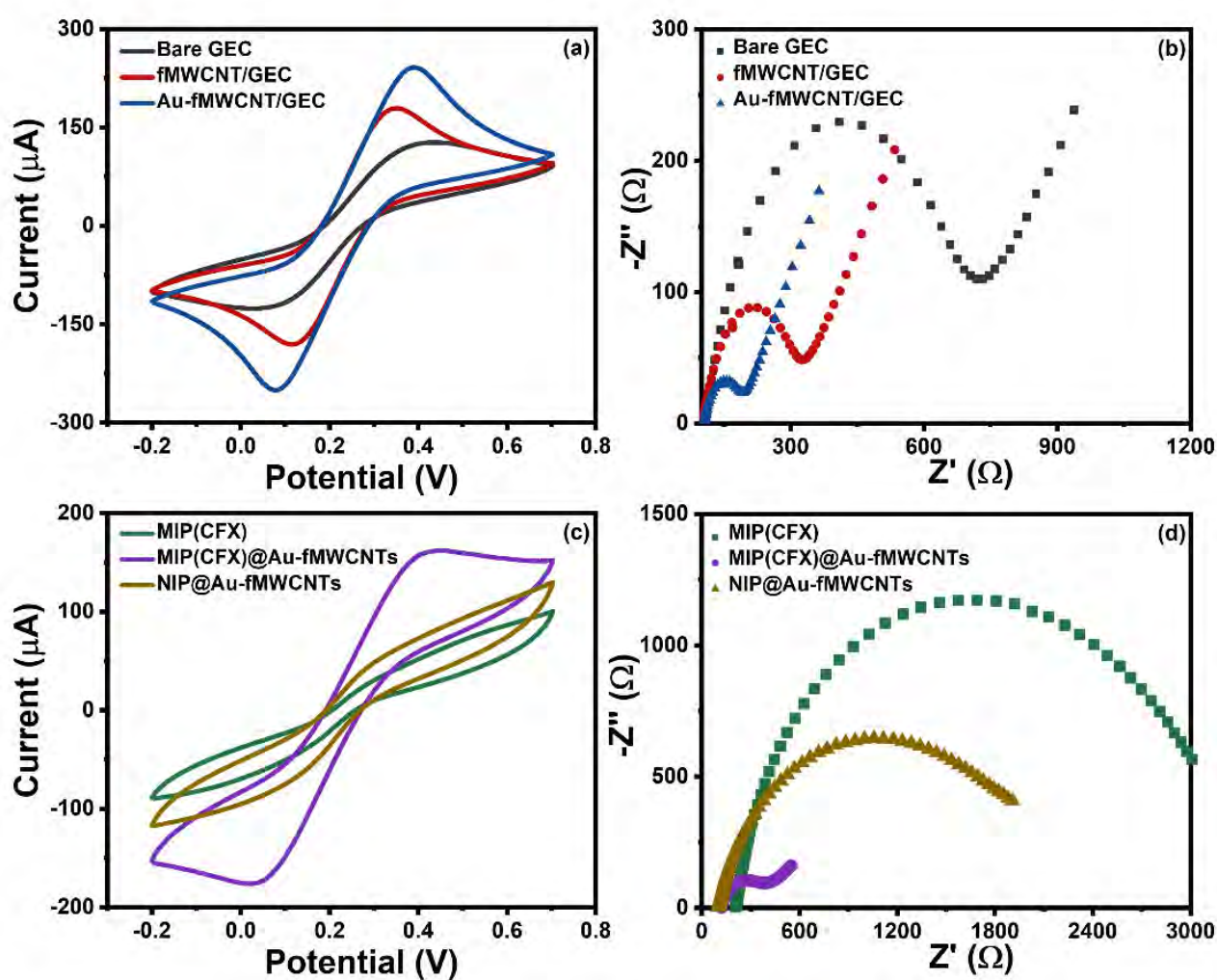


**Figure S5.** Electrochemical characterization of the sensor response towards a 5 mM  $[\text{Fe}(\text{CN})_6]^{3-/4-}$  solution in PBS during the different steps involved in the preparation of the sensors by (a,c) cyclic voltammetry and (b,d) electrochemical impedance spectroscopy.

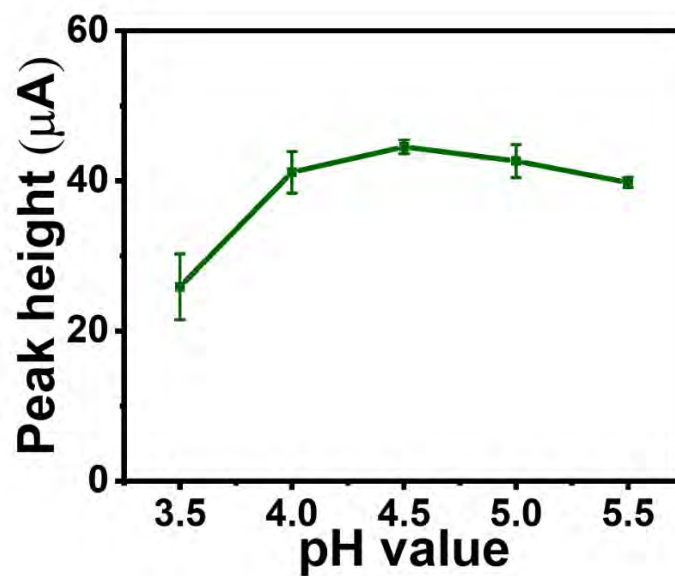


**Figure S6.** Effect of the pH of acetate buffer on the MIP(CFX)@Au-fMWCNTs sensor response towards a 10  $\mu$ M CFX solution.

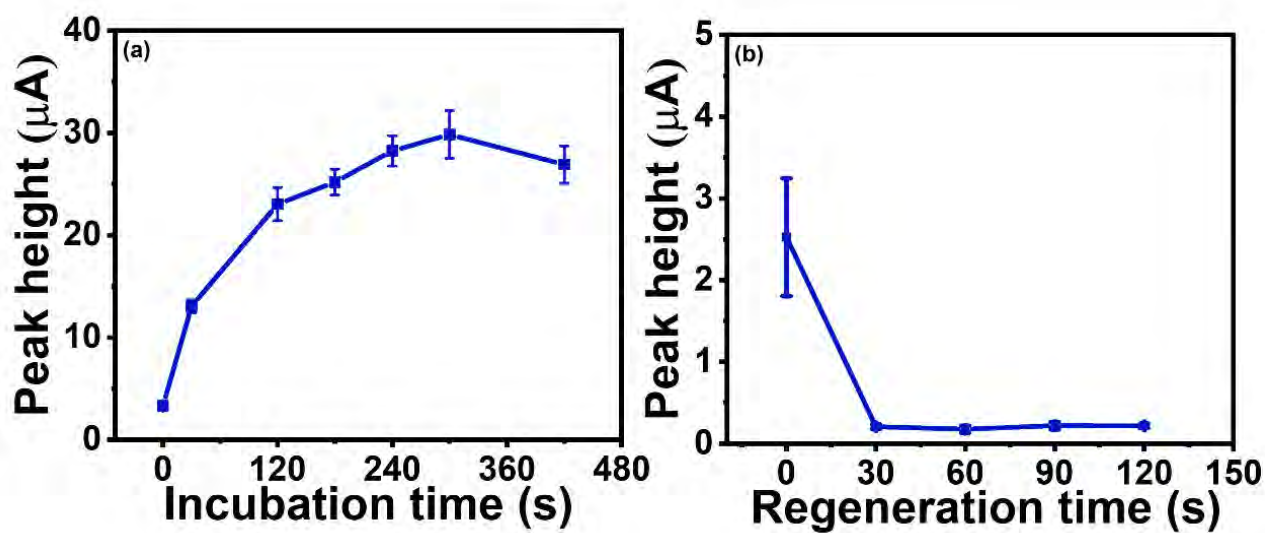


**Figure S7.** Effect on the sensor response of (a) the incubation time with the template and (b) the regeneration time after each measurement. The peak height was taken from DPV measurements with MIP(CFX)@Au-fMWCNTs sensor towards a 10  $\mu$ M CFX solution.



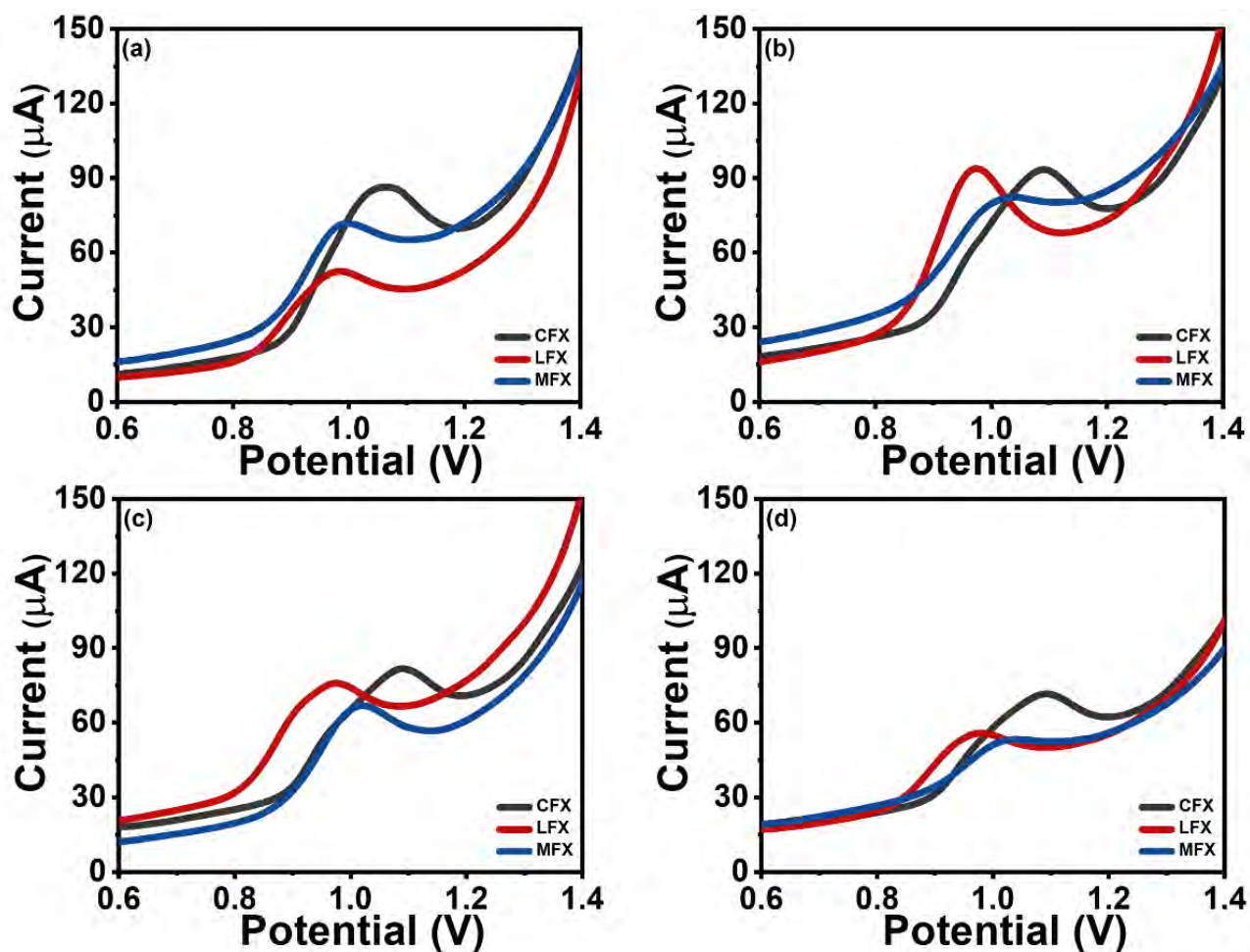


**Figure S8.** Raw DPV curves of (a) MIP(CFX)@Au-fMWCNTs, (b) MIP(LFX)@Au-fMWCNTs, (c) MIP(MFX)@Au-fMWCNTs and (d) NIP@Au-fMWCNTs towards a  $10\mu\text{M}$  solution of: (black) CFX, (red) LFX and (blue) MFX.

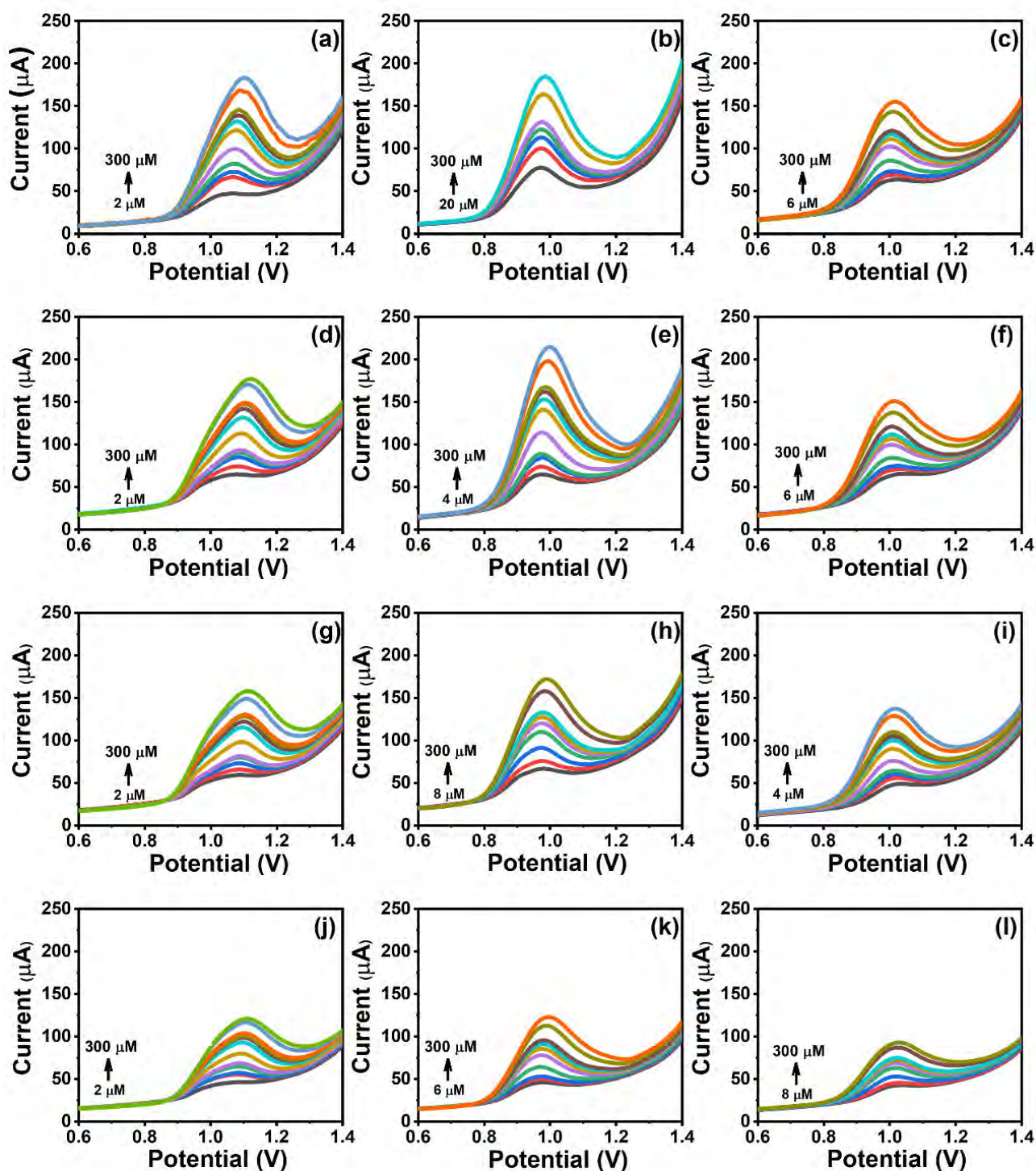


**Figure S9.** DPV curves in the corresponding linear concentration range of (a-c) MIP(CFX)@Au-fMWCNTs towards CFX, LFX and MFX (d-f) MIP(LFX)@Au-fMWCNTs towards CFX, LFX and MFX (g-i) MIP(MFX)@Au-fMWCNTs towards CFX, LFX and MFX and (j-l) NIP@Au-fMWCNTs towards CFX, LFX and MFX.

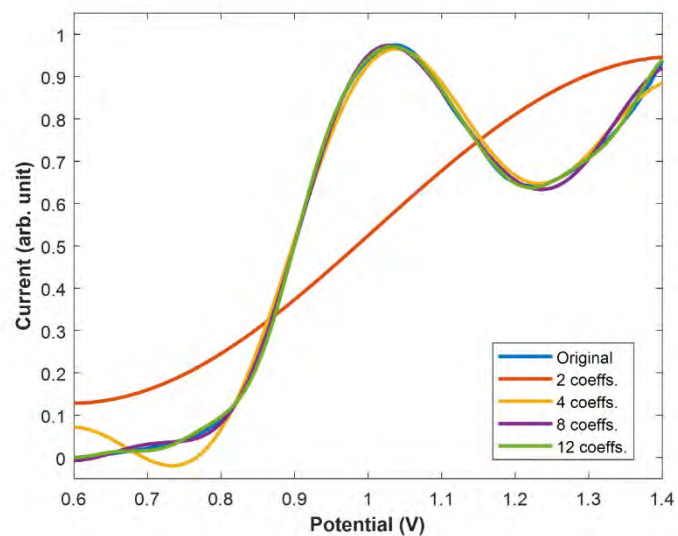


**Figure S10.** Effect of the number of coefficients taken during DCT compression step on the reconstruction of the original voltammetric signal.

**Table S1.** Analytical parameters of MIP(FQs)@Au-fMWCNTs sensors towards the three FQs calculated from DPV measurements.

Analyte	Sensor	$B_{\max}$ ( $\mu\text{A}$ )	$K_D$ ( $\mu\text{M}$ )
CFX	MIP(CFX)	114	23.4
	MIP(LFX)	108	22.3
	MIP(MFX)	88.1	21.7
	NIP	63.2	19.5
LFX	MIP(CFX)	155	3.76
	MIP(LFX)	165	33.2
	MIP(MFX)	148	60.9
	NIP	89.0	53.6
MFX	MIP(CFX)	109	49.0
	MIP(LFX)	99.4	54.2
	MIP(MFX)	94.5	37.3
	NIP	61.8	59.9

## **Acknowledgements**

Barcelona, when I landed from the Flight CA839 on 2 November, 2018, except my husband beside me, I knew nothing about the strange city. After going through years of pandemic, ups and downs in research work, and many unexpected surprises and serendipities of life, now I'm about to leave. As it draws to a close, I would like to thank you all so much for walking and growing with me on my PhD journey.

I appreciate my supervisor, Manel, for allowing me to join GSB and lighting a path for me as a newcomer. As the group leader, you not only give us scientific advices, but also lead a dynamic working environment, always being inclusive and considerate.

I am especially grateful to my co-supervisor, Xavier, for all his continuously patient instructions and warm helps. In the past years, every time when I stuck in the daunting bottleneck in research work, it was you pull me back from the edge of the implosion, extricate me from the dilemma of discouragement, provide me with so many useful instructions. In all sincerity, you are my *Scorpio Power* in Barcelona.

Thank my labmates, Marta, Dioni, Anna, Munmi, Qing, Elena, Yoana, Fracisco, Edervado and Pheem, working and studying in GSB leaves me countless beautiful moments.

Heartly, thank my families in China. Thank my parents and young brother who trust and love me. Thank my parents-in-law who understand and support us. Thank my bestie, Miao, who cares and encourages me.

Particularly, thank you, Wenhai, my super husband. From China to Barcelona, from master to doctor, from school uniform to wedding dress, you have been writing me a long-lasting and touching confession with the consistent companionship. You are my brightest star in the dark night, always.

By here, there are many memory clips rewinding in my mind. Anyway, thank for all encounters.

Mingyue Wang  
Bellaterra, July 2022